2008

# Investigation of Antimonide Structure Types and the Structural Studies of Molybdates

Dixie Plaisance Gautreaux
*Louisiana State University and Agricultural and Mechanical College, dgautr4@lsu.edu*

# INVESTIGATION OF ANTIMONIDE STRUCTURE TYPES AND THE STRUCTURAL STUDIES OF MOLYBDATES

A Dissertation

Submitted to the Graduate Faculty of the
Louisiana State University and
Agricultural and Mechanical College
in partial fulfillment of the
requirements for the degree of
Doctor of Philosophy

in

The Department of Chemistry

by
Dixie Plaisance Gautreaux
B.S., Nicholls State University, 2003
August 2008

**TABLE OF CONTENTS**

## LIST OF TABLES

**LIST OF FIGURES**

**ABSTRACT**

This dissertation highlights the investigation of ternary lanthanide antimonide structure types and their physical properties. In particular, these ternary phases allow for the systematic investigation of the structure in an effort to correlate structure and properties. The ternary antimonides are layered structures with two-dimensional square sheets or nets, which influence the properties of these materials. In an effort to determine how structural changes influence the physical properties, various single crystals of compounds relating to the orthorhombic $CeNiSb_3$ structure have been grown and characterized. The layered $CeNiSb_3$ structure consists of Sb sheets, $NiSb_6$ distorted octahedra, and $CeSb_9$ monocapped square anti-prisms. $LnNi(Sn,Sb)_3$ and $LnPdSb_3$ differ slightly from the $CeNiSb_3$ structure in the packing of the transition metal layer. The structures and physical properties of $LnNi(Sn,Sb)_3$ ($Ln$ = La-Nd, Sm, Gd, Tb) are studied as a function of lanthanide. The stability of the $CeNiSb_3$ structure was investigated by the substitution of Co or Cu for Ni in $CeNiSb_3$ resulting in $CeNi_xCo_{1-x}Sb_3$ and $Ln(Ni_{1-x}Cu_x)_ySb_2$ compounds. Also, the effect of Ni substitution for Cu in $Ce(Cu_{1-x}Ni_x)Sb_2$ $(0 \leq x \leq 0.8)$ compounds on the magnetoresistance is investigated.

This dissertation also explores the different structure types of molybdates $Rb_4M(MoO_4)_3$ ($M$ = Mn, Zn, and Cu). Each analogue adopts a different structure type and contain similar subunits. The full structure determinations of each of these compounds are important to be able to understand the promising magnetic and electrical properties.

# CHAPTER 1 – INTRODUCTION

## 1.1    Research Focus

Our research focus is on the interface of chemistry and physics, specifically the solid-state crystal growth of various materials for structure determination and physical properties of the new materials.  One of our primary goals is to identify structural features in extended solids that favor signature behaviors such as magnetoresistance, superconductivity, heavy-fermions, electrocatalysts, and multiferroics.  Gaining a better understanding of structural effects on the physical properties of highly correlated compounds will help enable the rational design of materials of the future.

The growth of high quality single crystals is essential to the discovery of new materials and their applications.  Only with high quality single crystal can detailed property measurements be done.  As Paul Canfield states, "the key is to search for materials with specific properties in a phase space that favors finding such compounds."[1]  This directly refers to our goal of understanding structural features that may be predominate in materials that possess the desired properties.  Once specific structural features have been identified, tuning of the physical properties of that material can begin by methods such as applying chemical pressure by substitution or doping other elements into the structure.

Many antimonides also possess unique structural features such as two-dimensional square sheets or nets and highly layered structures, which promote unusual physical properties.[2] Ternary rare earth (*Ln*) - transition metal - antimonides display unusual bonding and interesting physical properties such as magnetoresistance.  In particular, these ternary phases allow one to study the systematics in an effort to correlate structure and properties.  The magnetic rare earth element contributes to the magnetism and the coupling of *f*-electrons with a transition metal sublattice may lead to exotic properties.  The transition metal adds conduction electrons to the

1

magnetic structure as well as another structural layer. The addition of the main group element antimony, which resides along the metal – insulating border, makes this phase space attractive to investigate.

## 1.2 Synthesis

Crystal growth requires significant planning involving starting materials, the temperature profile, reaction vessel, and the stoichiometric ratios of each element involved. The primary crystal growth technique used in our lab is the self flux growth method, where the flux is a specific metal that acts as a "solution" to allow the melting of the other elements at high temperatures. The flux should melt at relatively low temperatures relative to the high melting metals so that the reaction mixture can be cooled to allow the desired phase to crystallize out of solution.[3] As the melt is slowly cooled, the desired phase will crystallize and excess flux can be removed via centrifugation or chemical etching.[3,4]

Other parameters to consider include atmosphere, the heat treatment of the sample, as well as the container used during the growth. Most metals will oxidize in high temperature environments so it is important to have an oxygen-free atmosphere. Ar or $N_2$ atmospheres are generally used to ensure that no $O_2$ is present within the sample. The reaction vessel used in the reaction must not react with any of the elements present and also must not melt at the temperatures achieved in the reaction. Examples of typical reaction vessels include Ta, $Al_2O_3$, Nb, Mo, steel, or W crucibles.[5] The crucible may then be sealed in a fused silica tube under an inert atmosphere.[3]

Phase diagrams are useful guides for determining stoichiometric ratios. To avoid unwanted binaries when synthesizing a ternary phase, temperatures and compositions of binary phases must be determined. If a ternary phase involving Ce-Ni-Sb is to be synthesized using Sn flux, one should consider the examination of Ce-Ni, Ni-Sb, Ce-Sb, Ce-Sn, Ni-Sn, and Sb-Sn

phase diagrams. Figure 1.1 shows the Ni-Sn binary temperature-composition phase diagram.[6]

To avoid the synthesis of $Ni_3Sn_4$, the molar ratio of Sn should be high enough for the reaction to

be in the liquidus state. We note that Sn melts at 232 °C, and hence to only isolate the desired

phase without Sn encapsulation, one would either remove the reaction from the furnace above

the melting point of Sn or etch the Sn from the surface of the samples.

An alternative to the flux growth method commonly used in our laboratory is an arc-

melting technique. Arc-melting is essentially a "brute-force" welding technique. This technique
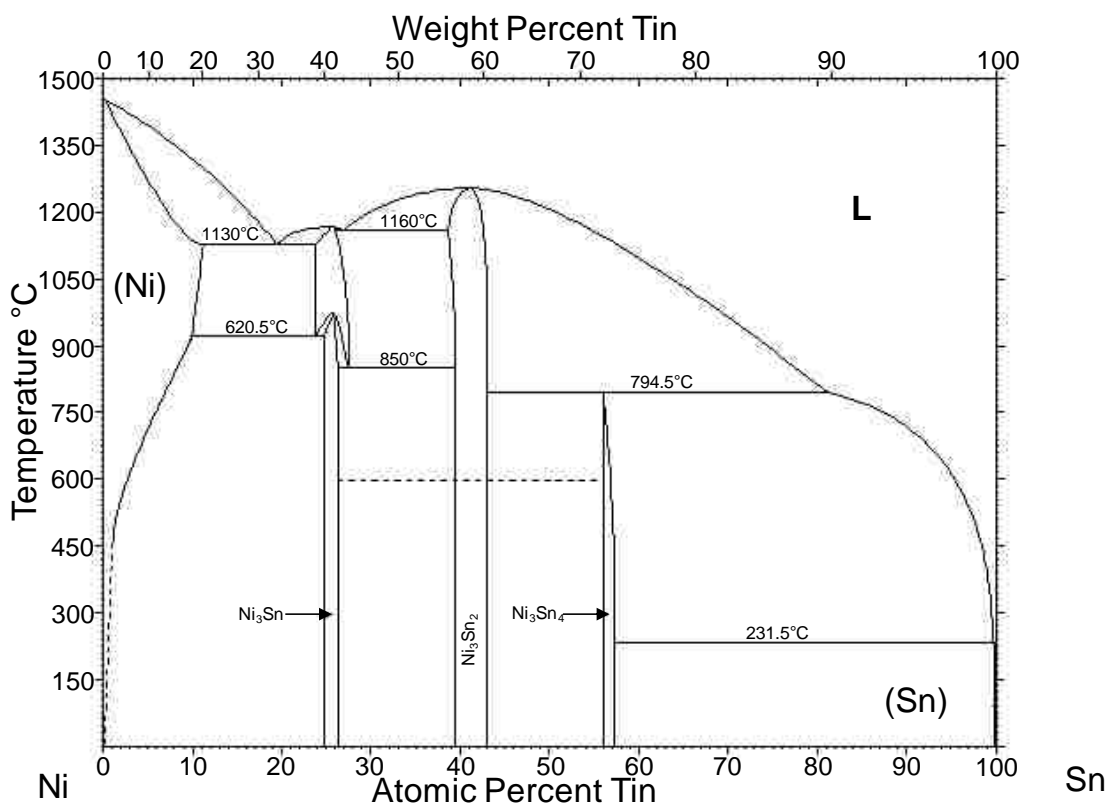


**Figure 1.1**    Ni-Sn Phase Diagram adapted from Nash's Ni-Sn Binary Alloy
Phase Diagram

is sometimes used when multiple flux-growth experiments have not yielded the desired results.

It is also an easy way to bypass the thermodynamic effects that allow undesired phases to form in

your reaction mixture. Constituent elements are weighed out on stoichiometry to the desired

phase. The elements are then placed together in an electric arc which rapidly melts and binds the

3

elements together into a button.  Then, the arc-melted button is annealed at high temperatures

under vacuum in our furnaces.  Occasionally, single crystals are obtained directly from the

annealing process.  However, most samples obtained from this method are polycrystalline in

nature.  Typically, the polycrystalline sample is then placed in an alumina crucible and a flux is

then added and the reaction vessel undergoes the flux-growth method described above.

Another synthetic technique is used to synthesize polycrystalline oxide samples.  Samples

are prepared using a combination of grinding and mixing the constituent oxide powders.  The

amounts of oxide powder used are based on the stoichiometry of a solid – state reaction yielding

the desired product.  The resulting mixture is then pressed into a small pellet.  The pellet is then

heat treated at high temperatures for a predetermined period of time.  The resulting pellet is then

ground and remixed again followed by a higher temperature heat treatment.  Between each heat

treatment, a powder XRD pattern is taken to identify the phase.  This process is continued until

the solid solution is reached with no unreacted oxides remaining.  The unreacted oxides show up

as extra peaks in the XRD powder pattern.  This technique typically yields only polycrystalline

samples.

## 1.3     Characterization

### 1.3.1    Single Crystal X-Ray Diffraction

Single crystal X-ray diffraction is an indispensable technique for determining the crystal

structure of highly crystalline compounds.  A beam of X-rays are collinated at the sample and

after impact, the X-rays are scattered in various directions by the electrons and atoms in the

lattice.[7]   When Bragg's law ($\lambda = 2d\sin\theta$, where $\lambda$ is the wavelength of the X-rays, $d$ is the

distance between adjacent planes, and $\theta$ is the Bragg angle) is satisfied, diffraction occurs.[8]   The

scattered X-rays are then recorded by a detector.  X-rays are a form of electromagnetic radiation

and possess both amplitude and a phase.  The current detectors can record only the amplitude, so

only half of the diffraction information needed to calculate electron density is recorded.  This is a well known problem known as the "Phase Problem".  Different techniques have been developed to overcome the phase problem, and direct methods is the technique used in our group to solve our structures.  Space group, lattice parameters, and atomic positions are obtained from successfully refined structural models.  Structural information such as bond distances, bond angles, site occupancy, and disorder can also be acquired and are invaluable to fully understanding the structure.

The Enraf Nonius Kappa CCD Diffractometer was used for all single crystal work in this document.  The X-rays are generated by a Mo $K_\alpha$ X-ray tube where $\lambda = 0.71073$ Å.  A crystal is mounted onto the tip of a glass fiber of the goniometer with epoxy and/or vacuum grease.  Temperature is regulated with a cooled nitrogen gas stream produced by an Oxford Cryostream Cooler.  The unit cell parameters were determined from images taken at a rotation of 15 °φ.  The structures were solved using the SIR97 direct methods program.[9]  The preliminary model of the structures were then refined using the SHELXL97 program package.[10]  Refinement of the model of the structure allows for the correction of many aspects of a crystal structure such as the addition of extinction coefficients, anisotropic parameters, size, temperature, site occupancy, and disorder.  This part of the process can produce the most correct model for that particular structure based on the data collected.

Occasionally special sample handling is necessary, particularly if the crystals are air-sensitive or hygroscopic.  In these cases, air exposure must be limited to protect the integrity of the crystals.  The crystals are placed in either mineral oil or paratone-N oil to protect the crystal surface.  Typically, a cooled nitrogen gas stream produced by an Oxford Cryostream Cooler is used to regulate the temperature of the crystal.  For sensitive crystals, the cooled nitrogen gas stream serves as an additional protective barrier and is used even for room temperature data

collections. At low temperatures (typically below 250 K) the epoxy used to secure the crystal to the tip of the goniometer becomes brittle. For low temperature data collections, the crystal is simply placed on the tip of the goniometer using either mineral oil or Paratone-N oil. Both of these oils harden at low temperatures and do not allow the crystal to move while on the tip of the goniometer. Low temperature data collections are typically used to search for phase transitions. However, low temperature data is sometimes better than room temperature because the thermal vibrations of atoms within the crystal are reduced at lower temperatures.

### 1.3.2 Powder X-Ray Diffraction

Each crystalline sample has a unique powder diffraction pattern. X-ray powder data are displayed as a pattern with intensity as a function of $2\theta$. The angles are dependent on the lattice parameters, lattice type, and wavelength of radiation. The intensity of each peak is dependent on the scattering of the elements present as well as the amount of sample. Most samples are compared to the powder patterns in the database from the Joint Committee on Powder Diffraction Standards (JCPDS) to check for known phases. An unknown sample can be identified by comparing the pattern to a calculated pattern from a refined model of the new structure.

X-ray powder diffraction data were collected on a Bruker D8 Advance Powder Diffractometer with monochromatic Cu $K_\alpha$ radiation ($\lambda = 1.540562$ Å) at room temperature. Data analysis was accomplished using DIFFRAC$^{plus}$ Evaluation Program.[11] The ground, polycrystalline sample is placed onto a no-background holder. It is essential that the powder sample be flat to avoid errors associated with sample displacement. Figure 1.2 shows the setup of a powder diffractometer as well as the no-background sample holder used to collect data.
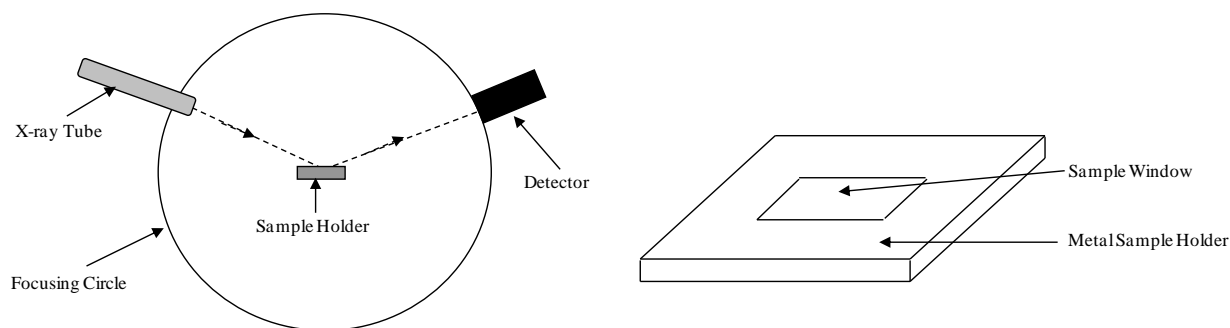
**Figure 1.2**    Illustration of powder diffractometer geometry and sample holder

### 1.3.3    Neutron Powder Diffraction

Neutron powder diffraction is a complementary technique used when X-ray diffraction cannot provide sufficient information.  The scattering power of neutrons is advantageous because the atomic nuclei rather than the electrons are responsible for scattering the radiation.   It is extremely useful in locating light atoms and is able to distinguish between atoms that have similar scattering.  Magnetic structure analysis is also possible with neutron powder diffraction because the magnetic dipole moment of neutrons may interact with unpaired electrons in the structure.   Neutron powder diffraction (NPD) data were collected at National Institute of Standards and Technology (NIST) Center for Neutron Research on the powder diffractometer BT-1.  A Cu(311) monochromator with a wavelength ($\lambda$) of 1.5403 Å was used.

### 1.3.4    Elemental Analysis

Because X-ray diffraction cannot distinguish between elements with similar *Z*, alternative characterization techniques must be used.   The first elemental analysis method used is inductively coupled plasma-optical emission spectroscopy (ICP-OES) on a Perkin Elmer Optima Model 5300V.  The plasma excites each of the atoms present and upon relaxation light is emitted and with a polychromatic detector, the amount of each element present can be determined.  The second elemental analysis method employed is energy dispersive spectroscopy.  A Hitachi S-3600N extra-large chamber variable pressure Scanning Electron Microscope (VP-SEM) with an

7

integrated energy dispersive (EDS) feature was used to collect data. The electrons at ground state are excited by the beam and an electron from the inner shell is ejected. Then a higher-energy electron fills the hole left by the inner shell electron and an X-ray is emitted which has characteristics specific to the element from which it was emitted. This technique is capable of giving quantitative elemental information and is an excellent complementary technique to X-ray crystallography.

## 1.4     Property Measurements

### 1.4.1   Magnetic Property Measurements

Magnetic susceptibility data (*M* vs *T*) were measured by a Quantum Design Physical Property Measurement System, where *M* is the magnetization and *T* is the temperature. Inverse susceptibility data above the ordering temperature are fitted to Curie-Weiss law to obtain the magnetic moment and the Weiss temperature, $\theta$.[12] The Curie Weiss law is $\chi = \dfrac{M}{H} = \dfrac{C}{T - \theta}$ , where $\chi$ is the magnetic susceptibility, *C* is the Curie constant, *T* is the temperature, and $\theta$ is the Weiss constant. Occasionally, a modified version of this law is used when the inverse susceptibility deviates from Curie-Weiss behavior and an additional constant, $\chi_0$, is subtracted from the magnetic susceptibility. The modified Curie-Weiss equation is $\chi - \chi_0 = \dfrac{M}{H} = \dfrac{C}{T - \theta}$, where $\chi_0$ is the temperature-independent contribution to the susceptibility. For most of the magnetic materials in this document $\chi_0$ is negligible.

The magnetization as a function of field (*M* vs *H*) was also measured by a Quantum Design Physical Property Measurement System, where *M* is the magnetization and *H* is the applied magnetic field. The saturation moment from this data is compared to a calculated value. The calculated saturation moment, $\mu_{\text{sat}} = -g\mu_B\mathbf{J}$, where *g* is given by the Landé equation, $\mu_B$ is a bohr magneton, and **J** is the sum of the orbital and spin angular momenta.[12] The Landé equation

is defined as $g = 1 + \frac{J(J+1) + S(S+1) - L(L+1)}{2J(J+1)}$ for a free atom. Typically, the magnetization curve for a ferromagnet displays hysteresis.

### 1.4.2 Transport Property Measurements

Resistivity as a function of temperature is typically measured on a single crystal and is defined as the resistance generated by collisions of electrons with phonons or impurities in the crystal lattice.[12] Electrical resistivity is defined as $\rho = R\frac{A}{L}$, where $R$ is the resistance, $A$ is the area of the crystal, and $L$ is the length of the crystal. A sudden drop in the resistivity to zero indicates a superconducting transition. Identifying and understanding materials with these superconducting transitions may lead to the design of materials with superconducting behavior at room temperature. Magnetoresistance is defined as $\frac{\rho - \rho_0}{\rho_0} \times 100\%$ and is plotted as a function of changing field.[12] The magnetoresistance of a typical metal is on the order of ~10 %. Materials that possess larger magnetoresistance behavior at room temperature have potential applications as various spintronic materials. Understanding both of these transport property behaviors are important in understanding and designing new materials.

## 1.5 Systems Investigated in This Document

The systems that are discussed in this dissertation focus on the structural studies of selected antimonides and double molybdates. Chapter 2 will focus on the synthesis, structure determination, and physical properties of $Ln$Ni(Sb,Sn)$_3$ ($Ln$ = La-Nd, Sm, Gd, Tb). The relationship of this structure type to other similar antimonide structure types will be explored. Chapter 3 will discuss the ramifications of substituting Co for Ni in both the structure and physical properties of CeNi$_x$Co$_{1-x}$Sb$_3$. Chapter 4 involves the systematic substitution of Ni for Cu in Ce(Cu$_{1-x}$Ni$_x$)$_y$Sb$_2$ and focuses on the effects on the magnetoresistance behavior. Structural

effects and magnetic properties are also explored.  Chapter 5 presents a structural study of the effects of transition metal substitution of double molybates $Rb_4M(MoO_4)_3$ ($M$ = Mn, Zn, and Cu).  The Zn and Cu analogues both adopt new structure types.  Temperature dependent phase transitions are explored for all analogues.  Chapter 6 provides brief conclusions and general overview of the dissertation.  The appendices include structural studies of various side projects.  Appendix 1 focuses on the structural determination of $Ln$PdSb$_3$, which is a new structure type.  Appendix 2 discusses the structure and physical properties of $EuCu_9Sn_4$.  Appendix 3 presents the structural confirmation of $VB_2$.  Accurate lattice parameters were necessary for energy band calculations.  Appendix 4 provides structural data from neutron powder diffraction and magnetic properties of $Y_{2-x}Ce_xTi_2O_7$.  Appendix 5 contains unpublished crystallographic information files for the molybdates discussed in Chapter 5.  Letters of permission to reuse published work are provided in Appendix 6.

## 1.6    References

(1)    Canfield, P. C. *Nature* **2008**, *4*, 167-169.

(2)    Papoian, G. A.; Hoffmann, R. *Angew. Chem. Int. Ed.* **2000**, *39*, 2409-2448.

(3)    Canfield, P. C.; Fisk, Z. *Philos. Mag. B* **1992**, *65*, 1117-23.

(4)    Kanatzidis, M. G.; Pöttgen, R.; Jeitschko, W. *Angew. Chem. Int. Ed.* **2005**, *44*, 6996-7023.

(5)    Fisk, Z.; Remeika, J. P. *Handbook on the Physics and Chemistry of Rare Earths*; Elsevier: Amsterdam, 1989; Vol. 12.

(6)    Nash, P.; Nash, A. *Bull. Alloy Phase Diagrams* **1985**, *6*, 350-359.

(7)    Cullity, B. D. *Elements of X-Ray Diffraction*; 2nd ed.; Addison-Wesley Publishing Company, Inc: Reading, Massachusetts, 1978.

(8)    Clegg, W.; Blake, A. J.; Gould, R. O.; Main, P. *Crystal Structure Analysis Principles and Practice*; Oxford University Press: Oxford, NY, 2001.

(9)     Altomare, A.; Burla, M. C.; Camalli, M.; Cascarno, G. L.; Giacovazzo, A.; Guagliardi, A.; Moliterni, A. G. G.; Polidori, G.; Spagna, R. J. *J. Appl. Crystallogr.* **1999**, *32*, 115-119.

(10)    Sheldrick, G. M.; University of Gottingen: Germany, 1997.

(11)    6.0 ed.; Bruker, AXS: Karlsruhe, West Germany, 2000.

(12)    Kittel, C.; 7th ed.; John Wiley & Sons, Inc.: New York, 1995.

**CHAPTER 2 – *Ln*Ni(Sn,Sb)$_3$**

**2.1 Introduction**

Ternary rare earth antimonides show unusual bonding and interesting physical properties such as large magnetoresistance and Kondo behavior.[1-3] The systematic studies of these ternary phases allow correlation of structure and properties. Structural features such as two-dimensional square sheets or nets and highly layered structures promote unusual physical properties.[4] The Ce, Pr, Nd and Sm analogues of *Ln*CrSb$_3$, which crystallize in the orthorhombic space group *Pbcm* with lattice parameters of $a \sim 12$ Å, $b \sim 6$ Å, $c \sim 6$ Å, each display two different magnetic transitions due to the Cr and lanthanide sublattices.[5-10] However, the Gd, Tb, and Dy analogues of *Ln*CrSb$_3$ each show only one magnetic transition due to the lanthanide.[6,11,12] YbCrSb$_3$, where Yb is divalent, was found to have a long range ferromagnetic ordering at $T_C \sim 280$ K.[14] $\alpha$-CeNiSb$_3$, which crystallizes in the orthorhombic space group *Pbcm* with lattice parameters of $a \sim 12$ Å, $b \sim 6$ Å, $c \sim 18$ Å, orders ferromagnetically at 6 K while the other lanthanide analogues of $\alpha$-*Ln*NiSb$_3$ (*Ln* = Pr, Nd and Sm) all order antiferromagnetically below 5 K.[15-17] The Dy and Ho analogues of the layered *Ln*NiSb$_2$ display large magnetoresistance (MR) of $\sim 115$ % and $\sim 165$ % respectively, while the Y analogue is linear up to $\sim$150 % at 3 K and 9 T.[18]

Tin flux was used in our efforts to grow larger crystals of CeNiSb$_3$ for magnetic and transport measurements and a new polymorph of this phase was discovered, previously known as $\beta$-CeNiSb$_3$.[19] $\beta$-CeNiSb$_3$ adopts the CePdSb$_3$ structure type with the orthorhombic space group *Pbcm* and lattice parameters $a \sim 12$ Å, $b \sim 6$ Å, $c \sim 12$ Å.[20,21] $\beta$-CeNiSb$_3$ orders ferromagnetically below 6 K and Kondo lattice behavior is observed.[19] To determine the structural stability of this structure type, we grew several lanthanide analogues. Further

---

investigation of this structure led to the discovery that Sn was incorporated into the crystal structure. The crystal growth, structure, magnetic properties of $Ln$Ni(Sn,Sb)$_3$ ($Ln$ = La, Ce, Pr, Nd, Sm, Gd, and Tb) are reported herein.

## 2.2 Experimental

### 2.2.1 Synthesis

Single crystals of $Ln$Ni(Sn,Sb)$_3$ ($Ln$ = La, Ce, Pr, Nd, Sm, Gd, or Tb) were prepared using excess Sn as the flux. La, Ce, Pr, Nd, Sm, Gd, or Tb pieces (99.9%, Alfa Aesar), Ni powder (99.999%, Alfa Aesar), Sb shot (99.999%, Alfa Aesar), and Sn shot (99.8%, Alfa Aesar) were placed in an alumina crucible in a 1:2:3:15 molar ratio. The crucible was sealed into an evacuated fused-silica tube. The reaction vessel was heated to 1150 °C where the temperature was held constant for 24 h and then cooled 5 °C h$^{-1}$ to 300 °C. After dwelling at 300 °C, the excess Sn flux was removed by centrifugation. The reaction mixtures contained silver plate-like crystals with dimensions up to 0.08 x 3 x 5 mm$^3$ for all analogues except Tb which contained plate-like crystals with dimensions up to 0.08 x 0.5 x 0.5 mm$^3$. Most samples also contained silver rod shaped crystals with dimensions of 1 x 1 x 5 mm$^3$. The plates were determined to be the desired product, while the predominant phase is the rod-shaped binary, Ni$_3$Sn$_4$. When exposed to air and moisture, there is no visible surface degradation to both compounds over a period of months.

Flux growth syntheses with other molar ratios such as 1:1:3:20 and 1:1:3:15 for the latter rare earth analogues with Sn flux were investigated; however, yield was less than 10%. The addition of excess Ni (1:2:3:15) resulted in an increased yield of $Ln$Ni(Sn,Sb)$_3$. We note that smaller lanthanide metals, Dy and Yb, yielded binary phases. Adjusting the spin temperature from 300 °C to 670 °C or 450 °C, also yielded different results. At 670 °C, CeNi(Sn,Sb)$_3$ and CeSb were obtained while at 450 °C CeNi(Sn,Sb)$_3$, CeSb, and Ni$_3$Sn$_4$ were obtained. However,

13

the yield of the desired $CeNi(Sn,Sb)_3$ was lower at both 670 °C and 450 °C than at 300 °C. Arc-melting the constituent elements Ce, Ni, and Sb (1:1:3) without Sn yields the $\alpha$-$CeNiSb_3$ structure type, therefore $\alpha$-$CeNiSb_3$ must be a line compound. Arc-melting Ce:Ni:Sb with 5 or 10% Sn followed by annealing at 1150 °C for 3 days in an evacuated fused-silica tube, allows for the substitution of Sn within the $\alpha$-$CeNiSb_3$ structure. This is determined by an increase of the lattice parameters obtained from single-crystal X-ray diffraction. Single crystals of $\alpha$-$CeNiSb_3$ can be "transformed" into $CeNi(Sn,Sb)_3$.[19] Unground single crystals of $\alpha$-$CeNiSb_3$ were placed into an alumina crucible with a 20 fold excess of Sn flux. After placing the crucible into an evacuated fused-silica tube, the reaction vessel underwent the heat treatment described above and was removed from the furnace at 300 °C. Approximately half of the crystals were "transformed" into $CeNi(Sn,Sb)_3$ while the other half maintained the $\alpha$-$CeNiSb_3$ structure type. These results were confirmed by single crystal X-ray diffraction.

2.2.2    Single Crystal X-ray Diffraction

A typical crystal with dimensions of ~ 0.08 x 0.08 x 0.1 mm$^3$ was mounted onto a glass fiber of a goniometer with epoxy and placed on a Nonius Kappa CCD X-ray diffractometer ($MoK_\alpha$ = 0.71073 Å). Data collection parameters and crystallographic data are listed in Table 2.1 for $LnNi(Sn,Sb)_3$ ($Ln$ = Pr, Sm, Gd, Tb). The unit cell parameters were determined from images taken at a rotation of 15 °$\varphi$. The model of the structure was refined by direct methods using SHELXL97.[22] The data were corrected for absorption and the displacement parameters were refined as anisotropic. Atomic coordinates and anisotropic displacement parameters are provided in Table 2.2. The R-factors for all compounds are reasonable with the exception of the Nd analogue. After multiple data collections, it was determined that this analogues has lower crystal quality based on higher chi$^2$ values.

14

**Table 2.1**  Crystallographic Data for $Ln$Ni(Sn,Sb)$_3$ ($Ln$ = Pr, Sm, Gd, or Tb)

| | La | Ce | Pr | Nd | Sm | Gd | Tb |
|---|---|---|---|---|---|---|---|
| Space Group | *Pbcm* | *Pbcm* | *Pbcm* | *Pbcm* | *Pbcm* | *Pbcm* | *Pbcm* |
| $a$ (Å) | 13.0970(2) | 12.9170(2) | 12.843(3) | 12.771(2) | 12.651(1) | 12.565(2) | 12.450(1) |
| $b$ (Å) | 6.1400(4) | 6.1210(5) | 6.105(7) | 6.093(4) | 6.083(2) | 6.072(3) | 6.060(2) |
| $c$ (Å) | 12.1270(4) | 12.0930(6) | 12.056(6) | 12.021(4) | 11.994(2) | 11.973(4) | 11.935(2) |
| $V$ (Å$^3$) | 975.20(4) | 956.13(9) | 945.3(12) | 935.4(7) | 923.0(3) | 913.5(6) | 900.5(3) |
| Size (mm$^3$) | 0.02/0.05/0.05 | 0.08/0.08/0.1 | 0.01/0.04/0.05 | 0.08/0.08/0.01 | 0.01/0.03/0.05 | 0.02/0.05/0.05 | 0.01/0.03/0.06 |
| Z | 8 | 8 | 8 | 8 | 8 | 8 | 8 |
| Temp (°C) | 25(2) | 25(2) | 24(2) | 25(2) | 25(2) | 25(2) | 25(2) |
| Density(g cm$^{-1}$) | 7.668 | 7.837 | 7.938 | 8.069 | 8.266 | 8.452 | 8.599 |
| $\theta$ Range (°) | 1.55-30.03 | 3.15-29.99 | 3.17-30.08 | 3.19-29.97 | 3.22-30.04 | 3.25-29.98 | 3.27-30.01 |
| $\mu$ (mm$^{-1}$) | 28.573 | 29.728 | 30.747 | 31.755 | 33.655 | 35.670 | 37.163 |
| $R_{int}$ | 0.0396 | 0.0181 | 0.0610 | 0.0626 | 0.0629 | 0.0557 | 0.0478 |
| Collected Ref. | 2677 | 2601 | 2541 | 2384 | 2492 | 2434 | 2469 |
| Unique Ref. | 1491 | 1445 | 1439 | 1400 | 1400 | 1377 | 1380 |
| $h$ | $-17 \le h \le 17$ | $-17 \le h \le 17$ | $-17 \le h \le 17$ | $-17 \le h \le 17$ | $-17 \le h \le 17$ | $-17 \le h \le 17$ | $-17 \le h \le 17$ |
| $k$ | $-8 \le k \le 8$ | $-8 \le k \le 8$ | $-8 \le k \le 8$ | $-8 \le k \le 8$ | $-8 \le k \le 8$ | $-8 \le k \le 8$ | $-8 \le k \le 8$ |
| $l$ | $-16 \le l \le 16$ | $-16 \le l \le 16$ | $-16 \le l \le 16$ | $-16 \le l \le 16$ | $-16 \le l \le 16$ | $-16 \le l \le 16$ | $-16 \le l \le 16$ |
| $\Delta\rho_{max}$ (e Å$^{-3}$) | 7.531 | 5.514 | 4.551 | 9.921 | 6.822 | 8.931 | 7.860 |
| $\Delta\rho_{min}$ (e Å$^{-3}$) | -5.625 | -1.705 | -3.704 | -10.886 | -12.674 | -8.063 | -12.168 |
| Extinction | 0.0056(5) | 0.00030(7) | 0.00050(10) | 0.0014(3) | 0.0064(5) | 0.00057(19) | 0.0064(5) |
| $^a R[F^2 > 2\sigma(F^2)]$ | 0.0627 | 0.0282 | 0.0522 | 0.0970 | 0.0745 | 0.0855 | 0.0618 |
| $^b wR_2(F^2)$ | 0.1779 | 0.0716 | 0.1314 | 0.2639 | 0.1832 | 0.2092 | 0.1621 |

$^a$ $R_1(F) = \sum \left| |F_0| - |F_c| \right| / \sum |F_0|$

$^b$ $R_w(F_0^2) = \sum [w(F_0^2 - F_c^2)] / \sum [w(F_0^2)^2]^{1/2}$ ; $w = 1/[\sigma^2(F_0^2) + (0.1403P)^2 + 1.2003P]$,

$w = 1/[\sigma^2(F_0^2) + (0.0140P)^2 + 12.8728P]$  $w = 1/[\sigma^2(F_0^2) + (0.0697P)^2 + 8.8849P]$, $w = 1/[\sigma^2(F_0^2) + (0.1728P)^2]$,

$w = 1/[\sigma^2(F_0^2) + (0.1232P)^2 + 2.3454P]$, $w = 1/[\sigma^2(F_0^2) + (0.1586P)^2]$, $w = 1/[\sigma^2(F_0^2) + (0.1078P)^2 + 9.3692P]$

for La, Ce, Pr, Nd, Sm, Gd, and Tb respectively

## 2.2.3    Elemental Analysis

Elemental analysis using EDX was performed using a Hitachi S-3600N variable pressure

scanning electron microscope (VP-SEM) and a stoichiometry of $Ln$NiSnSb$_2$ was obtained.

Elemental analysis of the Sn:Sb composition of the crystals was performed using Optical

Emission Spectroscopy (ICP-OES) on a Perkin Elmer Optima Model 5300V for all analogues

(Pr, Nd, Sm, Gd, Tb).  The Sn:Sb compositions obtained for each analogue are as follows: Pr –

Sn$_{0.97}$Sb$_{2.03}$, Nd – Sn$_{0.92}$Sb$_{2.08}$, Sm – Sn$_{1.24}$Sb$_{1.76}$, Gd – Sn$_{0.99}$Sb$_{2.01}$, Tb – Sn$_{0.59}$Sb$_{2.41}$.    This

confirms the presence of Sn in the structure and is consistent with the EDX results previously

mentioned.

**Table 2.2**　Atomic Positions and Displacement Parameters for $Ln$Ni(Sn,Sb)$_3$
($Ln$ = La, Ce, Pr, Sm, Gd, or Tb; X = Sn/Sb)

| Atom | Wyckoff site | $x$ | $y$ | $z$ | $U_{eq}$ (Å$^2$)$^a$ |
|------|------|------|------|------|------|
| La1 | 4$c$ | 0.69985(7) | ¼ | 0 | 0.0077(3) |
| La2 | 4$d$ | 0.30410(7) | 0.26099(11) | ¾ | 0.0077(3) |
| Ni1 | 8$e$ | 0.10248(10) | 0.0302(2) | 0.86359(9) | 0.0105(4) |
| X1 | 4$c$ | 0.97547(8) | ¼ | 0 | 0.0128(3) |
| X2 | 4$d$ | 0.78994(8) | 0.25128(12) | ¾ | 0.0080(3) |
| X3 | 8$e$ | 0.50131(5) | 0.50751(9) | 0.87603(4) | 0.0087(3) |
| X4 | 4$c$ | 0.21497(8) | ¼ | 0 | 0.0079(3) |
| X5 | 4$d$ | 0.94673(7) | 0.88313(14) | ¾ | 0.0121(3) |
| Ce1 | 4$c$ | 0.69921(4) | ¼ | 0 | 0.0070(1) |
| Ce2 | 4$d$ | 0.30482(4) | 0.26209(7) | ¾ | 0.0068(1) |
| Ni1 | 8$e$ | 0.10429(6) | 0.0302(1) | 0.86352(6) | 0.0094(2) |
| X1 | 4$c$ | 0.97482(5) | ¼ | 0 | 0.0112(2) |
| X2 | 4$d$ | 0.78593(5) | 0.25134(8) | ¾ | 0.0075(2) |
| X3 | 8$e$ | 0.50154(3) | 0.50804(6) | 0.8759(3) | 0.0081(1) |
| X4 | 4$c$ | 0.21859(5) | ¼ | 0 | 0.0074(2) |
| X5 | 4$d$ | 0.94614(4) | 0.8837(1) | ¾ | 0.0109(2) |
| Pr1 | 4$c$ | 0.69919(7) | ¼ | 0 | 0.0123(3) |
| Pr2 | 4$d$ | 0.30501(7) | 0.26236(17) | ¾ | 0.0120(3) |
| Ni1 | 8$e$ | 0.10491(13) | 0.0301(3) | 0.86371(14) | 0.0146(4) |
| X1 | 4$c$ | 0.97501(10) | ¼ | 0 | 0.0164(3) |
| X2 | 4$d$ | 0.78459(9) | 0.2512(2) | ¾ | 0.0131(3) |
| X3 | 8$e$ | 0.50157(6) | 0.50801(14) | 0.87592(6) | 0.0130(3) |
| X4 | 4$c$ | 0.22006(9) | ¼ | 0 | 0.0126(3) |
| X5 | 4$d$ | 0.94559(9) | 0.8841(2) | ¾ | 0.0167(3) |
| Nd1 | 4$c$ | 0.69855(10) | ¼ | 0 | 0.0057(4) |
| Nd2 | 4$d$ | 0.30558(9) | 0.26297(17) | ¾ | 0.0058(4) |
| Ni1 | 8$e$ | 0.10590(13) | 0.0304(3) | 0.86355(15) | 0.0075(5) |
| X1 | 4$c$ | 0.97456(11) | ¼ | 0 | 0.0082(5) |
| X2 | 4$d$ | 0.78284(12) | 0.25064(19) | ¾ | 0.0058(5) |
| X3 | 8$e$ | 0.50177(6) | 0.50821(15) | 0.87595(7) | 0.0068(5) |
| X4 | 4$c$ | 0.22184(12) | ¼ | 0 | 0.0058(5) |
| X5 | 4$d$ | 0.94564(9) | 0.8848(2) | ¾ | 0.0087(5) |
| Sm1 | 4$c$ | 0.69875(6) | ¼ | 0 | 0.0078(3) |
| Sm2 | 4$d$ | 0.30574(6) | 0.26435(13) | ¾ | 0.0078(3) |
| Ni1 | 8$e$ | 0.10733(10) | 0.0297(2) | 0.86354(11) | 0.0092(4) |
| X1 | 4$c$ | 0.97476(8) | ¼ | 0 | 0.0107(3) |
| X2 | 4$d$ | 0.77989(9) | 0.25034(14) | ¾ | 0.0081(3) |
| X3 | 8$e$ | 0.50213(4) | 0.50858(11) | 0.87599(6) | 0.0090(3) |
| X4 | 4$c$ | 0.22485(9) | ¼ | 0 | 0.0079(3) |
| X5 | 4$d$ | 0.94515(7) | 0.88488(16) | ¾ | 0.0106(3) |
| Gd1 | 4$c$ | 0.69800(8) | ¼ | 0 | 0.0077(4) |
| Gd2 | 4$d$ | 0.30634(8) | 0.26474(17) | ¾ | 0.0077(4) |
| Ni1 | 8$e$ | 0.10870(16) | 0.0295(3) | 0.86342(14) | 0.0103(5) |
| X1 | 4$c$ | 0.97487(11) | ¼ | 0 | 0.0115(4) |
| X2 | 4$d$ | 0.77844(12) | 0.2497(2) | ¾ | 0.0086(4) |

16

**Table 2.2** (cont.)

| Atom | Wyckoff site | $x$ | $y$ | $z$ | $U_{eq}$ (Å$^2$)$^a$ |
|------|------|------|------|------|------|
| X3 | 8$e$ | 0.50226(7) | 0.50904(15) | 0.87588(7) | 0.0099(4) |
| X4 | 4$c$ | 0.22648(12) | ¼ | 0 | 0.0081(4) |
| X5 | 4$d$ | 0.94488(11) | 0.8846(2) | ¾ | 0.0116(4) |
| Tb1 | 4$c$ | 0.69785(7) | ¼ | 0 | 0.0068(3) |
| Tb2 | 4$d$ | 0.30665(7) | 0.26545(13) | ¾ | 0.0064(3) |
| Ni1 | 8$e$ | 0.11013(12) | 0.0288(3) | 0.86377(12) | 0.0085(4) |
| X1 | 4$c$ | 0.97497(9) | ¼ | 0 | 0.0097(3) |
| X2 | 4$d$ | 0.77590(10) | 0.24843(16) | ¾ | 0.0073(3) |
| X3 | 8$e$ | 0.50259(5) | 0.50885(12) | 0.87582(6) | 0.0075(3) |
| X4 | 4$c$ | 0.22913(10) | ¼ | 0 | 0.0070(3) |
| X5 | 4$d$ | 0.94480(8) | 0.88451(18) | ¾ | 0.0106(3) |

$^a U_{eq}$ is defined as one-third of the trace of the orthogonalized $U_{ij}$ tensor.

### 2.2.4     Physical Property Measurements

Magnetic measurements on single crystals of $Ln$Ni(Sn,Sb)$_3$ oriented in the same direction were performed using a Quantum Design MPMS Superconducting Quantum Interference Device (SQUID) magnetometer.  Temperature-dependent susceptibility data were measured with applied fields of 0.1 T, 0.5 T, 1 T or 5 T from 2 K to 300 K.  Magnetization as a function of field was measured up to 5 T at 4 K or 5 K.  The resistivity (between 2 K - 300 K) and magnetoresistance (up to 9 T) was measured on single crystals employing the standard four wires and AC lock-in techniques (with thin Pt wires attached using silver epoxy) in a Quantum Design Physical Property Measurement System (PPMS) at ambient pressure.

## 2.3.     Results and Discussion

### 2.3.1     Structure

$Ln$Ni(Sn,Sb)$_3$ ($Ln$ = Pr, Nd, Sm, Gd, Tb) crystallizes in the CePdSb$_3$ structure type with lattice parameters $a \sim 12$ Å, $b \sim 6$ Å, $c \sim 12$ Å.[21]  The use of Sn flux allowed crystal growth to occur over a greater temperature range thus stabilizing the new compounds.  The structure is an intermediate between the CeCrSb$_3$ and $\alpha$-CeNiSb$_3$ structure types based on the lattice parameters and the arrangement and distortion of the subunits.  The polyhedral representation of the structures of $\alpha$-CeNiSb$_3$ and CeNi(Sn,Sb)$_3$ are shown in Figure 2.1.  The two compounds differ
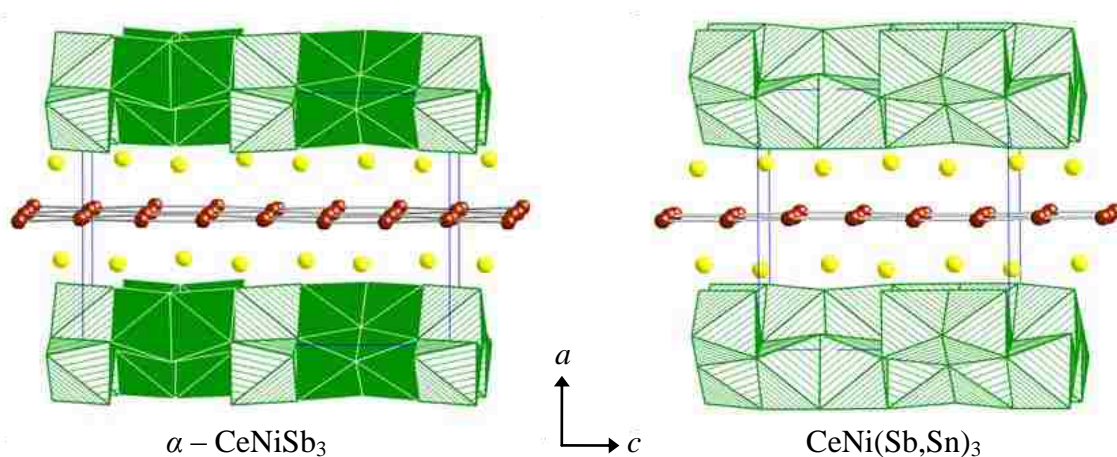
**Figure 2.1** Polyhedral representation of α-CeNiSb$_3$ and CeNi(Sb,Sn)$_3$, where the yellow spheres are the Ce atoms, the maroon spheres are Sb or (Sb,Sn) atoms, the green striped polyhedra are Ni1 octahedra, and the dark green polyhedra are Ni2 octahedra.

in the packing of the transition metal layer. This difference in the packing leads to the difference in the $c$-axis of the unit cell. Because we cannot determine the exact location of Sn within the CeNi(Sn,Sb)$_3$ structure, the nomenclature X, where X = Sn/Sb, will be used to refer to the main group site. This structure consists of layers of nearly square sheets of X atoms, with a layer of square anti-prismatic $Ln$X$_8$ and mono-capped square anti-prismatic $Ln$X$_9$ both above and below the Sn/Sb square sheets. There are $Ln$ atoms in the capping position of $Ln$X$_8$ square anti-prisms, however the inter-atomic distance is too far to be considered bonding as seen in Figure 2.2. Layers of distorted face- and edge- sharing NiX$_6$ octahedra are located next to the $Ln$ layers. The compounds that adopt the LaPdSb$_3$ structure with lattice parameters ~ 12 Å x 6 Å x 12 Å are related to the $\alpha$-$Ln$NiSb$_3$ (~12 Å x 6 Å x 18 Å) structure type and the main variation is in the stacking of the transition metal subunits.[5,15,19]

A decrease in volume, consistent with lanthanide contraction, was also observed in the $\alpha$-$Ln$NiSb$_3$ analogues ($Ln$ – Ce, Pr, Nd, Sm).[17] Figure 2.3 displays the $Ln$-X distances between the $Ln$ atoms and X-sheets for both $\alpha$-$Ln$NiSb$_3$ and $Ln$Ni(Sn,Sb)$_3$ as a function of ionic radii. As the
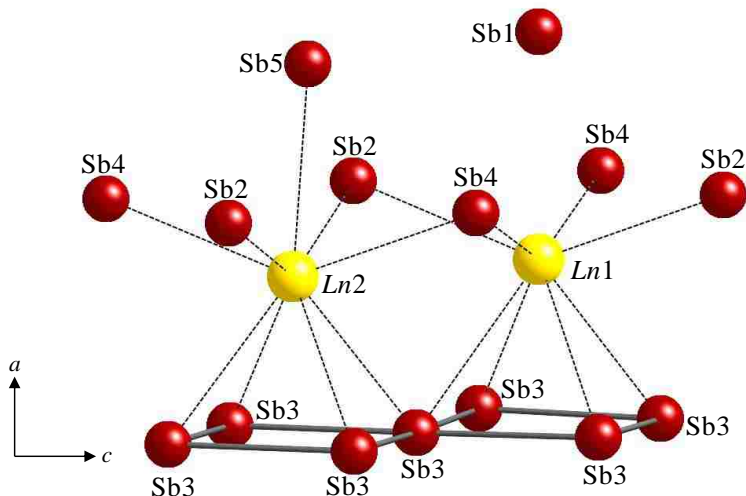
**Figure 2.2** Environment of *Ln* sites of *Ln*Ni(Sn,Sb)$_3$ as viewed down the *b*-axis. *Ln*1 adopts a square anti-prismatic environment, while *Ln*2 adopts a mono-capped square anti-prism.

lanthanide radii decreases, the distance between the *Ln* atoms and Sb or Sn/Sb nets decreases. Selected interatomic distances of *Ln*Ni(Sn,Sb)$_3$ (*Ln* = La-Nd, Sm, Gd, or Tb) are shown in Table 2.3. As expected, the *Ln*-X distances along the *a*-axis decrease as a function of smaller lanthanide. In *Ln*Ni(Sn,Sb)$_3$, the Sn/Sb net layer is formed by four-bonded X3 atoms while in the $\alpha$-phase, the Sb square net is formed by four Sb1 and Sb3 atoms and is highly distorted.[15] As smaller lanthanides are substituted into the structure, the X - X distances within the sheets decrease slightly, and the angles are slightly more distorted. Under our growth conditions, the *Ln*Ni(Sn,Sb)$_3$ phase can be adopted for Ce, Pr, Nd, Sm, Gd, and Tb while only Ce, Pr, Nd, and Sm analogues can be adopted for the $\alpha$-*Ln*NiSb$_3$ structure type. This may be due to the decrease in lanthanide to Sb net distances, leading to a strain on the structure type. It is also important to note that for smaller rare earth elements, Gd – Er, and Y, the tetragonal *Ln*NiSb$_2$ structure type is adopted under our growth conditions. The Gd and Tb analogues of *Ln*Ni(Sn,Sb)$_3$ the experimental yield was extremely small and the crystal size was almost microscopic. This is

further indication that the structure type is strained and leads to the more stable $Ln$NiSb$_2$ structure type.
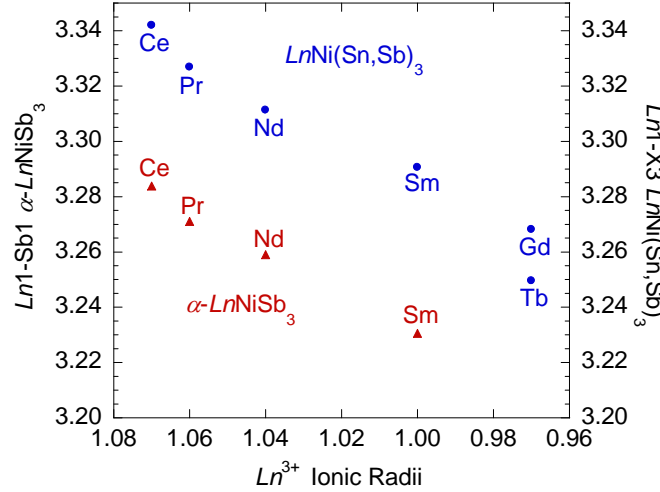


**Figure 2.3** Plot of $Ln$-X (X = Sn,Sb) distances as a function of lanthanide for both $\alpha$-$Ln$NiSb$_3$ and $Ln$Ni(Sn,Sb)$_3$.

**Table 2.3** Selected Interatomic Distances (Å) of $Ln$Ni(Sn,Sb)$_3$ ($Ln$ = La, Ce, Pr, Sm, Gd, or Tb; X = Sn/Sb)

|  | La | Ce | Pr | Nd | Sm | Gd | Tb |
|---|---|---|---|---|---|---|---|
| $Ln$1-X1 | 3.6099(13) | 3.501(8) | 3.5423(17) | 3.5249(18) | 3.4918(12) | 3.4789(17) | 3.4501(14) |
| $Ln$1-X2 (x2) | 3.2533(5) | 3.2241(3) | 3.2074(15) | 3.1923(11) | 3.1693(6) | 3.1593(11) | 3.1380(7) |
| $Ln$1-X3 (x2) | 3.3791(9) | 3.3419(5) | 3.3269(15) | 3.3074(14) | 3.2906(9) | 3.2681(13) | 3.2496(10) |
| $Ln$1-X3 (x2) | 3.3942(9) | 3.3562(3) | 3.3408(15) | 3.3188(14) | 3.2976(9) | 3.2759(13) | 3.2506(10) |
| $Ln$1-X4 (x2) | 3.2672(5) | 3.2395(3) | 3.224(3) | 3.212(2) | 3.1914(11) | 3.1808(15) | 3.1634(11) |
|  |  |  |  |  |  |  |  |
| $Ln$2-X2 | 3.2526(10) | 3.2159(7) | 3.198(4) | 3.179(2) | 3.1485(15) | 3.131(2) | 3.1021(16) |
| $Ln$2-X2 | 3.3633(10) | 3.3388(7) | 3.326(4) | 3.320(2) | 3.3091(15) | 3.304(2) | 3.2974(16) |
| $Ln$2-X3 (x2) | 3.3545(9) | 3.3158(6) | 3.2994(16) | 3.2795(14) | 3.2575(9) | 3.2351(13) | 3.2115(10) |
| $Ln$2-X3 (x2) | 3.3613(10) | 3.3232(6) | 3.3055(15) | 3.2867(14) | 3.2654(9) | 3.2453(13) | 3.2221(10) |
| $Ln$2-X4 (x2) | 3.2503(5) | 3.2228(3) | 3.2063(15) | 3.1908(11) | 3.1695(7) | 3.1582(11) | 3.1374(7) |
| $Ln$2-X5 | 3.3697(12) | 3.3261(7) | 3.3032(17) | 3.2930(17) | 3.2576(12) | 3.2394(17) | 3.2126(13) |
|  |  |  |  |  |  |  |  |
| X3-X3 | 3.0083(11) | 3.0020(7) | 2.994(2) | 2.985(2) | 2.9772(14) | 2.9748(19) | 2.9667(15) |
| X3-X3 | 3.0568(11) | 3.0464(7) | 3.036(2) | 3.028(2) | 3.0221(15) | 3.0142(19) | 3.0034(15) |
| X3-X3 | 3.0702(2) | 3.0607(6) | 3.053(4) | 3.047(2) | 3.0420(10) | 3.0365(15) | 3.0307(10) |
|  |  |  |  |  |  |  |  |
| Ni-X1 | 2.25957(13) | 2.5901(8) | 2.584(2) | 2.582(2) | 2.5790(15) | 2.580(2) | 2.5730(17) |
| Ni-X1 | 2.7066(14) | 2.7456(15) | 2.699(2) | 2.701(2) | 2.6997(15) | 2.701(2) | 2.6968(17) |
| Ni-X2 | 2.6105(14) | 2.6093(9) | 2.606(2) | 2.605(2) | 2.6033(16) | 2.596(2) | 2.5968(18) |
| Ni-X4 | 2.5927(13) | 2.5913(8) | 2.586(2) | 2.583(2) | 2.5857(15) | 2.580(2) | 2.5760(17) |
| Ni-X5 | 2.6217(15) | 2.6193(9) | 2.619(2) | 2.615(2) | 2.6153(15) | 2.618(2) | 2.6163(18) |
| Ni-X5 | 2.6477(14) | 2.6444(10) | 2.641(3) | 2.638(2) | 2.6390(17) | 2.636(2) | 2.638(2) |
|  |  |  |  |  |  |  |  |
| Ni-Ni | 2.755(2) | 2.7459(15) | 2.742(4) | 2.730(4) | 2.724(3) | 2.716(3) | 2.716(3) |

2.3.2    Physical Properties

The magnetic susceptibility ($\chi$ vs $T$) measured at applied fields of 0.1 T, 0.5 T, 1 T or 5T for several single crystals of $PrNi(Sn,Sb)_3$, $NdNi(Sn,Sb)_3$, $SmNi(Sn,Sb)_3$ and $GdNi(Sn,Sb)_3$, respectively are shown in Figure 2.4.  The inset of Figure 2.4 shows the magnetic susceptibility (M vs T) measured at an applied field of 0.1 T of a 1.99mg single crystal of $CeNi(Sn,Sb)_3$ in
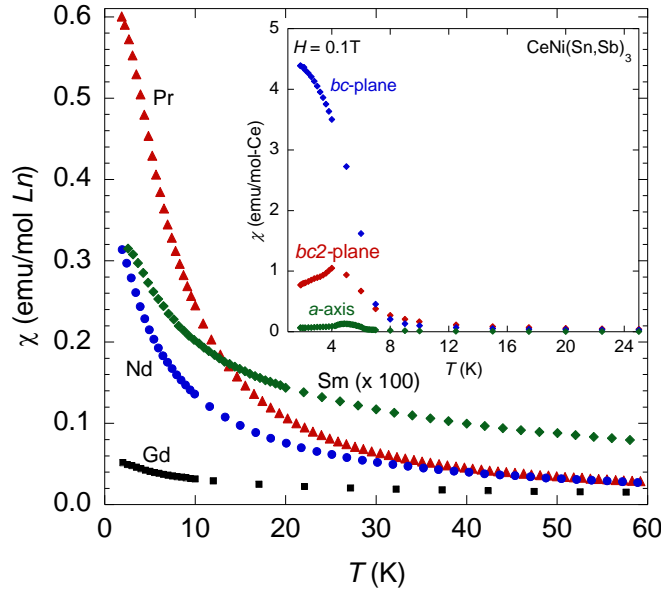


**Figure 2.4**  Magnetic susceptibility as a function of temperature between 2 K - 300 K for $PrNi(Sn,Sb)_3$ ($H$ = 0.1 T), $NdNi(Sn,Sb)_3$ ($H$ = 0.5 T), $SmNi(Sn,Sb)_3$ ($H$ = 1 T), and $GdNi(Sn,Sb)_3$ ($H$ = 1 T) where the red triangles, blue circles, green diamonds, and black squares refer to $PrNi(Sn,Sb)_3$, $NdNi(Sn,Sb)_3$, $SmNi(Sn,Sb)_3$, and $GdNi(Sn,Sb)_3$, respectively.    The inset displays the magnetic measured at an applied field of 0.1 T of a 1.99mg single crystal of $\beta$-$CeNiSb_3$ in three directions.  The inset is the inverse susceptibility of the same plot. The data for $SmNi(Sn,Sb)_3$ has been multiplied by 100 to fit the scale.

three directions.  The magnetic field is applied parallel to the $bc$ − plane of the crystals for all analogues with the exception of Ce which the field was oriented in three different directions and are labeled as such on the figure.  The properties of $TbNi(Sn,Sb)_3$ were not measured due to small yield.    A summary of the resulting magnetic data and fit parameters are shown in Table 2.4.  A ferromagnetic transition is observed for $CeNi(Sn,Sb)_3$ at ~ 6 K in each direction which is

similar to the $\chi(T)$ of the $\alpha$-form.[23]  From the inverse susceptibility along the $a$, $b$ and $c$-axes, the experimental effective moments of 1.80, 2.45 and 2.38 $\mu_B$ and Weiss temperatures ($\theta$) of 22.8, 8.6 and 1.4 K respectively along each axis obeys Curie-Weiss law.  The average $\mu_{eff}$ of 2.23 $\mu_B$ is slightly smaller than the calculated 2.54 $\mu_B$ for the $Ce^{3+}$ ion.  PrNi(Sn,Sb)$_3$ does not appear to order down to 2 K.  However, the possibility remains that this sample may order below 2 K as signs of ordering can be seen in the magnetization near 2 K.  An effective moment of 3.65 $\mu_B$ and a Weiss temperature ($\theta$) of $\sim$ -1 K were obtained from a modified Curie Weiss fit $\chi = \chi_0 +$ C/(T+$\theta$) between 100 K – 300 K.  The $\mu_{eff}$ of 3.68 $\mu_B$ is slightly larger than the calculated moment of 3.57 $\mu_B$ for the $Pr^{3+}$ ion and is consistent with the magnetic contribution coming solely from the Pr.  NdNi(Sn,Sb)$_3$ is paramagnetic down to 2 K.  Fits to the inverse susceptibility between 2 K – 300 K reveal an effective moment of 3.93 $\mu_B$ and a Weiss temperature, $\theta \sim$ -4 K. The experimental moment of 3.93 $\mu_B$ is slightly larger than the calculated moment of 3.62 $\mu_B$ for the $Nd^{3+}$ ion.  SmNi(Sn,Sb)$_3$ appears be paramagnetic down to 2.5 K.  An effective moment of 0.65 $\mu_B$ and a Weiss temperature ($\theta$) of $\sim$ -19 K were obtained with a Curie-Weiss fit from 50 – 300 K. The experimental moment is slightly smaller than the expected moment of 0.84 $\mu_B$ for $Sm^{3+}$.  GdNi(Sn,Sb)$_3$ is also paramagnetic down to 2 K and an effective moment of 7.47 $\mu_B$ and a Weiss temperature ($\theta$) of $\sim$ -403 K were obtained from the modified Curie-Weiss fit.  The expected moment for $Gd^{3+}$ is 7.94 $\mu_B$ which is slightly larger than the experimental moment.  The fact that these analogues (Pr, Nd, Sm, Gd) do not seem to order while CeNi(Sn,Sb)$_3$ orders ferromagnetically at 6 K, and $\alpha$-$Ln$NiSb$_3$ orders antiferromagnetically for $Ln$ = Pr, Nd, Sm with $T_{Neel} \leq$ 5K, is quite surprising.[19]   The evolution of the Curie-Weiss temperatures (except Gd) follows the de Gennes factors across the $Ln$ series as expected[24], and are close to the values found in the $\alpha$-analogues.

22

**Table 2.4** Summary of Magnetic Susceptibility Data

|  | Ce | Pr | Nd | Sm | Gd |
|---|---|---|---|---|---|
| $H$ (T) | 0.1 | 1 | 0.5 | 1 | 1 |
| $\chi_0$ | N/A | -0.0001 | -0.0035 | 0.000937 | -0.00059 |
| C | N/A | 1.69 | 1.93 | 0.053 | 6.94 |
| $\theta$ (K) | 8.6 | -0.97 | -3.92 | -19.33 | -403.51 |
| $\mu_{calc}$ ($\mu_B$) | 2.54 | 3.57 | 3.62 | 0.84 | 7.94 |
| $\mu_{eff}$ ($\mu_B$) | 2.23 | 3.68 | 3.93 | 0.65 | 7.45 |

The magnetization of single crystals of PrNi(Sn,Sb)$_3$, NdNi(Sn,Sb)$_3$, SmNi(Sn,Sb)$_3$ and GdNi(Sn,Sb)$_3$ as a function of field ($M$ vs $H$) at temperatures of 5 K or 4 K are shown in Figure 2.5 and the magnetization of $\beta$-CeNiSb$_3$ is shown in the inset. At ~1.5 T, the magnetization of CeNi(Sn,Sb)$_3$ shows obvious signs of saturation and the calculated saturation moment ($\mu_{sat}$) for
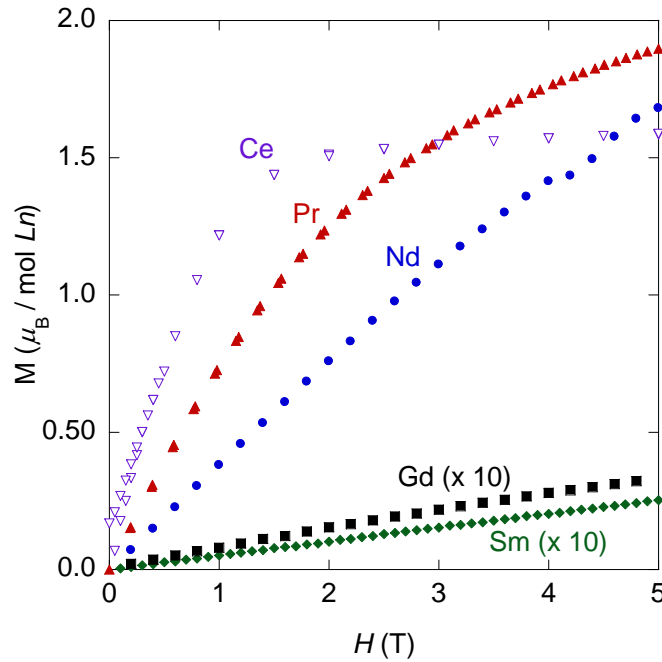


**Figure 2.5** Field dependent magnetization of single crystals of CeNi(Sn,Sb)$_3$ ($T = 2$ K), PrNi(Sn,Sb)$_3$ ($T = 5$ K) and NdNi(Sn,Sb)$_3$ ($T = 4$ K), SmNi(Sn,Sb)$_3$ ($T = 4$ K) and GdNi(Sn,Sb)$_3$ ($T = 4$ K) where the purple open triangles, red triangles, blue circles, green diamonds, and black squares refer to CeNi(Sn,Sb)$_3$, PrNi(Sn,Sb)$_3$, SmNi(Sn,Sb)$_3$, NdNi(Sn,Sb)$_3$ and GdNi(Sn,Sb)$_3$, respectively  The data for the Sm- and Gd-analogues have been multiplied by 10 to fit the scale.

Ce is 2.14 $\mu_B$/Ce. The magnetization of PrNi(Sn,Sb)$_3$ begins to show signs of saturation at around 4 T, well below the theoretical saturation moment of 3.2 $\mu_B$. The difference points to the importance of short range correlations in the proximity of a magnetic instability in this compound, as also evidenced by the anomalous behavior of resistivity (see below). The magnetization for the other analogues is nearly linear up to fields of 5 T. The diamagnetic background contribution is less than 3 % of the total signal for all samples. Moreover, the magnetization values at 5 T are consistent with the corresponding $\alpha$-analogues, suggesting similar magneto-crystalline anisotropy and crystal field splitting in both structure types. The magnetization of the Gd-analogue, however, is anomalously small. This, coupled to the small effective moment, suggests either a strong anisotropy or partial screening of the Gd moments by conduction electrons.

The resistivity as a function of temperature for $Ln$Ni(Sn,Sb)$_3$ ($Ln$ = Pr, Nd, Sm, Gd) is displayed in Figure 2.6. All analogues display simple metallic behavior with a small ratio of room temperature to low temperature resistivity. The Ce analogue displays metallic Kondo behavior, with a resistivity minimum around 20 K and a pronounced drop below the Curie temperature (6 K) while the La analogue displays simple metallic behavior.[19] The resistivity of the Ce analogue differs slightly from the previous report and is more representative of the compound. There is also a superconducting transition seen in all samples ~ 3.5 K which we attribute to Sn flux on the surface of the crystals (not shown). We also note that the resistivity of the Pr analogue has a quasi-linear temperature dependence below 50 K. This, together with a small Curie-Weiss temperature, suggests that PrNi(Sn,Sb)$_3$ is close to a magnetic instability.

The magnetoresistance (MR) as a function of field for $Ln$Ni(Sn,Sb)$_3$ ($Ln$ = Pr, Nd, Sm, Gd) is shown in Figure 2.7. All analogues show a small positive MR at $T$ = 5 K with a nearly quadratic field dependence and no signs of saturation up to 9 T, with a similar magnitude as the
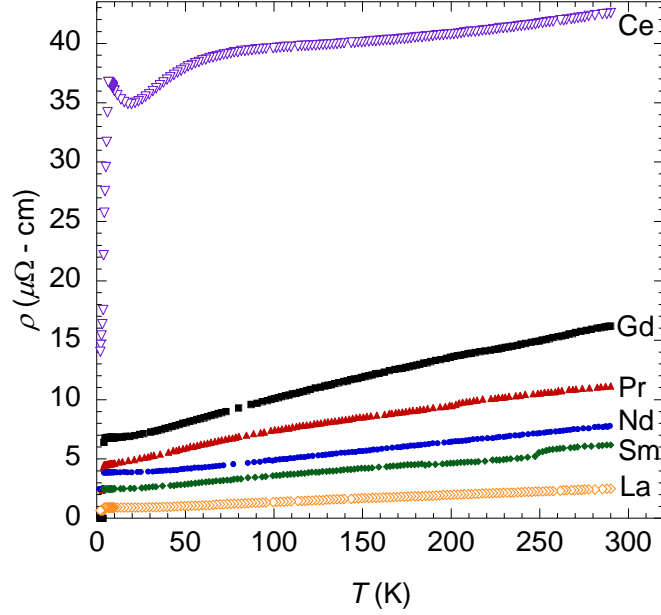
**Figure 2.6** Temperature dependent resistivity of single crystals of $Ln$Ni(Sn,Sb)$_3$ ($Ln$ = La, Ce, Pr, Nd, Sm, Gd) where the orange open diamonds, purple open triangles, red triangles, blue circles, green diamonds, and black squares refer to LaNi(Sn,Sb)$_3$, CeNi(Sn,Sb)$_3$, PrNi(Sn,Sb)$_3$, NdNi(Sn,Sb)$_3$, SmNi(Sn,Sb)$_3$, and GdNi(Sn,Sb)$_3$, respectively.
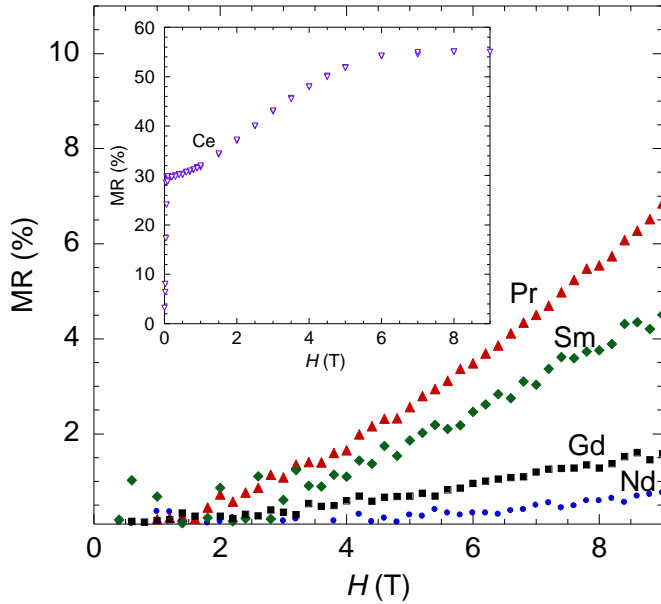


**Figure 2.7** Magnetoresistance of single crystals of PrNi(Sn,Sb)$_3$ (5 K), NdNi(Sn,Sb)$_3$ (5 K), SmNi(Sn,Sb)$_3$ (5 K), and GdNi(Sn,Sb)$_3$ (5 K). The purple open triangles, red triangles, blue circles, green diamonds, and black squares refer to $\beta$-CeNiSb$_3$, PrNi(Sn,Sb)$_3$, NdNi(Sn,Sb)$_3$, SmNi(Sn,Sb)$_3$, and GdNi(Sn,Sb)$_3$, respectively. The data for $\beta$-CeNiSb$_3$ (3 K) is located in the inset of the plot.

La analogue. This indicates that the MR is mostly dominated by the positive contribution, although one cannot exclude that a small negative contribution, due to the quenching of spin fluctuations by magnetic field, still persists at low temperatures. Indeed, the MR at $H$ = 9 T changes sign upon warming and a negative MR is recovered at temperatures above 100 K in all compounds (not shown). Assuming localized $f$-electrons, these compounds should have a similar density of charge carriers. In this case, the difference between the compounds is presumably due to the interplay between the orbital and the spin contributions. In contrast, the positive MR in the magnetic phase of $CeNi(Sn,Sb)_3$ at $T$ = 3 K, above the saturation field, also shown in Figure 2.7, is an order of magnitude larger and saturates around 6 T. The positive non-saturating MR is reminiscent of other planar materials including structurally related $LnSb_2$ ($Ln$ = La, Pr, Sm, Nd) whose structure also contains square Sb sheets, however the analogues investigated here have a significantly smaller magnetoresistance than these other compounds.[25]

## 2.4 References

(1)     Mills, A. M.; Lam, R.; Ferguson, M. J.; Deakin, L.; Mar, A. *Coord. Chem. Rev.* **2002**, *233-234*, 207-222.

(2)     Sologub, O.; Salamakha, P. S. *Handbook on the Physics and Chemistry of Rare Earths*; Elsevier: Netherlands, 2003; Vol. 33.

(3)     Kauzlarich, S. M. *Chemistry, Structure, and Bonding in Zintl Phases and Ions*; VCH Publishers: New York, 1996.

(4)     Papoian, G. A.; Hoffmann, R. *Angew. Chem. Int. Ed.* **2000**, *39*, 2409-2448.

(5)     Hartjes, K.; Jeitschko, W.; Brylak, M. *J. Magn. Magn. Mater.* **1997**, *173*, 109-116.

(6)     Leonard, M.; Saha, S.; Ali, N. *J. Appl. Phys.* **1999**, *85*, 4759-4561.

(7)     Leonard, M. L.; Dubenko, I. S.; Ali, N. *J. Alloys Compd.* **2000**, *303-304*, 265-269.

(8)     Jackson, D. D.; Torelli, M.; Fisk, Z. *Phys. Rev. B* **2001**, *65*, 014421.

(9)     Deakin, L.; Ferguson, M. J.; Mar, A. *Chem. Mater.* **2001**, *13*, 1407-1412.

(10)     Jackson, D. D.; Fisk, Z. *J. Magn. Magn. Mater.* **2003**, *256*, 106-116.

(11)     Jackson, D. D.; Fisk, Z. *J. Alloys Compd.* **2004**, *377*, 243-247.

(12)     Deakin, L.; Mar, A. *Chem. Mater.* **2003**, *15*, 3343-3346.

(13)     Gautreaux, D. P.; Capan, C.; DiTusa, J. F.; Young, D. P.; Chan, J. Y. *J. Solid State Chem.* **2008**, *In Press*.

(14)     Crerar, S. J.; Deakin, L.; Mar, A. *Chem. Mater.* **2005**, *17*, 2780-2784.

(15)     Macaluso, R. T.; Wells, D. M.; Sykora, R. E.; Albrecht-Schmitt, T. E.; Mar, A.; Nakatsuji, S.; Lee, H.; Fisk, Z.; Chan, J. Y. *J. Solid State Chem.* **2004**, *177*, 293-298.

(16)     Siderov, V. A.; Bauer, E. D.; Lee, H.; Nakatsuji, S.; Thompson, J. D.; Fisk, Z. *Phys. Rev. B* **2005**, *71*, 094422-1 - 094422-4.

(17)     Thomas, E. L.; Macaluso, R. T.; Lee, H.; Fisk, Z.; Chan, J. Y. *J. Solid State Chem.* **2004**, *177*, 4228-4236.

(18)     Thomas, E. L.; Moldovan, M.; Young, D. P.; Chan, J. Y. *Chem. Mater.* **2005**, *17*, 5810-5816.

(19)     Thomas, E. L.; Gautreaux, D. P.; Lee, H. O.; Fisk, Z.; Chan, J. Y. *Inorg. Chem.* **2007**, *46*, 3010-3016.

(20)     Thamizhavel, A.; Nakashima, H.; Shiromoto, T.; Obiraki, Y.; Matsuda, T. D.; Haga, Y.; Ramakrishnan, S.; Takeuchi, T.; Settai, R.; Onuki, Y. *J. Phys. Soc. Jpn.* **2005**, *74*, 2617-2621.

(21)     Thomas, E. L.; Gautreaux, D. P.; Chan, J. Y. *Acta Crystallogr. Sect. E: Struct. Rep. Online* **2006**, *E62*, i96-i98.

(22)     Sheldrick, G. M.; University of Gottingen: Germany, 1997.

(23)     Lee, H.-O.; Nakatsuji, S.; Chen, Y.; Bao, W.; Hundley, M. F.; Macaluso, R. T.; Chan, J. Y.; Carter, B.; Klavins, P.; Schlottmann, P.; Fisk, Z.

(24)     Jensen, J.; Mackintosh, A. R. *Rare Earth Magnetism Structure and Excitations*; Clarendon Press: Oxford, 1991.

(25)     Bud'ko, S. L.; Canfield, P. C.; Mielke, C. H.; Lacerda, A. H. *Phys. Rev. B* **1998**, *57*, 13624-13638.

**CHAPTER 3 – CeNi$_x$Co$_{1-x}$Sb$_3$**

**3.1    Introduction**

Doping is a method of introducing an element into a known compound to modify the compound's physical properties and structure.   Co is one of the five naturally occurring ferromagnetic elements and has a Curie temperature of 1388 K.[1]   Fe and Ni are also ferromagnetic below their Curie temperatures of 1043 K and 627 K respectively.[1]  Lanthanide – cobalt compounds have also demonstrated a phenomenon known as itinerant electron metamagnetism (IEM) where a first order transition from a nonmagnetic state to a ferromagnetic state occurs.[3]  This transition is caused by the ordering of the Co sublattice and generally occurs in addition to the local magnetic moment caused by the rare earth element.[4]  FeSi, a narrow-gap semiconductor has been doped with Co to produce a compound with extraordinary magnetoconductance.[5]   Another study showed that when FeSi is doped with Co a Curie temperature of 53 K is obtained along with a very high Hall conductance which are important developments for spintronics materials.[6]  By substituting Co for Ni in $\alpha$-CeNiSb$_3$, the number of carriers might change which can affect the magnetic or transport behavior.  The crystal growth and structure as well as physical properties of CeNi$_x$Co$_{1-x}$Sb$_3$ are reported herein.

**3.2    Experimental**

3.2.1   Synthesis

Single crystals of CeNi$_x$Co$_{1-x}$Sb$_3$, where $x = 0.8$, were prepared using an excess Sb flux growth method.  Ce ingot (99.9%, Alfa Aesar), Ni powder (99.999%, Alfa Aesar), Co powder (99.999%, Alfa Aesar), and Sb shot (99.999%, Alfa Aesar) were placed in an alumina crucible in a 1:0.8:0.2:20 molar ratio.  The crucible was sealed into an evacuated fused-silica tube.  The

---

reaction vessel was heated to 1150 °C where the temperature was held constant for 24 h and then cooled 5 °C h$^{-1}$ to 670 °C. After dwelling at 670 °C, the excess Sb flux was removed by centrifugation. Silvery, metallic plates with dimensions of approximately 0.5 x 0.5 x 0.025mm were obtained. When exposed to air and moisture, there is no visible surface degradation to both compounds over a period of months.

Though the focus will be CeNi$_x$Co$_{1-x}$Sb$_3$ where $x$ = 0.8, the attempted syntheses of CeNi$_x$Co$_{1-x}$Sb$_3$ compounds where $x$ = 0.5 - 0.9 and the results are shown in Table 3.1. When $x$ = 0.7 or 0.5, no crystals of the CeNi$_x$Co$_{1-x}$Sb$_3$ were obtained. When $x$ = 0.9, CeNi$_x$Co$_{1-x}$Sb$_3$ crystals were obtained however the lattice was similar to CeNi$_x$Co$_{1-x}$Sb$_3$ when $x$ = 0.8.

**Table 3.1**      Attempted Crystal Growths of CeNi$_x$Co$_{1-x}$Sb$_3$

| Sample | Ce:Ni:Co:Sb Ratio | Growth Conditions | Result |
|---|---|---|---|
| MP001 | 1:0.8:0.2:20 | 1150 °C for 24 h, slow-cooled 5 °C/h to 670 °C | CeNi$_x$Co$_{1-x}$Sb$_3$ |
| MP002 | 1:0.5:0.5:20 | 1150 °C for 24 h, slow-cooled 5 °C/h to 670 °C | CeSb$_2$ binary |
| MP003 | 1:0.2:0.8:20 | 1150 °C for 24 h, slow-cooled 5 °C/h to 670 °C | no crystals |
| MP004 | 1:1:0:15 | 1150 °C for 24 h, slow-cooled 5 °C/h to 670 °C | $\alpha$-CeNiSb$_3$ |
| MP007 | 1:0.8:0.2:20 | 1150 °C for 24 h, slow-cooled 5 °C/h to 670 °C | CeNi$_x$Co$_{1-x}$Sb$_3$ |
| MP008 | 1:1:1:20 | 1150 °C for 24 h, slow-cooled 5 °C/h to 670 °C | CeSb$_2$ binary |
| MP010 | 1:0.9:0.1:20 | 1150 °C for 24 h, slow-cooled 5 °C/h to 670 °C | CeNi$_x$Co$_{1-x}$Sb$_3$ |
| MP011 | 1:0.7:0.3:20 | 1150 °C for 24 h, slow-cooled 5 °C/h to 670 °C | polycrystalline material |

### 3.2.2   Single Crystal X-Ray Diffraction

A plate-shaped crystal with dimensions of 0.04 x 0.04 x 0.01 mm$^3$ was mounted onto a glass fiber of a goniometer with epoxy and placed on a Nonius Kappa CCD X-ray diffractometer

(Mo K$_\alpha$ = 0.71073 Å).  Data were collected at 25 °C.  Data collection parameters and crystallographic data are listed in Table 3.2.  The unit cell parameters were determined from images taken at a rotation of 15 °φ.  The structure was solved by direct methods using SHELXL97.[7]  The transition metal sites could be refined as either Ni or Co and not affect the overall R value or thermal parameters.  After refinement of the structure was complete, the data were corrected for absorption and the displacement parameters were refined as anisotropic.  Atomic coordinates and anisotropic displacement parameters are provided in Table 3.3.

**Table 3.2**     Crystallographic Data for $\alpha$-CeNiSb$_3$ and CeNi$_x$Co$_{1-x}$Sb$_3$

| Formula | $\alpha$-**CeNiSb$_3$** | **CeNi$_x$Co$_{1-x}$Sb$_3$** |
|---|---|---|
| Formula units (amu) | 564.08 | 564.11 |
| Space Group | *Pbcm* | *Pbcm* |
| $a$ (Å) | 12.65200(10) | 12.6480(2) |
| $b$ (Å) | 6.2120(3) | 6.2060(4) |
| $c$ (Å) | 18.4190(5) | 18.3860(8) |
| $V$ (Å$^3$) | 1447.63(8) | 1443.18(11) |
| Crystal Size (mm$^3$) | 0.025 x 0.045 x 0.050 | 0.010 x 0.040 x 0.040 |
| $Z$ | 12 | 12 |
| Temperature (°C) | 25(2) | 25(2) |
| $\theta$ range (°) | 2.74 – 30.03 | 2.74 – 30.06 |
| $\mu$ (mm$^{-1}$) | 29.452 | 21.868 |
| Collected reflections | 3921 | 3938 |
| Unique reflections | 2165 | 2165 |
| $h$ | $-17 \leq h \leq 17$ | $-17 \leq h \leq 17$ |
| $k$ | $-8 \leq k \leq 8$ | $-8 \leq k \leq 8$ |
| $l$ | $-25 \leq l \leq 25$ | $-25 \leq l \leq 25$ |
| $\Delta\rho_{max}$ (e Å$^{-3}$) | 5.871 | 6.565 |
| $\Delta\rho_{min}$ (e Å$^{-3}$) | -4.994 | -4.142 |
| Extinction coefficient | 0.00053(10) | 0.00018(4) |
| $^a R[F^2 > 2\sigma(F^2)]$ | 0.0604 | 0.0515 |
| $^b wR_2(F^2)$ | 0.1742 | 0.1330 |

$^a R_1(F) = \sum \left\| F_o \right| - \left| F_C \right\| / \sum \left| F_O \right|$

$^b R_w(F_o^2) = \sum \left[ w(F_o^2 - F_c^2) \right] / \sum \left[ w(F_o^2)^2 \right]^{1/2}$ : where $w = 1/[\sigma^2(F_o^2) + (0.1335P)^2 + 3.6415P]$ and $w = 1/[\sigma^2(F_o^2) + (0.0837P)^2 + 6.6619P]$ respectively

**Table 3.3**     Atomic Positions and Displacement Parameters for $CeNi_xCo_{1-x}Sb_3$

| Atom | Wyckoff site | $x$ | $y$ | $z$ | $U_{eq}$ $(Å^2)^a$ |
|------|------|------|------|------|------|
| Ce1 | 4$d$ | 0.30507(7) | 0.55270(16) | ¼ | 0.0089(2) |
| Ce2 | 8$e$ | 0.29910(5) | 0.02420(11) | 0.41677(3) | 0.0084(2) |
| $M1^b$ | 4$c$ | 0.89836(16) | ¼ | ½ | 0.0105(4) |
| $M2^b$ | 8$e$ | 0.90174(12) | 0.8252(3) | 0.17577(9) | 0.0116(4) |
| Sb1 | 8$e$ | 0.50321(5) | 0.78945(13) | 0.33405(4) | 0.0097(2) |
| Sb2 | 4$d$ | 0.21816(8) | 0.04743(19) | ¼ | 0.0096(3) |
| Sb3 | 4$c$ | 0.50359(8) | ¼ | ½ | 0.0102(3) |
| Sb4 | 8$e$ | 0.22288(6) | 0.52308(13) | 0.41567(4) | 0.0091(2) |
| Sb5 | 8$e$ | 0.97368(6) | 0.54075(13) | 0.41329 | 0.0116(2) |
| Sb5 | 4$d$ | 0.07541(8) | 0.68314(18) | ¼ | 0.0110(3) |

$^a U_{eq}$ is defined as one-third of the trace of the orthogonalized $U_{ij}$ tensor.
$^b M1$ and $M2$ represent a mixture of Ni and Co

### 3.2.3   ICP-Optical Emission Spectroscopy

Elemental analysis of $CeNi_xCo_{1-x}Sb_3$ using inductively coupled plasma-optical emission spectroscopy (ICP-OES) was performed at Galbraith Laboratories.  This analysis was performed due to the similar X-ray scattering of Ni and Co.  X-ray diffraction cannot distinguish between elements with similar $Z$.  Optical emission spectroscopy excites each of the atoms present and upon relaxation light is emitted and with a polychromatic detector, the amount of each element present can be determined.  This analysis was performed for Ni and Co and a stoichiometry of $CeNi_{0.780}Co_{0.220}Sb_3$ was obtained.  This is similar to the nominal composition of $CeNi_{0.80}Co_{0.20}Sb_3$.

### 3.2.4   Physical Property Measurements

Magnetic susceptibility data (between 2 K – 300 K) at an applied field of 0.1 T and magnetization (up to 9 T) at 3 K were measured using a Quantum Design Physical Property Measurement System (PPMS).  The resistivity (between 2 K - 300 K) was measured on a single crystal using the standard four wires and AC lock-in techniques (with thin Pt wires attached

using silver epoxy) in a Quantum Design Physical Property Measurement System (PPMS) at ambient pressure.

## 3.3 Results and Discussion

### 3.3.1 Structure

$CeNi_{0.80}Co_{0.20}Sb_3$ crystallizes in the $CeNiSb_3$ structure type.[8] The structure of $CeNi_{0.80}Co_{0.20}Sb_3$ is shown in Figure 3.1. The structure consists of layers of mono-capped square anti-prismatic $CeSb_9$ above and below a layer of Sb square nets. Layers of distorted face- and edge- sharing $MSb_6$ octahedra are located between the $CeSb_9$ layers. The transition metal site will be referred to as $M1$ and $M2$ which will be a mixture of Ni and Co on each site. Figure 3.2
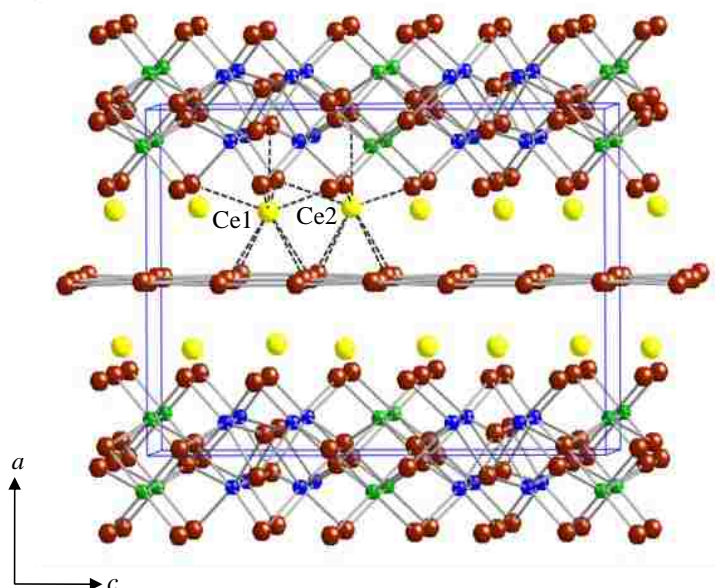


**Figure 3.1** The structure of $CeNi_xCo_{1-x}Sb_3$ viewed down the $b$-axis. The yellow spheres represent Ce atoms, blue and green spheres represent Ni/Co atoms, and maroon spheres represent Sb atoms.

shows the X-ray powder patterns of $CeNi_xCo_{1-x}Sb_3$ and $\alpha$-$CeNiSb_3$. Each reflection is indexed according to the structural data from single crystal X-ray diffraction. The atomic radius of Co is slightly larger than that of Ni so a peak shift to the left is expected and observed. The second

pattern in Figure 3.2 displays the 400 reflection and the slight shift once Co is introduced into the $\alpha$-CeNiSb$_3$ structure type.
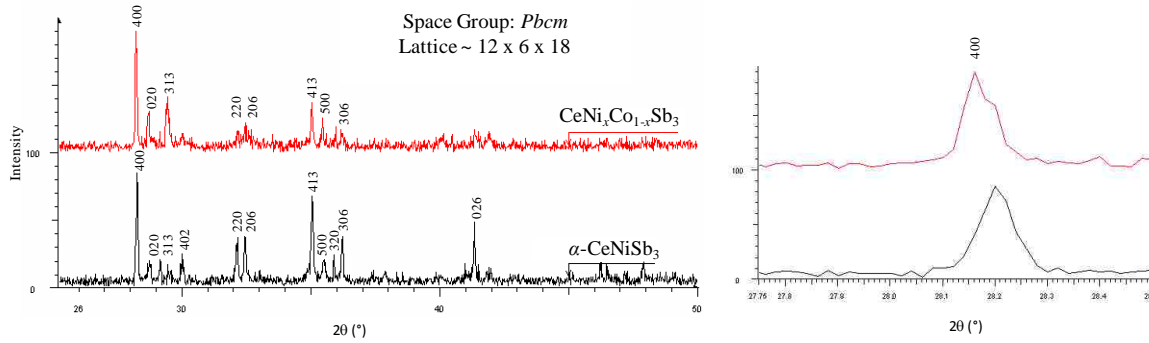


**Figure 3.2**     X-ray diffraction powder patterns of CeNi$_x$Co$_{1-x}$Sb$_3$ and $\alpha$-CeNiSb$_3$.  The pattern on the left is the full spectrum for each compound and the pattern to the right displays the shift seen in the 400 peak.

### 3.3.2    Physical Properties

The magnetic susceptibility ($\chi$ vs T) measured at an applied field of 0.2 T for 10 mg of single crystals of CeNi$_{0.78}$Co$_{0.22}$Sb$_3$ is shown in Figure 3.3.  The magnetic field is oriented along the *c*-axis of the crystals.  A ferromagnetic transition is observed at ~ 4.6 K  which is lower than the 6 K ordering temperature of the $\alpha$-CeNiSb$_3$.[9]  Although the Ni atoms in pure CeNiSb$_3$ do not contribute directly to the magnetism, the insertion of Co into this sublattice may disrupt the overall magnetic moment.  From the inverse susceptibility versus temperature plot from 50 K – 150 K, the experimental effective moment of 2.43 $\mu_B$/Ce and a Weiss temperature ($\theta$) of 41 K were obtained.  The $\mu_{eff}$ of 2.43 $\mu_B$ is close to the calculated 2.54 $\mu_B$ for the Ce$^{3+}$ ion.[1]  This is consistent with the magnetic contribution due solely to the Ce$^{3+}$.  The average effective moment of $\alpha$-CeNiSb$_3$ is 2.58 $\mu_B$/Ce and the values for the Weiss constant, $\theta$, are -156 along the *ab* plane and 29 K along the *c*-axis.[9]

The magnetization as a function of vield (M vs H) measured at 3 K on the same sample
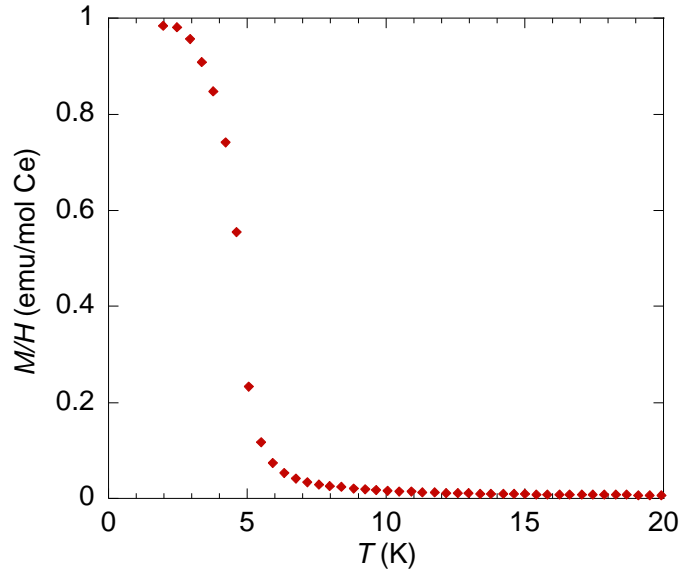
**Figure 3.3** The magnetic susceptibility (M vs T) measured at an applied field of 0.2 T of $CeNi_{0.780}Co_{0.220}Sb_3$.

of $CeNi_{0.78}Co_{0.22}Sb_3$ is shown in Figure 3.4. At $H \sim 1$ T, the magnetization begins to show signs of slow saturation well below the theoretical saturation moment of 2.14 $\mu_B$ for $Ce^{3+}$. A similar result is observed in the pure material, which has a large magnetocrystalline anisotropy and shows evidence for a modest Kondo interaction, with the ground state being a crystal-field-split doublet of Ce.[9]
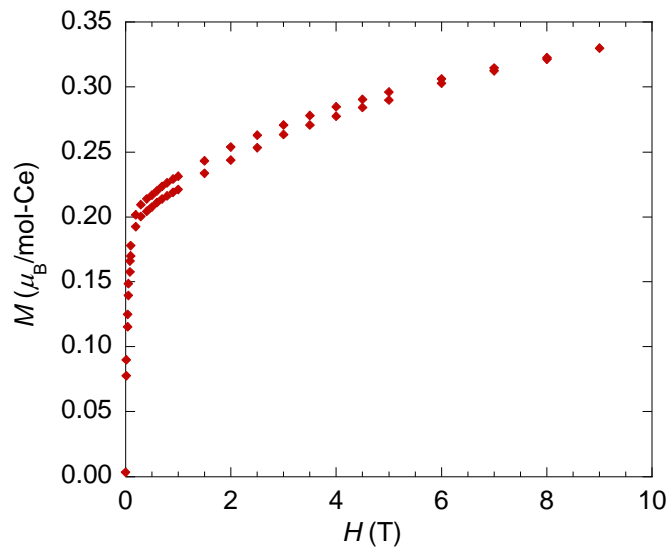


**Figure 3.4** The magnetization as a function of field (M vs H) measured at 3 K of $CeNi_{0.780}Ce_{0.220}Sb_3$.

The resistivity as a function of temperature for a single crystal of $CeNi_{0.78}Co_{0.22}Sb_3$ is shown in Figure 3.5. The current has been applied along the $b$-axis (in-plane). The overall shape of the curve is similar to that of $\alpha$-CeNiSb$_3$[8] and is weakly temperature dependent and characteristic of Kondo systems. However, the minimum observed near 27 K is much deeper here than it is for pure CeNiSb$_3$, which could be due to more Kondo-like behavior of the doped
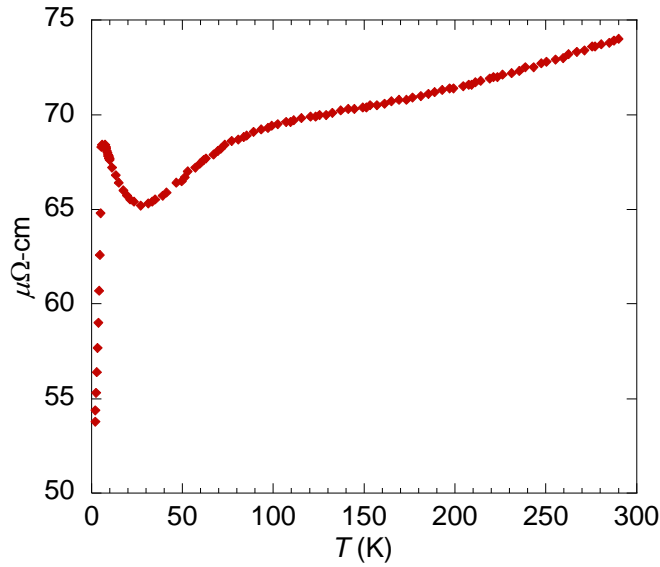


**Figure 3.5** The resistivity of $CeNi_{0.780}Co_{0.220}Sb_3$ measured between 2 and 290 K.

sample. This effect is analogous to the physical pressure effects observed in another Kondo lattice system, CeAl$_2$.[10] Below ~ 5 K ($T_c$) the resistivity decreases very quickly, in response to the reduction in the spin disorder scattering.

The magnetoresistance at 3 K of $CeNi_{0.78}Co_{0.22}Sb_3$ is shown in Figure 3.6. Unlike usual ferromagnets, the magnetoresistance is positive, increasing to over 10% by 9 T. The shape of the magnetoresistance essentially tracks the magnetization of the sample for the field applied along the same direction which may be due to the magnetic anisotropy of the crystal.

The slightly lower ferromagnetic ordering temperature, smaller saturation moment, and deeper minimum in the resistivity data summarize the effects of Co substitution on pure CeNiSb$_3$ for this concentration.
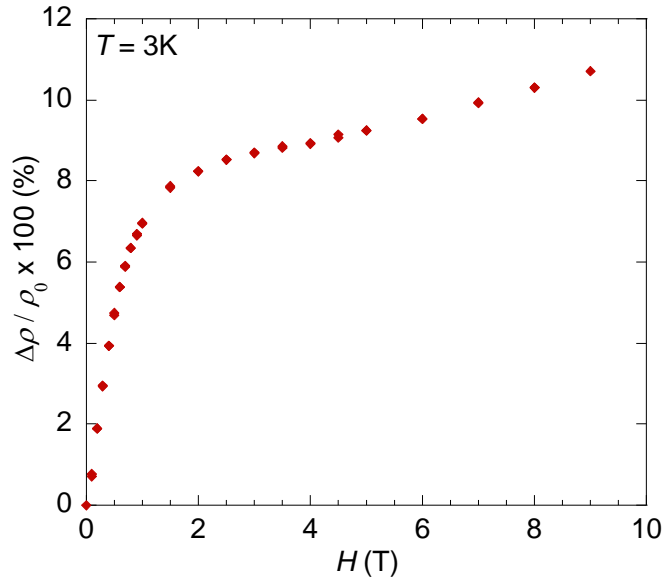


**Figure 3.6.** The magnetoresistance of CeNi$_{0.780}$Ce$_{0.220}$Sb$_3$ at 3 K taken from 0 to 9 T.

## 3.4 References

(1)    Kittel, C.; 7th ed.; John Wiley & Sons, Inc.: New York, 1995.

(2)    Gautreaux, D. P.; Parent, M.; Moldovan, M.; Young, D. P.; Chan, J. Y. *Physica B* **2008**, *403*, 1005-1006.

(3)    Duc, N. H.; Goto, T. *Handbook on the Physics and Chemistry of Rare Earths*; Elsevier Science: Netherlands, 1999; Vol. vol. 26.

(4)    Duc, N. H.; Hien, T. D.; Brommer, P. E.; Franse, J. J. M. *J. Magn. Magn. Mater.* **1992**, *104-107*, 1252.

(5)    Manyala, N.; Sidis, Y.; DiTusa, J. F.; Aeppli, G.; Young, D. P.; Fisk, Z. *Nature* **2000**, *404*, 581-584.

(6)    Manyala, N.; Sidis, Y.; DiTusa, J. F.; Aeppli, G.; Young, D. P.; Fisk, Z. *Nature Mater.* **2004**, *3*, 255-262.

(7)     Sheldrick, G. M.; University of Gottingen: Germany, 1997.

(8)     Macaluso, R. T.; Wells, D. M.; Sykora, R. E.; Albrecht-Schmitt, T. E.; Mar, A.; Nakatsuji, S.; Lee, H.; Fisk, Z.; Chan, J. Y. *J. Solid State Chem.* **2004**, *177*, 293-298.

(9)     Siderov, V. A.; Bauer, E. D.; Lee, H.; Nakatsuji, S.; Thompson, J. D.; Fisk, Z. *Phys. Rev. B* **2005**, *71*, 094422-1 - 094422-4.

(10)    Nicolas-Francillon, M.; Percheron, A.; Achard, J. C. *Solid State Comm.* **1972**, *11*, 845-849.

# CHAPTER 4 – $Ln(Cu_{1-x}Ni_x)_ySb_2$

## 4.1 Introduction

Antimonide compounds have been a focus of many research groups because of the interesting structural features and physical properties they possess.[1-4] All analogues of $LnSb_2$ ($Ln$ = La – Nd, Sm) show positive, linear magnetoresistance at 2 K.[5] Also of notable interest is LaSb$_2$, which has a positive, linear magnetoresistance below 10 K greater that 8,500 % with no signs of saturation up to 45 T.[6] Adopting a similar layered structure, $LnNi_{1-x}Sb_2$ ($Ln$ = Y, Dy, and Ho) analogues have large positive magnetoresistance above 100 % at 3 K.[7] Single crystalline CeNiSb$_2$ is reported to order ferromagnetically at 6 K and has a Sommerfeld coefficient ($\gamma$) of 55 mJ mol$^{-1}$ K$^{-2}$.[8] It is important to note that the full structural determination has not been reported for CeNiSb$_2$ and the physical properties are similar to the fully characterized orthorhombic CeNiSb$_3$ which orders ferromagnetically at 6 K and has a Sommerfeld coefficient ($\gamma$) of ~50 mJ mol$^{-1}$ K$^{-2}$.[4,9] Ce$M$Sb$_2$ ($M$ = Ni, Cu, Pd, and Ag) show dense Kondo behavior and polycrystalline CeNiSb$_2$ shows an enhanced electron mass.[10] The magnetoresistance of polycrystalline CeCuSb$_2$ has been reported to be ~12.5 % at 4.5 T and 4.5 K.[11] CeCuSb$_2$, both in the polycrystalline and single-crystalline form, orders antiferromagnetically between 7 – 8 K.[8,10,12-15] CeCuSb$_2$ is also a heavy fermion with reported Sommerfeld coefficients ($\gamma$) of 94, 100, and 200 mJ mol$^{-1}$ K$^{-2}$.[8,10,14,15]

In an effort to further determine structural stability of ternary Ce – Ni – Sb and Ce – Cu – Sb compounds, single crystals of various compositions of Ce(Cu$_{1-x}$Ni$_x$)$_y$Sb$_2$ were obtained. The crystal structure, elemental analysis, magnetic and transport properties of Ce(Cu$_{1-x}$Ni$_x$)$_y$Sb$_2$ ($x$ = 0, 0.25, 0.37, and 0.46) are reported herein.

## 4.2    Experimental

### 4.2.1    Synthesis

High quality single crystals of $Ln(Cu_{1-x}Ni_x)_ySb_3$ were synthesized via flux growth by placing fragments of La or Ce rod (99.9% Alfa Aesar), Ni powder (99.999% Alfa Aesar), Cu powder (99.999% Alfa Aesar) and Sb shot (99.999% Alfa Aesar) in an alumina crucible.  The nominal composition used was 1 : $x$ : 1-$x$ : 20 ($x$ = 0, 0.6, 0.7, 0.8) for Ce : Ni : Cu : Sb, where excess Sb was included as the flux.  For the La analogue, the nominal composition of 1 : 0.8 : 0.2 : 20 for La : Ni : Cu : Sb was used.  Silica wool was placed on top of the crucible and was sealed under vacuum in a fused silica tube and placed in a furnace.  The reaction vessel was heated to 1150 °C and held constant for 48 hours, then cooled to 670 °C at a rate of 5 °C h$^{-1}$.  Excess flux was removed by centrifugation.  Single crystals were extracted with sizes up to 0.5 x 1 x 2 mm$^3$ although the crystals tend to grow into larger, layered aggregates.  The tetragonal plates are silver with a metallic luster.  However, at lower concentrations of Cu, crystals gain a dull, blue-gray iridescence and begin to resemble crystals of CeNiSb$_3$.[4]  The crystals are stable in air over a period of months.  It is important to note that under our growth conditions, where the nominal value of $x$ > 0.8, single crystals of CeNiSb$_3$ were grown.  This will be discussed more in depth in the structural analysis section.

### 4.2.2    Single Crystal X-Ray Diffraction

A typical crystal with dimensions of ~ 0.05 x 0.10 x 0.175 mm$^3$ was mounted onto a glass fiber of a goniometer with epoxy and placed on a Nonius Kappa CCD X-ray diffractometer (MoK$_\alpha$ = 0.71073 Å).  After choosing the tetragonal space group $P4/nmm$ (No. 129),  the initial structural model was generated by SIR97[16] and the model was then refined by direct methods using SHELXL97.[17]   Due to the similarity of $Z$ for Ni and Cu, $X$-rays cannot accurately distinguish between the two.  Therefore, the mixed transition metal site was refined as pure Cu

39

for continuity and is designated as *M*. After refinement, the data were corrected for absorption and the displacement parameters were refined as anisotropic. An extinction coefficient was added and refined through multiple least squares cycles. A disagreeable thermal parameter for the transition metal site was observed and the site was allowed to be partially occupied. This is consistent with the partial transition metal occupancy observed in most other analogues of the $HfCuSi_2$ structure type. For simplicity, the exact partial occupancy will not be defined in the text for each compound as each value differs. It will be designated as *y* and the exact values will be listed in the crystallographic tables. Data collection parameters and crystallographic data are listed in Table 4.1. Atomic coordinates, anisotropic displacement parameters, and site occupancies are provided in Table 4.2.

### 4.2.3 Energy Dispersive Spectroscopy

Elemental analysis was performed on multiple single crystalline samples using the Hitachi S-3600N extra-large chamber variable pressure Scanning Electron Microscope (VP-SEM) with an integrated energy dispersive (EDS) feature. Data were collected over a small flux-free area on the surface of the crystals using an accelerating voltage of 20 kV and 50 s acquisition times. This analysis was performed due to the similar X-ray scattering of Ni and Cu. X-ray diffraction cannot distinguish between elements with similar *Z* and it is important to know the exact amounts of Ni and Cu in the sample. The transition metal site occupancy is consistent with the occupancy determined from single crystal X-ray diffraction data and formula compositions are located in Table 4.3. Is is important to note that the nominal and exact Ni/Cu concentrations do not agree, however there is a systematic increase of Ni in both the nominal and exact compositions. From this point on, the actual EDS compositions will be used.

**Table 4.1**  Crystallographic Data for $Ln(Cu_{1-x}Ni_x)_ySb_2$ ($Ln$ = La or Ce)

| Nominal $x$ | 0 | 0.6 | 0.7 | 0.8 | 0.8 |
|---|---|---|---|---|---|
| SC Formula | $CeCu_{0.841}Sb_2$ | $CeM_{0.707}Sb_2$ | $CeM_{0.738}Sb_2$ | $CeM_{0.665}Sb_2$ | $LaM_{0.779}Sb_2$ |
| Space Group | $P4/nmm$ | $P4/nmm$ | $P4/nmm$ | $P4/nmm$ | $P4/nmm$ |
| $a$ (Å) | 4.3650(2) | 4.3790(2) | 4.3780(3) | 4.3800(2) | 4.4000(2) |
| $c$ (Å) | 10.0010(6) | 9.8480(7) | 9.8160(8) | 9.7900(6) | 10.0490(9) |
| $V$ (Å$^3$) | 190.551(17) | 188.842(18) | 188.14(2) | 187.815(17) | 194.55(2) |
| Crystal size (mm$^3$) | 0.05/0.13/0.17 | 0.05/0.13/0.13 | 0.05/0.10/0.13 | 0.08/0.13/0.15 | 0.05/0.08/0.10 |
| $Z$ | 2 | 2 | 2 | 2 | 2 |
| Temperature (°C) | 25(2) | 25(2) | 25(2) | 25(2) | 25(2) |
| Density (g cm$^{-1}$) | 7.793 | 8.897 | 8.930 | 8.945 | 8.615 |
| $\theta$ Range (°) | 2.04-30.02 | 2.07-29.93 | 2.07-29.94 | 2.08-30.02 | 2.03-29.98 |
| $\mu$ (mm-1) | 30.989 | 36.104 | 36.239 | 36.302 | 34.326 |
| $R_{int}$ | 0.0386 | 0.0420 | 0.0613 | 0.0379 | 0.0360 |
| Collected Reflections | 541 | 466 | 356 | 489 | 460 |
| Unique Reflections | 204 | 203 | 181 | 194 | 207 |
| $h$ | $-6 \le h \le 6$ | $-6 \le h \le 6$ | $-6 \le h \le 6$ | $-6 \le h \le 6$ | $-6 \le h \le 6$ |
| $k$ | $-4 \le k \le 4$ | $-4 \le k \le 4$ | $-4 \le k \le 3$ | $-4 \le k \le 4$ | $-4 \le k \le 4$ |
| $l$ | $-14 \le l \le 14$ | $-10 \le l \le 13$ | $-13 \le l \le 9$ | $-13 \le l \le 2$ | $-14 \le l \le 10$ |
| $\Delta\rho_{max}$ (e Å$^{-3}$) | 3.005 | 3.4666 | 2.957 | 5.730 | 2.117 |
| $\Delta\rho_{min}$ (e Å$^{-3}$) | -1.709 | -5.727 | -5.933 | -4.593 | -1.959 |
| Extinction coefficient | 0.050(6) | 0.051(7) | 0.22(2) | 0.090(16) | 0.029(3) |
| [a] $R[F^2 > 2\sigma(F^2)]$ | 0.0379 | 0.0499 | 0.0466 | 0.0618 | 0.0286 |
| [b] $wR_2(F^2)$ | 0.1007 | 0.1207 | 0.1207 | 0.1661 | 0.0732 |

[a] $R_1(F) = \sum \left\| F_0 \right| - \left| F_c \right\| / \sum \left| F_0 \right|$

[b] $R_w(F_0^2) = \sum [w(F_0^2 - F_c^2)] / \sum [w(F_0^2)^2]^{1/2}$; $w = 1/[\sigma^2(F_0^2) + (0.0547P)^2 + 3.3374P]$,
$w = 1/[\sigma^2(F_0^2) + (0.1045P)^2 + 7.0979P]$, $w = 1/[\sigma^2(F_0^2) + (0.0613P)^2 + 1.7761P]$,
$w = 1/[\sigma^2(F_0^2) + (0.0840P)^2 + 3.5287P]$, $w = 1/[\sigma^2(F_0^2) + (0.0358P)^2 + 3.9432P]$ for $x$ = 0, 0.8, 0.7, 0.6, and 0.8(La) respectively

**Table 4.2**  Atomic Positions and Displacement Parameters for $Ln(Cu_{1-x}Ni_x)_ySb_2$ ($Ln$ = La or Ce, $M$ = mixture of Ni and Cu)

| | Atom | Wyckoff site | $x$ | $y$ | $z$ | $U_{eq}$ (Å$^2$)$^a$ | Occupancy |
|---|---|---|---|---|---|---|---|
| $CeCu_{0.841}Sb_2$ | | | | | | | |
| $x = 0$ | Ce1 | $2c$ | ¼ | ¼ | 0.75381(8) | 0.0066(4) | 1 |
| | Cu1 | $2a$ | ¾ | ¼ | 0 | 0.0103(8) | 0.841(10) |
| | Sb1 | $2c$ | ¼ | ¼ | 0.14829(12) | 0.0100(5) | 1 |
| | Sb2 | $2b$ | ¾ | ¼ | ½ | 0.0079(4) | 1 |

**Table 4.2** (cont.)

| | Atom | Wyckoff site | $x$ | $y$ | $z$ | $U_{eq}$ (Å$^2$)$^a$ | Occupancy |
|---|---|---|---|---|---|---|---|
| Ce$M_{0.665}$Sb$_2$ | | | | | | | |
| $x = 0.8$ | Ce1 | 2$c$ | ¼ | ¼ | 0.75909(15) | 0.0073(8) | 1 |
| | $M$1 | 2$a$ | ¾ | ¼ | 0 | 0.0063(14) | 0.665(17) |
| | Sb1 | 2$c$ | ¼ | ¼ | 0.1367(8) | 0.0136(8) | 1 |
| | Sb2 | 2$b$ | ¾ | ¼ | ½ | 0.0091(8) | 1 |
| Ce$M_{0.738}$Sb$_2$ | | | | | | | |
| $x = 0.7$ | Ce1 | 2$c$ | ¼ | ¼ | 0.24163(9) | 0.0062(6) | 1 |
| | $M$1 | 2$a$ | ¾ | ¼ | 0 | 0.0103(10) | 0.738(10) |
| | Sb1 | 2$c$ | ¼ | ¼ | 0.86089(13) | 0.0123(7) | 1 |
| | Sb2 | 2$b$ | ¾ | ¼ | ½ | 0.0075(7) | 1 |
| Ce$M_{0.707}$Sb$_2$ | | | | | | | |
| $x = 0.6$ | Ce1 | 2$c$ | ¼ | ¼ | 0.75771(11) | 0.0081(6) | 1 |
| | $M$1 | 2$a$ | ¾ | ¼ | 0 | 0.0083(10) | 0.707(11) |
| | Sb1 | 2$c$ | ¼ | ¼ | 0.14063(16) | 0.0139(6) | 1 |
| | Sb2 | 2$b$ | ¾ | ¼ | ½ | 0.0092(6) | 1 |
| La$M_{0.779}$Sb$_2$ | | | | | | | |
| $x = 0.8$ | La1 | 2$c$ | ¼ | ¼ | 0.75641(11) | 0.0067(4) | 1 |
| | $M$1 | 2$a$ | ¾ | ¼ | 0 | 0.0091(9) | 0.779(10) |
| | Sb1 | 2$c$ | ¼ | ¼ | 0.13948(14) | 0.0129(4) | 1 |
| | Sb2 | 2$b$ | ¾ | ¼ | ½ | 0.0082(4) | 1 |

$^a U_{eq}$ is defined as one-third of the trace of the orthogonalized $U_{ij}$ tensor.

**Table 4.3**    EDS Formula Compositions for Ce(Cu$_{1-x}$Ni$_x$)$_y$Sb$_2$

| Nominal Composition | Single Crystal Formula | EDS Formula |
|---|---|---|
| $x = 0.8$ | Ce($M$)$_{0.665}$Sb$_2$ | Ce(Ni$_{0.46}$Cu$_{0.54}$)$_{0.67}$Sb$_{2.16}$ |
| $x = 0.7$ | Ce($M$)$_{0.738}$Sb$_2$ | Ce(Ni$_{0.37}$Cu$_{0.63}$)$_{0.74}$Sb$_{1.86}$ |
| $x = 0.6$ | Ce($M$)$_{0.707}$Sb$_2$ | Ce(Ni$_{0.25}$Cu$_{0.75}$)$_{0.69}$Sb$_{2.16}$ |

### 4.2.4   Physical Property Measurements

Magnetic measurements on single crystals of Ce(Cu$_{1-x}$Ni$_x$)$_y$Sb$_2$ oriented in the same direction were performed using a Quantum Design Physical Property Measurement System (PPMS). Temperature-dependent susceptibility data were measured with an applied field of 0.1 T from 2 K to 300 K. Magnetization as a function of field was measured at 3 K up to 9 T. The

resistivity from 2 K – 300K and magnetoresistance at 3 K (up to 9 T) were measured using the standard four probe-AC method in the Quantum Design PPMS at ambient pressure.

## 4.3     Results and Discussion

### 4.3.1    Structural Changes

$Ln(Cu_{1-x}Ni_x)_ySb_2$ ($Ln$ = La, Ce) crystallizes in the tetragonal space group $P4/nmm$ with the HfCuSb$_2$ structure type.[18]   As indicated in Tables 4.1 and 4.3, the nominal and exact compositions of Ni and Cu do not agree.  However, there is a systematic increase of Ni in both the nominal and exact compositions.  For consistency throughout this document, the compounds will be referred to by their actual compositions.  We believe that there is a limit to the amount of Ni that can occupy the transition metal site when there is a large rare earth cation such as Ce present in the structure under our growth conditions.  When too much Ni is added to the reaction mixture, the tetragonal structure can no longer be supported and the stable phase that forms is the CeNiSb$_3$ structure type.[4]  This theory is supported by earlier work where pure $Ln$NiSb$_2$ can only be formed in the presence of smaller rare earth cations (Gd – Er, Y).[7]  In the presence of larger rare earth ions such as Ce – Sm, the orthorhombic $Ln$NiSb$_3$ structure is formed using the Sb flux growth method.[4,19]  We note that other experimental techniques such as arc-melting have yielded $Ln$NiSb$_2$ ($Ln$ = Pr, Nd, Sm).[12]

As previously stated, $Ln(Cu_{1-x}Ni_x)_ySb_2$ ($Ln$ = La, Ce) crystallizes in the tetragonal space group $P4/nmm$.  The structure consists of alternating layers of Sb2 square nets capped by $Ln$1 square antiprismatic layers and $M$1-Sb1 tetrahedral layers as shown in Figure 4.1.  The $Ln$ atoms are coordinated to four Sb1 atoms from the $M$ tetrahedral layer and four Sb2 atoms from the net layer, forming a slightly distorted square antiprism.  The $M$ atoms are surrounded by four Sb1 atoms adopting a somewhat distorted tetrahedral geometry.  This layered antimonide structure is

similar to the orthorhombic $Ln$Sb$_2$ structure type which also includes alternating layers of Sb nets and $Ln$Sb$_8$ square antiprismatic layers.[20]
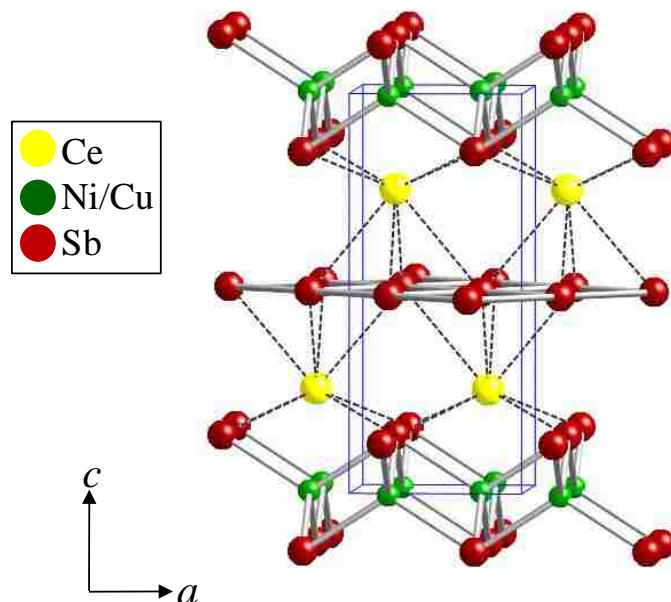


**Figure 4.1**    Crystal structure of Ce(Cu$_{1-x}$Ni$_x$)$_y$Sb$_2$ as viewed down the $b$-axis where the yellow spheres refer to the Ce atoms, the green spheres refer to a mixture of Ni and Cu atoms and the maroon spheres refer to the Sb atoms.

Table 4.4 contains selected interatomic distances and Sb2 $-$ $M$1 $-$ Sb2 tetrahedral angles. As more Ni is introduced into the structure, the overall volume decreases which is expected because Ni has a slightly smaller radius (1.15 Å) than Cu (1.17 Å). Also, the $M$1 tetrahedra show more distortion as the amount of Ni added to the structure is increased as indicated by the Sb2 $-$ $M$1 $-$ Sb2 angles listed in Table 4.4.    As expected, the $M$1 $-$ Sb2 distances decrease as a function of additional Ni introduced into the structure.  The $M$1 $-$ Sb2 distances range from 2.6387(7) Å for pure CeCu$_{0.84}$Sb$_2$ to 2.5668(12) Å for Ce(Cu$_{0.54}$Ni$_{0.46}$)$_{0.67}$Sb$_2$. The addition of Ni has very little effect on the Sb2 square nets as the Sb2 $-$ Sb2 distances show hardly any change (3.08652(14) Å $-$ 3.09713(14) Å), and there is no visible distortion as the Ni content increases.

**Table 4.4**     Selected Interatomic Distances (Å) and Angles (°) for $Ce(Cu_{1-x}Ni_x)_ySb_2$

|  | $x = 0.46$ | $x = 0.37$ | $x = 0.25$ | $x = 0$ |
|---|---|---|---|---|
| Ce1-Sb1(x4) | 3.2607(9) | 3.2552(5) | 3.2543(6) | 3.2381(4) |
| Ce1-Sb2(x4) | 3.3511(12) | 3.3502(7) | 3.3519(8) | 3.2902(6) |
| $M$1-Sb1(x4) | 2.5668(12) | 2.5800(7) | 2.5907(9) | 2.6387(7) |
| Sb2 – Sb2(x4) | 3.09713(14) | 3.0957(2) | 3.09642(14) | 3.08652(14) |
|  |  |  |  |  |
| Sb1 – $M$1 – Sb1(x2) | 117.12(9) | 116.09(5) | 115.37(6) | 111.61(4) |
| Sb1 – $M$1 – Sb1(x4) | 105.79(4) | 106.27(2) | 106.60(3) | 108.41(2) |

### 4.3.2   Physical Properties

The magnetic susceptibility of $Ce(Cu_{1-x}Ni_x)_ySb_2$ ($x$ = 0, 0.25, 0.37, 0.46) measured at an applied magnetic field of 0.1 T is shown in Figure 4.2.  The actual compositions of $x$ will be used to describe the samples in this section and the value of $y$ is ~ 0.7.  The Ni substituted $Ce(Cu_{1-x}Ni_x)_ySb_2$ analogues ($x$ = 0.25, 0.37) appear to be paramagnetic down to 2 K.  For $Ce(Cu_{1-x}Ni_x)_ySb_2$ ($x$ = 0.46), a sharp kink in the data is observed at 11 K.  This feature is consistent with
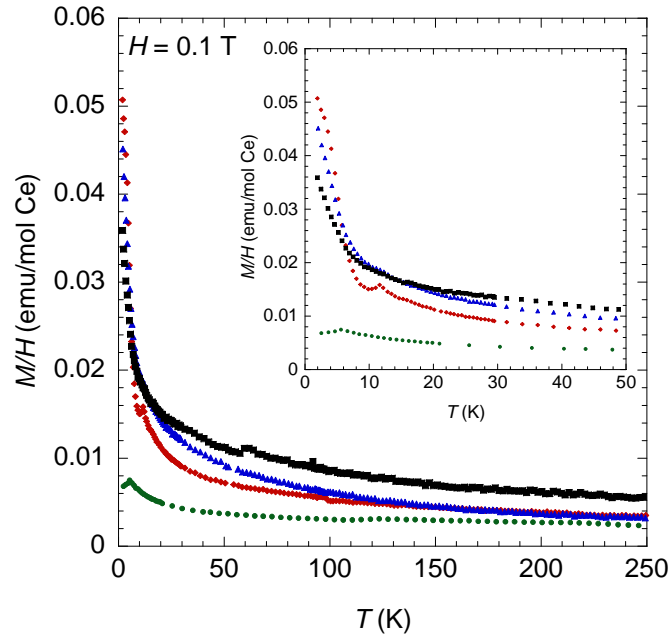


**Figure 4.2**     Magnetic susceptibility of $Ce(Cu_{1-x}Ni_x)_ySb_2$ measured at a field of 0.1 T where the green circles, black squares, blue triangles, and red diamonds refer to $x$ = 0, 0.25, 0.37, and 0.46 respectively.  The inset displays a close-up of the susceptibility from 2 – 20 K.

the onset of long-range antiferromagnetic order. $CeCu_{0.84}Sb_2$ ($x = 0$) orders antiferromagnetically at ~ 6 K which is consistent with literature reports.[8,10,12-15] The effective moments for each sample were calculated using a modified Curie-Weiss equation, $\chi = \chi_0 + C/(T - \theta)$, where $\chi$ is the magnetic susceptibility, $\chi_0$ is the temperature-independent contribution, $C$ is the Curie constant, $T$ is the temperature, and $\theta$ is the Weiss constant. Experimental effective moments of 2.32 $\mu_B$, 2.44 $\mu_B$, 2.38 $\mu_B$, and 2.31 $\mu_B$ were calculated for compounds with $x = 0.46$, 0.37, 0.25, and 0 respectively, and all are in agreement with the calculated moment of 2.54 $\mu_B$ for the free $Ce^{3+}$ ion. Curie temperatures of ~ -62, -35, -25, and -225 were observed for compounds with $x = 0.46$, 0.37, 0.25, and 0, respectively and indicate that there are antiferromagnetic correlations within the structures. A summary of the magnetic data are located in Table 4.5.

**Table 4.5** Summary of Magnetic Data for $Ce(Cu_{1-x}Ni_x)_ySb_2$ ($x = 0.8, 0.7, 0.6,$ and 0)

| $x^a$ | 0.46 | 0.37 | 0.25 | 0 |
|---|---|---|---|---|
| Fit Range | 50 – 275 K | 50 – 275 K | 100 – 275 K | 75 – 250 K |
| $T_N$ (K) | 11 | - | - | 8 |
| $\chi_0$ | 0.00125 | 0.000578 | 0.00296 | 0.00102 |
| C | 0.6716 | 0.7455 | 0.7058 | 0.6685 |
| $\theta$ (K) | -62.54 | -34.593 | -24.72 | -225.17 |
| $\mu_{calc}$ ($\mu_B$) | 2.32 | 2.44 | 2.38 | 2.31 |
| $\mu_{eff}$ ($\mu_B$) | 2.54 | 2.54 | 2.54 | 2.54 |

$^a x$ = composition as obtained from elemental analysis

The magnetization of $Ce(Cu_{1-x}Ni_x)_ySb_2$ ($x = 0.46, 0.37, 0.25,$ and 0) as a function of field (up to 9 T) measured at 3 K are shown in Figure 4.3. The magnetization of pure $CeCu_{0.84}Sb_2$ is linear with field, consistent with antiferromagnetism below 6K. None of the Ni-substituted compounds show any signs of saturation. The calculated saturation moment for a $Ce^{3+}$ free ion is 2.14 $\mu_B$. The magnetization of each analogue follows the same general curvature. There are no signs of any hysteresis in any of the compounds measured. The magnetization of all

analogues measured is small which suggests either a strong anisotropy or partial screening of the Ce moments by conduction electrons.
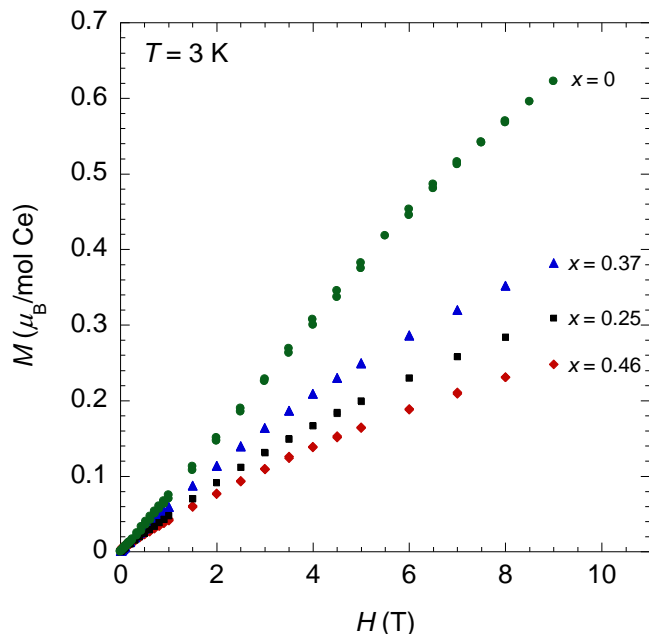


**Figure 4.3**    Magnetism of Ce(Cu$_{1-x}$Ni$_x$)$_y$Sb$_2$ measured at 3 K where the green circles, black squares, blue triangles, and red diamonds refer to $x = 0$, 0.25, 0.37, and 0.46 respectively.

Resistivity data were measured as a function of temperature for each analogue and are displayed in Figure 4.4.  All of the analogues display broad shoulders in the resistivity data as the temperature decreases which is indicative of Kondo behavior.  Also, the classic upturn of the resistivity at low temperatures is seen for Ce(Cu$_{1-x}$Ni$_x$)$_y$Sb$_2$ ($x = 0.37$ and 0.25).  The resistivity data coupled with the screening of the Ce$^{3+}$ moment seen in the magnetization data are signals that these compounds are more Kondo-like.  A sharp kink in the resistivity data for the $x = 0$ and $x = 0.46$ samples is observed at their ordering temperatures, consistent with a decrease in the spin-disorder scattering (Figure 4.4, arrows).

The magnetoresistance at fields up to 9 T measured at 3 K is displayed in Figure 4.5 for the Ce analogues.  The magnetoresistance for all analogues is larger than typical metals.  The magnetoresistance of CeCu$_y$Sb$_2$ increases quickly up to ~ 1 T then increases at a slower rate up
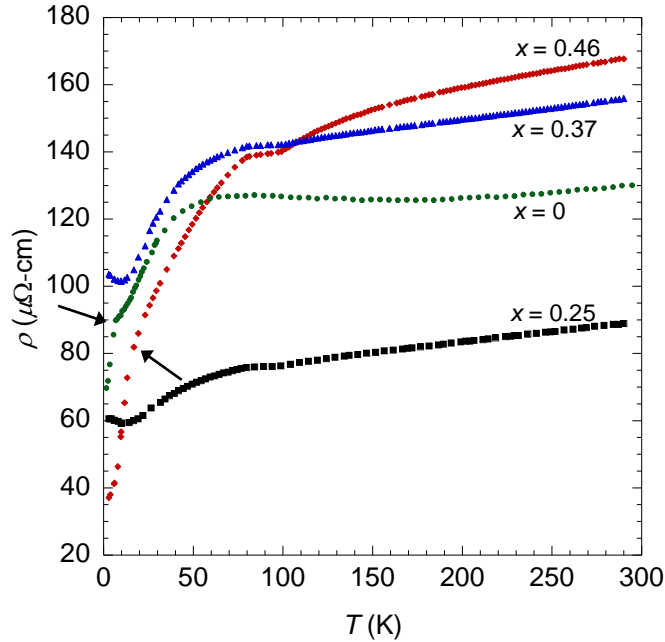
**Figure 4.4** Resistivity of $Ce(Cu_{1-x}Ni_x)_ySb_2$ where the green circles, black squares, blue triangles, and red diamonds refer to $x = 0$, 0.25, 0.37, and 0.46 respectively.
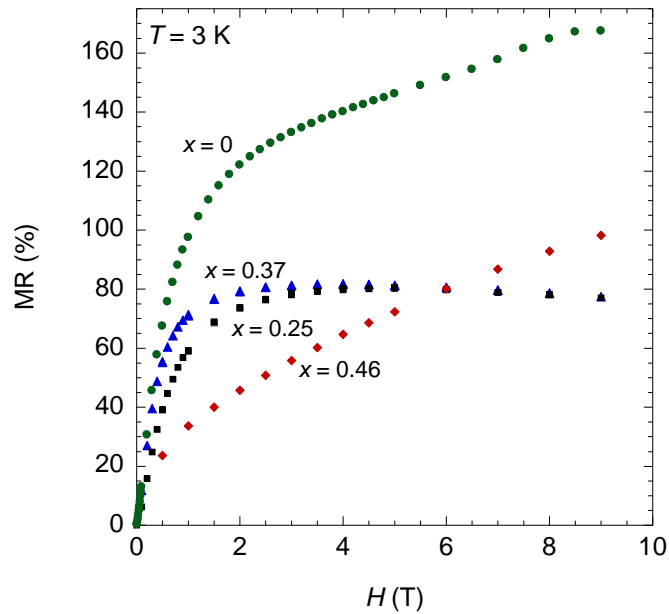


**Figure 4.5** Magnetoresistance of $Ce(Cu_{1-x}Ni_x)_ySb_2$ measured at 3 K where the green circles, black squares, blue triangles, and red diamonds refer to $x = 0$, 0.25, 0.37, and 0.46 respectively.

to ~165 % at 9 T. The magnetoresistance increases quickly up to ~ 1 T then begins to saturate at

77 %, and 80 % for $x = 0.25$, and 0.37 respectively. The magnetoresistance for $Ce(Cu_{1-x}Ni_x)_ySb_2$

($x$= 0.46) is similar to the other analogues up to ~ 1 T, then the behavior deviates and increases with no signs of saturation up to 100 % at 9 T.  The magnetoresistance is not proportional to $H^2$ for all analogues, indicating that the magnetoresistive behavior is not classical.   The magnetoresistance of nominal La(Cu$_{0.2}$Ni$_{0.8}$)$_y$Sb$_2$ measured at 3 K up to fields of 9 T is displayed in Figure 4.6.  The magnetoresistance is significantly larger than the Ce analogues with the magnetoresistance saturating at ~ 300 %.  This is not surprising as many La analogues have larger magnetoresistive behavior than other rare earth analogues such as LaSb$_2$.[5,6]
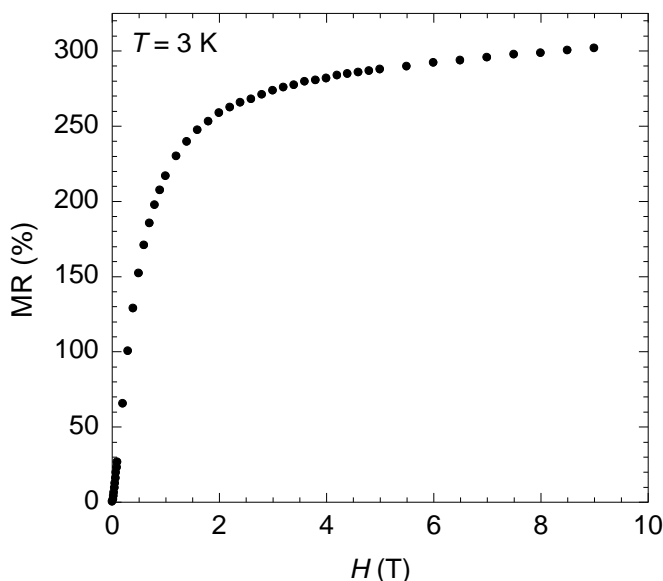


**Figure 4.6**     Magnetoresistance of La(Cu$_{1-x}$Ni$_x$)$_y$Sb$_2$ (nominal $x$ = 0.8) measured at 3 K.

## 4.4  References

(1)     Mills, A. M.; Lam, R.; Ferguson, M. J.; Deakin, L.; Mar, A. *Coord. Chem. Rev.* **2002**, *233-234*, 207-222.

(2)     Sologub, O.; Salamakha, P. S. *Handbook on the Physics and Chemistry of Rare Earths*; Elsevier: Netherlands, 2003; Vol. 33.

(3)     Kauzlarich, S. M. *Chemistry, Structure, and Bonding in Zintl Phases and Ions*; VCH Publishers: New York, 1996.

(4)     Macaluso, R. T.; Wells, D. M.; Sykora, R. E.; Albrecht-Schmitt, T. E.; Mar, A.; Nakatsuji, S.; Lee, H.; Fisk, Z.; Chan, J. Y. *J. Solid State Chem.* **2004**, *177*, 293-298.

(5)     Bud'ko, S. L.; Canfield, P. C.; Mielke, C. H.; Lacerda, A. H. *Phys. Rev. B* **1998**, *57*, 13624-13638.

(6)     Young, D. P.; Goodrich, R. G.; DiTusa, J. F.; Guo, S.; Adams, P. W.; Chan, J. Y.; Hall, D. *Appl. Phys. Lett.* **2003**, *82*, 3713-3715.

(7)     Thomas, E. L.; Moldovan, M.; Young, D. P.; Chan, J. Y. *Chem. Mater.* **2005**, *17*, 5810-5816.

(8)     Thamizhavel, A.; Takeuchi, T.; Okubo, T.; Yamada, M.; Asai, R.; Kirit, S.; Galatanu, A.; Yamamoto, E.; Ebihara, T.; Inada, Y.; Settai, R.; Onuki, Y. *Phys. Rev. B* **2003**, *68*, 54427.

(9)     Siderov, V. A.; Bauer, E. D.; Lee, H.; Nakatsuji, S.; Thompson, J. D.; Fisk, Z. *Phys. Rev. B* **2005**, *71*, 094422-1 - 094422-4.

(10)    Muro, Y.; Takeda, N.; Ishikawa, M. *J. Alloys Compd.* **1997**, *257*, 23-29.

(11)    Lakshmi, K. V.; Menon, L.; Nigam, A. K.; Das, A.; Malik, S. K. *Physica B* **1996**, *223 & 224*, 289-291.

(12)    Sologub, O.; Hiebl, K.; Rogl, P.; Noël, H.; Bodak, O. *J. Alloys Compd.* **1994**, *210*, 153-157.

(13)    Flandorfer, H.; Sologub, O.; Godart, C.; Hiebl, K.; Leith-Jasper, A.; Rogl, P.; Noel, H. *Solid State Commun.* **1996**, *97*, 561-565.

(14)    Koyama, T.; Matsumoto, M.; Wada, S.; Muro, Y.; Ishikawa, M. *J. Phys. Soc. Jpn.* **2001**, *70*, 3667-3672.

(15)    Thamizhavel, A.; Okubo, T.; Yamada, M.; Galatanu, A.; Yamamoto, E.; Inada, Y.; Ebihara, T.; Onuki, Y. *Physica B* **2003**, *327*, 374-377.

(16)    Altomare, A.; Burla, M. C.; Camalli, M.; Cascarno, G. L.; Giacovazzo, A.; Guagliardi, A.; Moliterni, A. G. G.; Polidori, G.; Spagna, R. J. *J. Appl. Crystallogr.* **1999**, *32*, 115-119.

(17)    Sheldrick, G. M.; University of Gottingen: Germany, 1997.

(18)    Andrukhiv, L. S.; Lysenko, L. O.; Yarmolyuk, Y. P.; Hladyshevsky, E. I. *Dopov. Akad. Nauk Ukr. RSR, Ser. A* **1975**, *7*, 645-648.

(19)    Thomas, E. L.; Macaluso, R. T.; Lee, H.; Fisk, Z.; Chan, J. Y. *J. Solid State Chem.* **2004**, *177*, 4228-4236.

(20)    Wang, R.; Steinfink, H. *Inorg. Chem.* **1967**, *6*, 1685-1692.

# CHAPTER 5 – Rb$_4$$M$(MoO$_4$)$_3$

## 5.1 Introduction

The existence of ferroelectricity and magnetism in a single material has generated interest in recent years because the two phenomena were previously thought to not coexist in the same material. This new, exciting field has been termed multiferroics and researchers are working to understand the mechanisms by which these two phenomena can coexist simultaneously. This research is fueled by the promise of numerous practical applications such as conventional actuators, transducers, data storage, or memory media.[1]

One of the more well known mechanisms for ferroelectricity in a perovskite such as BaTiO$_3$, has the Ti$^{4+}$ ion shifted towards the corner of the unit cell which creates electric polarization inducing a charge transfer from filled oxygen $2p$ orbitals into the empty $d$-orbitals of the transition metal.[1,2] Empty $d$-orbitals are necessary for magnetism to exist, so this mechanism is not conducive to multiferroism. Another mechanism for off-center distortion of the transition metal site is found in materials with a $ns^2$ lone pair which displaces the parent cation leading to the loss of inversion symmetry.[1] There are both proper and improper inversion symmetry breaking mechanisms.[3] Covalent bonding between $3d^0$ transition metal and oxygen seen in BaTiO$_3$ and $6s^2$ lone pair polarization seen in compounds such as BiMnO$_3$, BiFeO$_3$, and Pb(Fe$_{2/3}$W$_{1/3}$)O$_3$ are examples of the proper mechanism for losing inversion symmetry.[3] Examples of improper loss of inversion symmetry mechanisms include structural transitions as seen in K$_2$SeO$_4$, Cs$_2$CdI$_4$, and hexagonal RMnO$_3$, charge ordering as seen in LuFe$_2$O$_4$, and magnetic ordering as seen in RMn$_2$O$_5$, CoCr$_2$O$_4$, and the orthorhombic RMnO$_3$.[3] These mechanisms apply only to ferroelectricity and typically do not allow for the simultaneous presence of a magnetic moment.

Multiferroic materials were in short supply until 2003, when Kimura *et al.* discovered that spin frustration causes antiferromagnetic ordering in $TbMnO_3$.[4] This rekindled interest in multiferroic materials and the quest was on to understand and discover more of these intriguing materials with frustrated spin systems. In 2007, another mechanism came to light in frustrated magnets where a magnetic spiral structure breaks inversion symmetry and leads to the presence of electric polarization.[3,5] In 2008 CuO, a centrosymmetric material, was identified as an induced-multiferroic which has a proper-screw magnetic.[6] This new mechanism will be useful in identifying other possible multiferroic materials.

As indicated above, crystal symmetry plays an integral role in predicting and understanding multiferroic behavior in materials. This is the motivation for the present work. Full structural determination, understanding temperature induced phase transitions, and the analyses of disorder in crystals are important in understanding the properties of these materials. The crystal structural studies of the possible multiferroic double molybdates, $Rb_4M(MoO_4)_3$, ($M$ = Mn, Zn, Cu) are reported herein.

## 5.2    Structural Studies by Single Crystal X-Ray Diffraction

The single crystal X-ray diffraction data of $Rb_4M(MoO_4)_3$ ($M$ = Mn, Zn, and Cu) were collected at various temperatures. Due to the extremely hygroscopic nature of the samples, the crystals were placed in Paratone-N oil to protect the sample from exposure to air and moisture. A crystal with approximate dimensions of ~ 0.05 x 0.125 x 0.125 mm$^3$ was mounted onto a glass fiber of the goniometer with epoxy and/or vacuum grease and placed on a Nonius Kappa CCD X-ray diffractometer ($MoK_\alpha$ = 0.71073 Å). Temperature was regulated with a cooled nitrogen gas stream produced by an Oxford Cryostream Cooler. The unit cell parameters were determined from images taken at a rotation of 15 °φ. Initial structural models were solved by

SIR97[7] and refined by direct methods using SHELXL97[8]. The data were corrected for absorption and the displacement parameters were refined as anisotropic.

### 5.2.1 $Rb_4Mn(MoO_4)_3$

The single crystal X-ray diffraction data was collected at various temperatures for $Rb_4Mn(MoO_4)_3$. Data were collected at 298 K, 270 K, and 100 K. The crystal measured had dimensions of ~ 0.05 x 0.125 x 0.125 $mm^3$. There were two suitable structural models in two different, hexagonal space group choices: $P\bar{6}2c$ (# 190) and $P6_3/mmc$ (# 194). $P\bar{6}2c$ (# 190) is a non-centrosymmetric space group while $P6_3/mmc$ (# 194) is a centrosymmetric space group. The main difference between the two space groups is the presence of three mirrors perpendicular to the rotation axis in the higher symmetry space group. The systematic absences are the same for both space groups. Powder patterns were calculated from the single crystal models and both patterns were identical and matched the experimental powder pattern as shown in Figure 5.1.
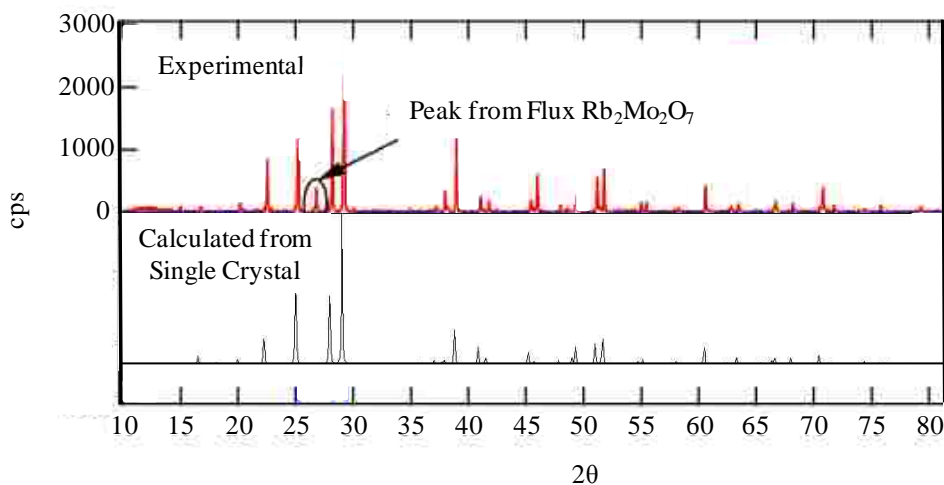


**Figure 5.1** Experimental (red) and calculated (black) powder patterns for $Rb_4Mn(MoO_4)_3$.

Previous structural reports indicate acceptable structural models in three hexagonal space groups: $P6_3/mmc$, $P6_3mc$, and $P\bar{6}2c$. However, the centrosymmetric $P6_3/mmc$ was ruled out due to

piezoelectric effects.[9] We chose the higher symmetry $P6_3/mmc$ model because the data was in slightly better agreement than the lower symmetry $P\bar{6}2c$ model based on R-factors of 2.88 % for the $P6_3/mmc$ model and 4.04 % for the $P\bar{6}2c$ model. Also, because the polarization measurements have not been measured on our crystals, we cannot use that as reasoning for choosing the non-centrosymmetric structural model. The crystallographic information for $Rb_4Mn(MoO_4)_3$ is located in Table 5.1 and the atomic parameters are located in Table 5.2.

**Table 5.1**     Crystallographic Data for $Rb_4Mn(MoO_4)_3$

| Sample | dixie67 | dixie68 | dixie69 |
|---|---|---|---|
| Formula | $Rb_4Mn(MoO_4)_3$ | $Rb_4Mn(MoO_4)_3$ | $Rb_4Mn(MoO_4)_3$ |
| Formula units (amu) | 876.64 | 876.64 | 876.64 |
| Space Group | $P6_3/mmc$ | $P6_3/mmc$ | $P6_3/mmc$ |
| $a$ (Å) | 6.0989(2) | 6.0919(3) | 6.0529(4) |
| $b$ (Å) | 6.0989(2) | 6.0920(3) | 6.0529(4) |
| $c$ (Å) | 23.7107(6) | 23.7248(9) | 23.7010(10) |
| $V$ (Å$^3$) | 763.80(4) | 762.51(6) | 752.01(8) |
| Crystal size (mm$^3$) | 0.025/0.075/0.075 | 0.025/0.075/0.075 | 0.025/0.075/0.075 |
| $Z$ | 2 | 2 | 2 |
| Temperature (K) | 298 | 270 | 100 |
| Density (g cm$^{-1}$) | 3.812 | 3.818 | 3.871 |
| $\theta$ Range (°) | 3.44-29.98 | 3.43-30.02 | 3.44-30.00 |
| $\mu$ (mm$^{-1}$) | 15.923 | 15.950 | 16.173 |
| $R_{int}$ | 0.0531 | 0.0725 | 0.0907 |
| Collected Reflections | 2762 | 2510 | 2530 |
| Unique Reflections | 489 | 489 | 482 |
| $h$ | $-8 \leq h \leq 8$ | $-8 \leq h \leq 8$ | $-8 \leq h \leq 8$ |
| $k$ | $-6 \leq k \leq 6$ | $-6 \leq k \leq 6$ | $-6 \leq k \leq 6$ |
| $l$ | $-32 \leq l \leq 32$ | $-33 \leq l \leq 25$ | $-28 \leq l \leq 33$ |
| $\Delta\rho_{max}$ (e Å$^{-3}$) | 0.892 | 1.514 | 1.380 |
| $\Delta\rho_{min}$ (e Å$^{-3}$) | -1.134 | -0.828 | -1.948 |
| Extinction coefficient | 0.0049(8) | 0.0040(7) | 0.0072(9) |
| [a] R(F) for $F_o^2 > 2\sigma(F_o^2)$ | 0.0288 | 0.0334 | 0.0396 |
| [b] $R_w(F_o^2)$ | 0.0749 | 0.0766 | 0.0949 |

[a] $R_1(F) = \sum \left\| F_0 \right| - \left| F_c \right\| / \sum \left| F_0 \right|$

[b] $R_w(F_o^2) = \sum[w(F_o^2 - F_c^2)^2] / \sum[w(F_o^2)^2]^{1/2}$ ;where $w = 1/[\sigma^2(F_0^2) + (0.0421P)^2 + 0.7989P]$,

$w = 1/[\sigma^2(F_0^2) + (0.0419P)^2]$, $w = 1/[\sigma^2(F_0^2) + (0.0568P)^2]$ for dixie67, dixie68, and dixie69 respectively.

**Table 5.2**      Atomic Positions and Displacement Parameters for $Rb_4Mn(MoO_4)_3$

| Atom | Wyckoff site | $x$ | $y$ | $z$ | $U_{eq}$ (Å$^2$)[a] | Occupancy |
|------|------|------|------|------|------|------|
| dixie67 – 298 K | | | | | | |
| Rb1 | 4f | ⅓ | ⅔ | 0.15755(3) | 0.0344(3) | 1 |
| Rb2 | 4f | ⅔ | ⅓ | 0.02849(3) | 0.0283(3) | 1 |
| Mn1 | 2a | 0 | 0 | ¼ | 0.0281(4) | 1 |
| Mo1 | 4e | 0 | 0 | 0.09016(2) | 0.0196(2) | 1 |
| Mo2 | 4f | ⅔ | ⅓ | 0.22782(6) | 0.0255(5) | 0.48 |
| O1 | 4e | 0 | 0 | 0.1645(2) | 0.056(2) | 1 |
| O2 | 12k | 0.1555(3) | 0.3109(6) | 0.06565(15) | 0.0406(9) | 1 |
| O3 | 4f | ⅔ | ⅓ | 0.1557(4) | 0.047(6) | 0.50 |
| O4 | 12j | 0.3859(12) | 0.3283(13) | ¼ | 0.041(2) | 0.51 |
| dixie68 – 270 K | | | | | | |
| Rb1 | 4f | ⅓ | ⅔ | 0.15755(3) | 0.0306(3) | 1 |
| Rb2 | 4f | ⅔ | ⅓ | 0.02850(4) | 0.0244(3) | 1 |
| Mn1 | 2a | 0 | 0 | ¼ | 0.0240(5) | 1 |
| Mo1 | 4e | 0 | 0 | 0.09006(3) | 0.0167(2) | 1 |
| Mo2 | 4f | ⅔ | ⅓ | 0.22787(7) | 0.0216(6) | 0.48 |
| O1 | 4e | 0 | 0 | 0.1647(2) | 0.053(2) | 1 |
| O2 | 12k | 0.1556(3) | 0.3112(7) | 0.06566(16) | 0.0352(10) | 1 |
| O3 | 4f | ⅔ | ⅓ | 0.1556(4) | 0.037(6) | 0.50 |
| O4 | 12j | 0.3840(13) | 0.3286(14) | ¼ | 0.037(3) | 0.52 |
| dixie69 – 100 K | | | | | | |
| Rb1 | 4f | ⅓ | ⅔ | 0.15728(4) | 0.0176(4) | 1 |
| Rb2 | 4f | ⅔ | ⅓ | 0.02879(4) | 0.0143(4) | 1 |
| Mn1 | 2a | 0 | 0 | ¼ | 0.0164(6) | 1 |
| Mo1 | 4e | 0 | 0 | 0.08945(3) | 0.0113(3) | 1 |
| Mo2 | 4f | ⅔ | ⅓ | 0.22778(9) | 0.0160(8) | 0.48 |
| O1 | 4e | 0 | 0 | 0.1649(3) | 0.033(3) | 1 |
| O2 | 12k | 0.1568(5) | 0.3136(10) | 0.0649(2) | 0.0233(13) | 1 |
| O3 | 4f | ⅔ | ⅓ | 0.1551(6) | 0.016(6) | 0.46 |
| O4 | 12j | 0.385(2) | 0.332(2) | ¼ | 0.028(3) | 0.50 |

[a]$U_{eq}$ is defined as one-third of the trace of the orthogonalized $U_{ij}$ tensor.

Figure 5.2 displays the structure of $Rb_4Mn(MoO_4)_3$ as well as the coordination around the Mn1 atom.   The structure consists of $MnO_5$ trigonal bipyramids surrounded by five Mo tetrahedra: two Mo2 tetrahedra in the capping positions and three Mo1 tetrahedra in the basal plane.   $Rb_4Mn(MoO_4)_3$ is isostructural to $Cs_4Cu(MoO_4)_3$.[9]   There are several atoms in this structure that are disordered.  The three O4 atoms in the basal plane of the Mn trigonal bipyramid and each Mo2, O3, and O4 atoms that comprise the Mo2 tetrahedra are disordered.  This disorder is displayed by ½ occupied sites in the atomic positions.  The Mo2 tetrahedra seem to be inverted

and staggered as seen in Figure 5.2, however each Mo2 and surrounding O atoms are ½ occupied throughout the entire extended structure.
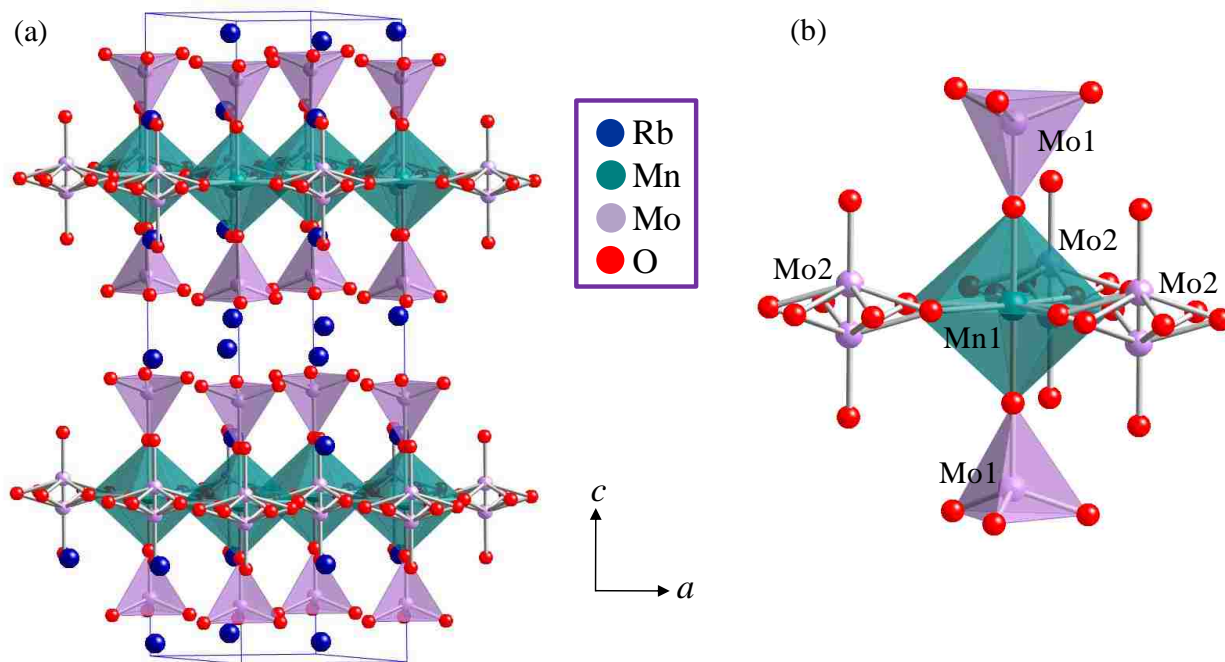


**Figure 5.2** (a) Crystal structure of $Rb_4Mn(MoO_4)_3$ where the blue, green, purple, and red spheres refer to Rb, Mn, Mo, and O atoms respectively. (b) The Mn bonding environment of $Rb_4Mn(MoO_4)_3$.

### 5.2.2   $Rb_4Zn(MoO_4)_3$

The lattice ($a$ = 10.90, $b$ = 22.42, and $c$ = 6.271 Å) and space group ($Pn2_1a$) were previously reported for $\beta$-$Rb_4Zn(MoO_4)_3$ however, no full structural determination was reported.[10] The crystal structure of $Rb_4Zn(MoO_4)_3$ was determined by X-ray diffraction and based on our experimentation, $Rb_4Zn(MoO_4)_3$ crystallizes in the orthorhombic space group *Pbca* (# 61) and adopts a new structure type with lattice parameters of $a$ = 12.574(2) Å, $b$ = 10.9130(10) Å, and $c$ = 22.3320(10) Å at room temperature. A crystal coated with Paratone-N oil and dimensions of ~ 0.05 x 0.10 x 0.125 mm$^3$ was measured at 290 K and 100 K. After collecting full data at 290 K, the crystal was slowly cooled and scans at a rotation of 15 °φ were taken in 20 K increments and no temperature induced structural transitions were observed for

56

$Rb_4Zn(MoO_4)_3$. Crystallographic information for $Rb_4Zn(MoO_4)_3$ is located in Table 5.3 and the atomic parameters are located in Table 5.4.

**Table 5.3**     Crystallographic Data for $Rb_4Zn(MoO_4)_3$

| Sample | dixie75 | dixie76 |
|---|---|---|
| Formula | $Rb_4Zn(MoO_4)_3$ | $Rb_4Zn(MoO_4)_3$ |
| Formula units (amu) | 887.07 | 887.07 |
| Space Group | *Pbca* | *Pbca* |
| $a$ (Å) | 12.574(2) | 12.485(2) |
| $b$ (Å) | 10.9130(10) | 10.8750(10) |
| $c$ (Å) | 22.3320(10) | 22.2660(10) |
| $V$ (Å$^3$) | 3064.4(6) | 3023.2(6) |
| Crystal size (mm$^3$) | 0.05/0.10/0.125 | 0.05/0.10/0.125 |
| $Z$ | 8 | 8 |
| Temperature (K) | 290 | 100 |
| Density (g cm$^{-1}$) | 3.845 | 3.898 |
| $\theta$ Range (°) | 2.44-30.04 | 2.45-30.02 |
| $\mu$ (mm$^{-1}$) | 16.617 | 16.843 |
| $R_{int}$ | 0.0703 | 0.0535 |
| Collected Reflections | 8345 | 8235 |
| Unique Reflections | 2478 | 2922 |
| $h$ | $-17 \le h \le 17$ | $-17 \le h \le 17$ |
| $k$ | $-15 \le k \le 15$ | $-15 \le k \le 15$ |
| $l$ | $-31 \le l \le 31$ | $-31 \le l \le 31$ |
| $\Delta\rho_{max}$ (e Å$^{-3}$) | 4.515 | 2.495 |
| $\Delta\rho_{min}$ (e Å$^{-3}$) | -2.607 | -1.940 |
| Extinction coefficient | 0.00052(4) | 0.000134(18) |
| [a] R($F$) for $F_o^2 > 2\sigma(F_o^2)$ | 0.0537 | 0.0456 |
| [b] $R_w(F_o^2)$ | 0.1132 | 0.0919 |

[a] $R_1(F) = \sum \lVert F_0 \rvert - \lvert F_c \rVert / \sum \lvert F_0 \rvert$

[b] $R_w(F_o^2) = \sum[w(F_o^2 - F_c^2)^2]/\sum[w(F_o^2)^2]^{1/2}$ ;where $w = 1/[\sigma^2(F_0^2) + (0.0579P)^2]$, $w = 1/[\sigma^2(F_0^2) + (0.0394P)^2 + 9.0735P]$ for dixie75 and dixie76 respectively.

**Table 5.4**     Atomic Positions and Displacement Parameters for $Rb_4Zn(MoO_4)_3$

| Atom | Wyckoff site | $x$ | $y$ | $z$ | $U_{eq}$ (Å$^2$)[a] |
|---|---|---|---|---|---|
| dixie75 – 290 K | | | | | |
| Rb1 | 8$c$ | 0.62666(7) | 0.91895(7) | 0.97177(4) | 0.0217(2) |
| Rb2 | 8$c$ | 0.87590(7) | 0.08521(7) | 0.03049(4) | 0.0277(2) |
| Rb3 | 8$c$ | 0.10741(7) | 0.57137(8) | 0.83923(3) | 0.0281(2) |
| Rb4 | 8$c$ | 0.62284(7) | 0.59654(8) | 0.84237(3) | 0.0297(2) |

**Table 5.4** (cont.)

| Atom | Wyckoff site | $x$ | $y$ | $z$ | $U_{eq}$ (Å$^2$)$^a$ |
|---|---|---|---|---|---|
| Zn1 | 8$c$ | 0.32058(8) | 0.71852(9) | 0.75362(4) | 0.0210(2) |
| Mo1 | 8$c$ | 0.37569(6) | 0.74745(6) | 0.90548(3) | 0.01751(18) |
| Mo2 | 8$c$ | 0.87314(6) | 0.75371(6) | 0.90623(3) | 0.01718(17) |
| Mo3 | 8$c$ | 0.37405(6) | 0.42351(6) | 0.73335(3) | 0.02164(19) |
| O1 | 8$c$ | 0.3700(5) | 0.7450(6) | 0.6745(3) | 0.0362(16) |
| O2 | 8$c$ | 0.4974(5) | 0.4610(6) | 0.7621(3) | 0.0361(15) |
| O3 | 8$c$ | 0.3952(5) | 0.7523(5) | 0.8246(2) | 0.0340(16) |
| O4 | 8$c$ | 0.5129(5) | 0.1799(5) | 0.9321(2) | 0.0325 (15) |
| O5 | 8$c$ | 0.2805(5) | 0.5423(5) | 0.7539(2) | 0.0301(15) |
| O6 | 8$c$ | 0.1731(5) | 0.7797(5) | 0.7613(2) | 0.0308(14) |
| O7 | 8$c$ | 0.2597(5) | 0.6703(6) | 0.9237(2) | 0.0424(17) |
| O8 | 8$c$ | 0.3684(5) | 0.8973(5) | 0.9332(3) | 0.0385(17) |
| O9 | 8$c$ | 0.3829(6) | 0.4163(6) | 0.6567(2) | 0.0429(19) |
| O10 | 8$c$ | 0.4835(5) | 0.6722(6) | 0.9368(2) | 0.0380(16) |
| O11 | 8$c$ | 0.6239(5) | 0.4062(5) | 0.9300(2) | 0.0320(15) |
| O12 | 8$c$ | 0.7604(5) | 0.6837(5) | 0.9353(2) | 0.0328(15) |
| dixie76 – 100 K | | | | | |
| Rb1 | 8$c$ | 0.62709(5) | 0.91860 (6) | 0.97183(3) | 0.01378(15) |
| Rb2 | 8$c$ | 0.87567(5) | 0.08440(6) | 0.03151(3) | 0.01385(15) |
| Rb3 | 8$c$ | 0.10545(6) | 0.57003(6) | 0.83948(3) | 0.01477(15) |
| Rb4 | 8$c$ | 0.62453(5) | 0.59903(6) | 0.84265(3) | 0.01486(16) |
| Zn1 | 8$c$ | 0.32067(7) | 0.71724(7) | 0.75429(3) | 0.01259(18) |
| Mo1 | 8$c$ | 0.37662(4) | 0.74717(5) | 0.90582(2) | 0.00993(13) |
| Mo2 | 8$c$ | 0.87294(4) | 0.75407(5) | 0.90704(2) | 0.01007(13) |
| Mo3 | 8$c$ | 0.37491(5) | 0.42223(5) | 0.73384(3) | 0.01156(14) |
| O1 | 8$c$ | 0.3690(4) | 0.7428(4) | 0.6740(2) | 0.0205(11) |
| O2 | 8$c$ | 0.4986(4) | 0.4614(4) | 0.7629(2) | 0.0165(10) |
| O3 | 8$c$ | 0.3980(4) | 0.7525(4) | 0.82513(19) | 0.0167(11) |
| O4 | 8$c$ | 0.5121(4) | 0.1802(4) | 0.9333(2) | 0.0188 (11) |
| O5 | 8$c$ | 0.2808(4) | 0.5400(4) | 0.75474(19) | 0.0168(10) |
| O6 | 8$c$ | 0.1704(4) | 0.7760(4) | 0.7622(2) | 0.0178(10) |
| O7 | 8$c$ | 0.2594(4) | 0.6681(5) | 0.9229(2) | 0.0224(12) |
| O8 | 8$c$ | 0.3683(4) | 0.8969(4) | 0.9333(2) | 0.0201(11) |
| O9 | 8$c$ | 0.3833(4) | 0.4173(4) | 0.65647(19) | 0.0195(11) |
| O10 | 8$c$ | 0.4851(4) | 0.6700(4) | 0.9381(2) | 0.0206(11) |
| O11 | 8$c$ | 0.6227(4) | 0.4084(4) | 0.92981(19) | 0.0167(11) |
| O12 | 8$c$ | 0.7585(4) | 0.6840(4) | 0.93782(19) | 0.0174(11) |

$^a U_{eq}$ is defined as one-third of the trace of the orthogonalized $U_{ij}$ tensor.

Figure 5.3 displays the crystal structure of $Rb_4Zn(MoO_4)_3$ as well as the Zn subunit. The layered structure consists of slightly distorted $ZnO_4$ tetrahedral units surrounded by four slightly less distorted Mo tetrahedra. The Zn tetrahedra form chains with Mo3 tetrahedra along the *b*-axis and are capped by Mo1 and Mo3 tetrahedra in the *c*-direction. The O-Mo-O angles range

**Figure 5.3** (a) Crystal structure of $Rb_4Zn(MoO_4)_3$ as viewed down the *a* axis where the blue, green, purple, and red spheres refer to Rb, Zn, Mo, and O atoms respectively. (b) Zn bonding environment of $Rb_4Zn(MoO_4)_3$.

from 107.9 ° - 111.1 ° for Mo1, 108.8 ° - 110.1 ° for Mo2, and 108.7 ° - 112.1 ° for Mo3 indicating a slight deviation from the expected angle of 109.5 °. The O-Zn-O angles range from 103.5 ° - 126.4 ° for the $ZnO_4$ tetrahedra indicating more distortion than the $MoO_4$ units. Selected interatomic distances and bond angles are located in Table 5.5. The distances are consistent with the ionic radii of $Rb^{1+}$, $Zn^{2+}$, and $Mo^{6+}$.[11] The notable difference between this structure and the $Rb_4Mn(MoO_4)_3$ structure is the lack of disorder and the bonding environment of the transition metal. The Mn analogue consists of a Mn trigonal bipyramid while the Zn analogue contains slightly distorted Zn tetrahedra.

**Table 5.5** Selected Interatomic Distances (Å) for $Rb_4Zn(MoO_4)_3$

| | | | | | |
|---|---|---|---|---|---|
| Mo1 – O7 | 1.740(5) | Rb1 – O9 | 2.860(4) | Rb2 – O10 | 2.866(5) |
| Mo1 – O8 | 1.742(5) | Rb1 – O8 | 2.915(5) | Rb2 – O12 | 2.886(5) |
| Mo1 – O10 | 1.748(5) | Rb1 – O4 | 2.939(5) | Rb2 – O11 | 2.965(4) |
| Mo1 – O3 | 1.817(4) | Rb1 – O7 | 3.018(5) | Rb2 – O8 | 3.152(5) |

**Table 5.5** (cont.)

| | | | | | |
|---|---|---|---|---|---|
| | | Rb1 – O12 | 3.126(5) | Rb2 – O10 | 3.159(5) |
| Mo2 – O4 | 1.746(5) | Rb1 – O11 | 3.263(5) | Rb2 – O4 | 3.173(5) |
| Mo2 – O11 | 1.754(4) | Rb1 – O4 | 3.300(5) | Rb2 – O11 | 3.203(5) |
| Mo2 – O12 | 1.758(5) | Rb1 – O12 | 3.309(5) | Rb2 – O7 | 3.268(5) |
| Mo2 – O1 | 1.808(5) | Rb1 – O10 | 3.319(5) | Rb2 – O7 | 3.334(5) |
| | | Rb1 – O8 | 3.352(5) | | |
| Mo3 – O9 | 1.727(4) | | | Rb4 – O2 | 2.805(4) |
| Mo3 – O2 | 1.727(5) | Rb3 – O4 | 2.820(5) | Rb4 – O11 | 2.840(4) |
| Mo3 – O5 | 1.800(5) | Rb3 – O8 | 2.830(5) | Rb4 – O10 | 2.853(5) |
| Mo3 – O6 | 1.802(5) | Rb3 – O7 | 2.878(5) | Rb4 – O12 | 2.853(5) |
| | | Rb3 – O2 | 2.893(5) | Rb4 – O5 | 2.986(5) |
| Zn1 – O3 | 1.889(5) | Rb3 – O5 | 2.908(5) | Rb4 – O6 | 3.079(5) |
| Zn1 – O1 | 1.908(5) | Rb3 – O6 | 2.939(4) | Rb4 – O3 | 3.307(5) |
| Zn1 – O6 | 1.990(5) | Rb3 – O9 | 3.234(5) | | |
| Zn1 – O5 | 1.991(5) | | | | |

### 5.2.3 $Rb_4Cu(MoO_4)_3$

$Rb_4Cu(MoO_4)_3$ undergoes two temperature dependent phase transitions.[12] Above room temperature the structure adopts a hexagonal structure, at room temperature the crystal adopts an orthorhombic structure, and around 103 K the crystal is reported to adopt a monoclinic structure.[12] Based on current experiments at 298 K, the compound adopts an orthorhombic structure (*Pnma* #62) with a lattice of $a = 10.581(2)$ Å, $b = 23.213(4)$ Å, and $c = 6.078(1)$ Å. One sample batch yielded a crystal that adopted the hexagonal structure (6.1 x 23.2 Å), however this result was not found in other batches of $Rb_4Cu(MoO_4)_3$ crystals. The crystallographic information for both the hexagonal and orthorhombic phases of $Rb_4Cu(MoO_4)_3$ are located in Table 5.6 and the atomic coordinates and displacement parameters are located in Table 5.7. A similar orthorhombic lattice was also reported for $\beta$-$Rb_4Zn(MoO_4)_3$ which adopts the $Pn2_1a$ space group, however no other structural information was reported for this compound.[10] The lattice is similar to the orthorhombic compound $K_4Zn(MoO_4)_3$ which crystallizes in the space group $P2_12_12_1$.[13,14] The space groups $P2_12_12_1$ and *Pnma* belong to the same sub group and both have $2_1$ screw axes in all three directions, while *Pnma* also has a mirror, glide planes, and an

60

**Table 5.6** Crystallographic Information for the Phases of $Rb_4Cu(MoO_4)_3$

| Sample | dixie51 | dixie78 |
|---|---|---|
| Formula | $Rb_4Cu(MoO_4)_3$ | $Rb_4Cu(MoO_4)_3$ |
| Formula units (amu) | 885.24 | 885.24 |
| Crystal System | hexagonal | orthorhombic |
| Space Group | $P6_3/mmc$ | $Pnma$ |
| $a$ (Å) | 6.088(5) | 10.581(2) |
| $b$ (Å) | 6.088(5) | 23.213(4) |
| $c$ (Å) | 23.157(4) | 6.078(1) |
| $V$ (Å$^3$) | 743.3(9) | 1492.9(5) |
| Crystal size (mm$^3$) | 0.05/0.125/0.125 | 0.075/0.15/0.175 |
| $Z$ | 2 | 4 |
| Temperature (K) | 298 | 298 |
| Density (g cm$^{-1}$) | 3.383 | 3.939 |
| $\theta$ Range (°) | 3.86-29.95 | 3.46-30.02 |
| $\mu$ (mm$^{-1}$) | 16.873 | 16.872 |
| $R_{int}$ | 0.0578 | 0.0295 |
| Collected Reflections | 2499 | 3948 |
| Unique Reflections | 467 | 1582 |
| $h$ | $-8 \leq h \leq 8$ | $-14 \leq h \leq 14$ |
| $k$ | $-6 \leq k \leq 6$ | $-32 \leq k \leq 32$ |
| $l$ | $-29 \leq l \leq 32$ | $-8 \leq l \leq 8$ |
| $\Delta\rho_{max}$ (e Å$^{-3}$) | 1.095 | 2.333 |
| $\Delta\rho_{min}$ (e Å$^{-3}$) | -1.201 | -1.226 |
| Extinction coefficient | 0.0036(9) | 0.00084(11) |
| [a] R($F$) for $F_o^2 > 2\sigma(F_o^2)$ | 0.0538 | 0.0508 |
| [b] $R_w(F_o^2)$ | 0.1250 | 0.1103 |

[a] $R_1(F) = \sum \left\| F_0 \right| - \left| F_c \right\| / \sum \left| F_0 \right|$

[b] $R_w(F_o^2) = \sum [w(F_o^2 - F_c^2)^2] / \sum [w(F_o^2)^2]^{1/2}$ ;where, $w = 1/[\sigma^2(F_0^2) + (0.0320P)^2 + 15.9950P]$ and $w = 1/[\sigma^2(F_0^2) + (0.00207P)^2 + 31.5979P]$ for dixie51 and dixie78 respectively.

inversion center. Because of the similarities in both the lattice and space groups, an attempt was made to refine the structural model of $Rb_4Cu(MoO_4)_3$ using the structural information from the $K_4Zn(MoO_4)_3$. An acceptable R-value was obtained, however the thermal parameters for multiple atoms were extremely large. Also, the intensities of the observed structure factors were generally higher than the calculated values indicating either a twinned or incorrect absolute structure. Also, the Zn in $K_4Zn(MoO_4)_3$ adopts a tetrahedral bonding environment, while the Cu

in $Rb_4Cu(MoO_4)_3$ adopts a distorted square planar environment. These differences all contribute to choosing the higher symmetry *Pnma* model over the published $P2_12_12_1$ model.

**Table 5.7**    Atomic Coordinates and Anisotropic Displacement Parameters for $Rb_4Cu(MoO_4)$

| Atom | Wyckoff site | $x$ | $y$ | $z$ | $U_{eq}$ $(Å^2)^a$ | Occupancy |
|---|---|---|---|---|---|---|
| dixie51 – 298 K | | | | | | |
| Rb1 | 4f | ⅓ | ⅔ | 0.16065(9) | 0.0481(7) | 1 |
| Rb2 | 4f | ⅔ | ⅓ | 0.02880(7) | 0.0248(5) | 1 |
| Cu1 | 2a | 0 | 0 | ¼ | 0.0219(7) | 1 |
| Mo1 | 4e | 0 | 0 | 0.09259(5) | 0.0187(4) | 1 |
| Mo2 | 4f | ⅔ | ⅓ | 0.22984(17) | 0.0605(19) | 0.54 |
| O1 | 4e | 0 | 0 | 0.1695(6) | 0.048(4) | 1 |
| O2 | 12k | 0.1547(8) | 0.3094(15) | 0.0672(4) | 0.043(2) | 1 |
| O3 | 4f | ⅔ | ⅓ | 0.1561(11) | 0.048(12) | 0.54 |
| O4 | 12j | 0.380(5) | 0.313(5) | ¼ | 0.087(13) | 0.51 |
| dixie78 – 298 K | | | | | | |
| Rb1 | 8d | 0.33338(8) | 0.47125(3) | 0.50086(12) | 0.0258(2) | 1 |
| Rb2 | 8d | 0.33349(10) | 0.66056(3) | 0.47298(16) | 0.0378(2) | 1 |
| Mo1 | 8d | 0.00050(6) | 0.59262(2) | 0.50809(10) | 0.01809(17) | 1 |
| Mo2 | 8d | 0.16952(16) | 0.73000(6) | 0.9616(3) | 0.0285(2) | 0.48 |
| Cu1 | 4c | 0.00041(14) | ¼ | 0.5088(2) | 0.0223(3) | 1 |
| O1 | 8d | 0.4181(6) | 0.5647(3) | 0.2159(10) | 0.0361(15) | 1 |
| O2 | 4c | 0.4590(12) | ¼ | 0.603(3) | 0.075(4) | 1 |
| O3 | 8d | 0.4280(7) | 0.5690(3) | 0.7497(11) | 0.0410(16) | 1 |
| O4 | 8d | -0.0003(8) | 0.6692(3) | 0.4940(14) | 0.054(2) | 1 |
| O5 | 8d | 0.1542(6) | 0.5672(3) | 0.5002(11) | 0.0388(15) | 1 |
| O6 | 4c | 0.8410(11) | ¼ | 0.325(2) | 0.057(3) | 1 |
| O7 | 4c | 0.6865(11) | ¼ | 0.927(2) | 0.070(4) | 1 |
| O8 | 8d | 0.1736(13) | 0.6559(5) | 0.983(2) | 0.044(4) | 0.51 |

$^a U_{eq}$ is defined as one-third of the trace of the orthogonalized $U_{ij}$ tensor.

The orthorhombic structure of $Rb_4Cu(MoO_4)_3$ is shown in Figure 5.4 and consists of distorted square planar $CuO_4$ bonded to two slightly distorted $MoO_4$ tetrahedral units in the *c*-direction. This square planar $CuO_4$ environment is also seen in other oxide structures such as $La_2CuO_4$.[15] Along the *a*-axis, disordered, slightly distorted $MoO_4$ tetrahedral units link the $CuO_4$ subunits. Table 5.8 lists selected interatomic distances and bond angles for $Rb_4Cu(MoO_4)_3$. Cu – O interatomic distances range from 1.876(6) – 2.023(11) Å and the in plane O – Cu – O angles

are 157.6(5)° and 179.0(5)° which indicate that the $CuO_4$ is highly distorted. Mo1 adopts a slightly distorted tetrahedral environment with interatomic distances ranging from 1.731(6) – 1.780(6) Å. Mo2 is also a slightly distorted tetrahedron with interatomic distances ranging from 1.674(13) – 1.805(12) Å. Mo2 is only half occupied which induces disorder throughout the structure. Rb1 is coordinated to ten oxygen atoms with bond distances ranging from 2.905(6) – 3.294(7) Å. Rb2 is coordinated to six oxygen atoms with bond distances ranging from 2.862(6) – 3.205(11) Å. The Rb polyhedra are disbursed throughout the unit cell. Cu superexchange is possible because the layers of Cu atoms are connected by Mo2 and O atoms.
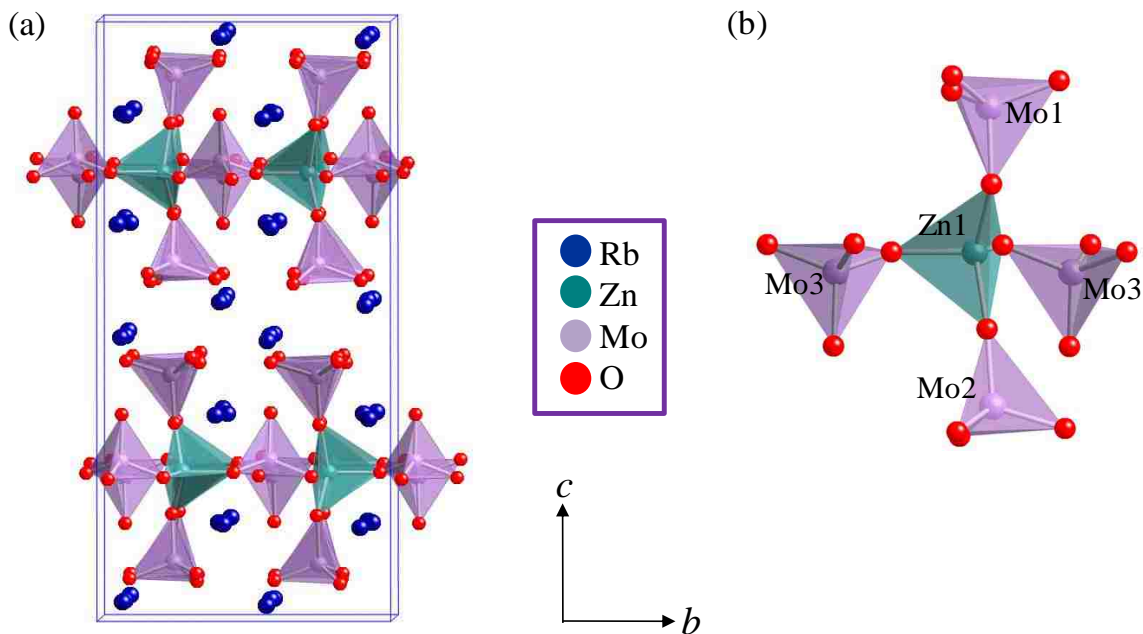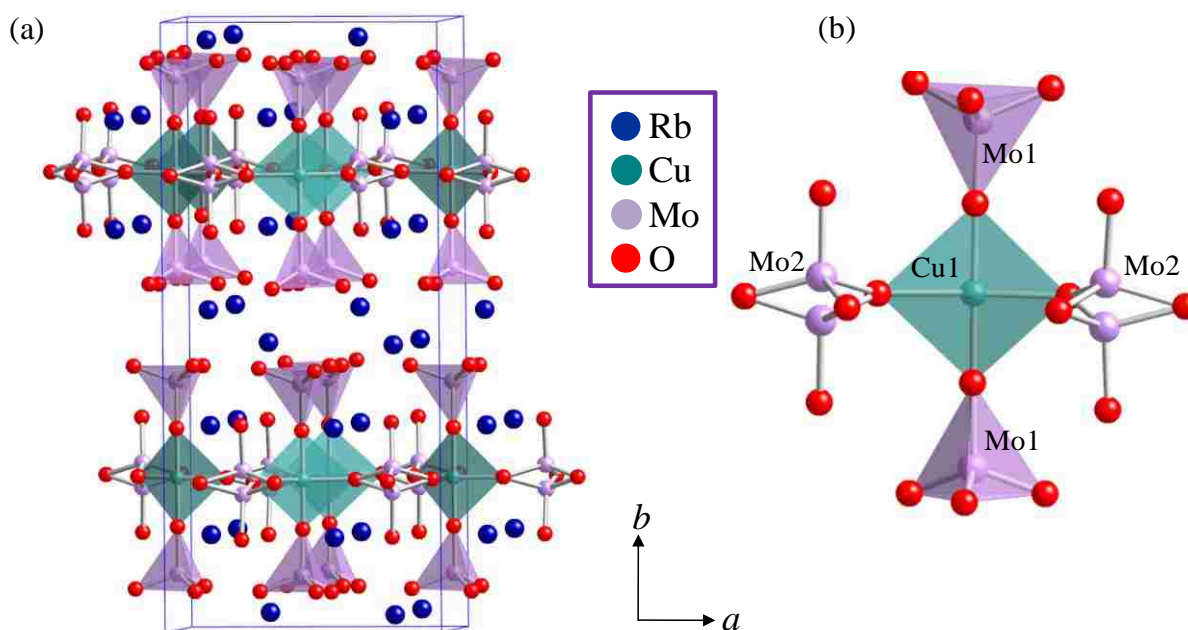


**Figure 5.4** (a) Crystal structure of $Rb_4Cu(MoO_4)_3$ as viewed down the *c*-axis where the blue, green, purple, and red spheres refer to Rb, Cu, Mo, and O atoms respectively. (b) Cu distorted square planar bonding environment of $Rb_4Cu(MoO_4)_3$.

**Table 5.8** Selected Interatomic Distances (Å) and Angles for Orthorhombic $Rb_4Cu(MoO_4)_3$

| | | | | | |
|---|---|---|---|---|---|
| Cu – O4 (x2) | 1.876(6) | Rb2 – O1 | 2.862(6) | O4 – Cu – O6(x2) | 89.7(3) ° |
| Cu – O7 | 2.007(12) | Rb2 – O5 | 2.884(7) | O4 – Cu – O7(x2) | 90.1(3) ° |

63

**Table 5.8** (cont.)

| | | | | | |
|---|---|---|---|---|---|
| Cu – O6 | 2.023(11) | Rb2 – O3 | 2.889(7) | O6 – Cu – O7 | 157.6(5) ° |
| | | Rb2 – O6 | 3.038(9) | O4 – Cu – O4 | 179.0(5) ° |
| Rb1 – O3 | 2.905(6) | Rb2 – O2 | 3.057(10) | | |
| Rb1 – O1 | 2.918(6) | Rb2 – O7 | 3.205(11) | O5 – Mo1 – O1 | 108.8(3) ° |
| Rb1 – O5 | 2.926(6) | | | O1 – Mo1 – O3 | 108.8(3) ° |
| Rb1 – O8 | 2.954(11) | Mo1 – O5 | 1.731(6) | O5 – Mo1 – O3 | 109.2(3) ° |
| Rb1 – O1 | 3.080(7) | Mo1 – O1 | 1.741(6) | O1 – Mo1 – O4 | 109.3(3) ° |
| Rb1 – O3 | 3.093(7) | Mo1 – O3 | 1.748(6) | O5 – Mo1 – O4 | 110.1(4) ° |
| Rb1 – O5 | 3.166(7) | Mo1 – O4 | 1.780(6) | O3 – Mo1 – O4 | 110.6(4) ° |
| Rb1 – O5 | 3.174(7) | | | | |
| Rb1 – O1 | 3.252(7) | Mo2 – O2 | 1.674(13) | O8 – Mo2 – O7 | 102.5(5) ° |
| Rb1 – O3 | 3.294(7) | Mo2 – O8 | 1.726(11) | O2 – Mo2 – O8 | 104.9(5) ° |
| | | Mo2 – O7 | 1.730(11) | O8 – Mo2 – O6 | 109.4(5) ° |
| | | Mo2 – O6 | 1.805(12) | O7 – Mo2 – O6 | 111.2(6) ° |
| | | | | O2 – Mo2 – O6 | 111.9(6) ° |
| | | | | O2 – Mo2 – O7 | 116.1(6) ° |

## 5.3    References:

(1)    Hill, N. A. *Annu. Rev. Mater. Res.* **2002**, *32*, 1-37.

(2)    Ederer, C.; Spaldin, N. A. *Nature Mater.* **2004**, *3*, 849-851.

(3)    Cheong, S. W.; Mostovoy, M. *Nature Mater.* **2007**, *6*, 13-20.

(4)    Kimura, T.; Goto, T.; Shintani, H.; Ishizaka, K.; Arima, T.; Tokura, Y. *Nature* **2003**, *426*, 55-58.

(5)    Arima, T. *J. Phys. Soc. Jpn.* **2007**, *76*.

(6)    Kimura, T.; Sekio, Y.; Nakamura, H.; Siegrist, T.; Ramirez, A. P. *Nature* **2008**, *7*, 291-294.

(7)    Altomare, A.; Burla, M. C.; Camalli, M.; Cascarno, G. L.; Giacovazzo, A.; Guagliardi, A.; Moliterni, A. G. G.; Polidori, G.; Spagna, R. J. *J. Appl. Crystallogr.* **1999**, *32*, 115-119.

(8)    Sheldrick, G. M.; University of Gottingen: Germany, 1997.

(9)    Solodovnikov, S. F.; Klevtsova, R. F.; Glinskaya, L. A.; Klevtsov, P. V. *Sov. Phys. Crystallogr.* **1988**, *33*, 820-824.

(10)    Trunov, K.; Efremov, V. A.; Velikodnyi, Y. A. *Crystal Chemistry and Properties of Double Molybdates and Tungstates [In Russian]*; Nauka: Leningrad, 1986.

(11)    Shannon, R. D. *Acta. Cryst.* **1976**, *32A*, 751-767.

(12)     Klevtsov, P. V.; Kim, V. G.; Kruglik, A. I.; Klevtsova, R. F. *Sov. Phys. Crystallogr.* **1989**, *34*, 384-386.

(13)     Gicquel-Mayer, C.; Mayer, M. M.; Perez, G. *Chimie Minerale* **1976**, *283*, 533-535.

(14)     Gicquel-Mayer, C.; Mayer, M.; Perez, G. *Rev. Chem. Min.* **1980**, *17*, 445-457.

(15)     Chaillout, C.; Cheong, S. W.; Fisk, Z.; Lehmann, M. S.; Marezio, M.; Morosin, B.; Schirber, J. E. *Physica Scripta.* **1989**, *T29*, 97-99.

**CHAPTER 6 – CONCLUSION**

One of the primary goals of this dissertation was to gain a better understanding of structural effects on the physical properties of highly correlated compounds. Identifying structural features in extended solids that favor a desired behavior will help with the design of future materials. More correlations of structure and properties are needed to understand the complex physical properties and to predict the properties of new materials. By growing high-quality single crystals of compounds, detailed structural analyses and physical property measurements can be done. For example, it is well known that layered compounds typically display magnetic anisotropy. It would be beneficial to be able to identify a certain structural features that could lead to desired or unconventional behavior. The key is simply knowing where to look.

The dominant theme of this dissertation revolves around layered antimonide compounds which typically possess unique structural features, unusual bonding, and interesting physical properties. Antimony resides along the metal – insulating border making this phase space attractive to investigate. A systematic study of the orthorhombic $CeNiSb_3$ structure type was conducted in an attempt to correlate structure and properties. By using Sn to grow larger single crystals of $CeNiSb_3$, a new pseudo-ternary compound, $Ln Ni(Sn,Sb)_3$, was discovered. The substitution of the magnetic rare earth element allows for the study of structural changes as well as physical property effects. Another study was done by the substitution of the transition metal Ni with Co or Cu of $LnNiSb_2$ i.e. what happens to the structure and physics when changing carrier density. It was discovered that Cu's coordination preferentially occupies the tetrahedral environment seen in the tetragonal $CeCuSb_2$ structure.

Another important part of this work is the structural study of the double molybdates $Rb_4M(MoO_4)_3$ ($M$ = Mn, Zn, Cu) compounds. These materials were chosen for investigation

because they have frustrated triangular lattices which may lead to polarization. Also the Cu analogue is expected to be a $S = ½$ system which exhibits both frustration and quantum fluctuation. Research of multiferroic materials is extremely attractive because of the promise of new practical applications. Crystal symmetry plays an integral role in predicting and understanding multiferroic behavior in materials. $Rb_4M(MoO_4)_3$ ($M$ = Mn, Zn, Cu) compounds have promising magnetic and electrical behaviors. The Zn and Cu analogues adopt different, orthorhombic structures which are both new structure types. The detailed structural study provided here will be vital in understanding and formulating a mechanism for any multiferroic behavior.

The appendices which follow this chapter provide information on collaborative projects. Structural details of compounds such as $Ln$PdSb$_3$, $EuCu_9Sn_4$, $VB_2$, and $Y_{2-x}Ce_xTi_2O_7$ are discussed within. These projects also follow the structure-property correlation theme that is seen throughout this dissertation.

**APPENDIX 1 – STRUCTURE DETERMINATION OF $Ln$PdSb$_3$ ($Ln$ = La, Ce)**

## A1.1   Introduction

There are seven ternary compounds in the Ce–Pd–Sb system that have been reported thus far: CePdSb,[2] CePd$_2$Sb$_2$,[3] CePdSb$_3$,[4] CePdSb$_2$,[5] Ce$_3$Pd$_6$Sb$_5$,[6] Ce$_8$Pd$_{24}$Sb,[7] and Ce$_2$Pd$_9$Sb$_3$.[8] Some of these phases show heavy fermion behavior.  Heavy fermions possess conduction electrons that have larger effective masses one-hundred times the mass of a free-electron.[9] This leads to a Sommerfeld coefficient ($\gamma$) greater than 100 mJ mol$^{-1}$ K$^{-2}$.  The Sommerfeld coefficient is obtained through a fit from heat capacity measurements after subtracting from the phonon contribution.  Ce$_8$Pd$_{24}$Sb, has a $\gamma$ of ~400 mJ mol$^{-1}$ K$^{-2}$,[10] while CePdSb$_2$ possesses a relatively large enhanced mass with $\gamma$ of ~100 mJ mol$^{-1}$ K$^{-2}$.[11] CePdSb$_3$, of the CaBe$_2$Ge$_2$ structure type,[12] shows no evidence of magnetic ordering and has a $\gamma$ of ~250 mJ mol$^{-1}$ K$^{-2}$.[4]

LaPdSb$_3$ and CePdSb$_3$ grown using flux growth rather than arc melting, crystallize in a different structure type than the previously reported tetragonal CePdSb$_3$ phase.[4]  More recently, magnetic, transport and heat capacity data CePdSb$_3$ was reported and shown to exhibit Kondo lattice behavior and ordered antiferromagnetically below 3.1 K.[13] However, Thamizhavel *et al* described the structure as having different Wyckoff positions from CeNiSb$_3$.[1] This is not the case, as the orthorhombic CePdSb$_3$ is in fact an entirely new structure type and is not the same structure type as CeNiSb$_3$.  $Ln$Ni(Sn,Sb)$_3$ discussed in Chapter 2 adopts this structure type.  The crystal growth and structural determination of $Ln$PdSb$_3$ ($Ln$ = La or Ce) are discussed herein.

## A1.2   Experimental

A1.2.1 Synthesis Optimization

Single crystals of LaPdSb$_3$ and CePdSb$_3$ were grown using excess Sb flux growth

---

[1] Portions of this chapter reprinted by permission of The International Union of Crystallography:  Thomas, E.L.; Gautreaux, D.P.; Chan, J.Y.; "The Layered Intermetallic Compound LaPdSb$_3$", *Acta Cryst.* **2006**, *E62,* I96-I98.

method.  La or Ce ingots (99.9% purity, Alfa Aesar), Pd powder (99.999% purity, Alfa Aesar), and Sb shot (99.9999% purity, Alfa Aesar) were placed into alumina crucibles in a 1:1:10 (*Ln*:Pd:Sb) molar ratio.  Each crucible was then sealed into a fused silica tube under vacuum. The samples were heated to 1150 °C where the temperature was held constant for 10 h then cooled at 5°C h$^{-1}$ to 670 °C.  After dwelling at 670 °C for approximately 24 h, the excess liquid Sb flux was removed by centrifugation.  Silvery plate-shaped crystals with dimensions up to 1 x 2 x 2 mm$^3$ were extracted.  Both the La and Ce analogues of each compound show little or no surface degradation when exposed to air and moisture for extended periods.  The crystal growth method listed above was the optimal synthetic conditions.  Table A1.1 lists the attempted crystal growth conditions for CePdSb$_3$ before the best experimental conditions were discovered.

**Table A1.1**     Attempted Crystal Growths for CePdSb$_3$

| Sample | Elements | Ratio | Temperature Profile | Results |
|--------|----------|-------|---------------------|---------|
| DPG011 | Ce:Pd:Sb | 1:2:20 | 1150 °C for 8 hrs<br>5 °C/hr to 670 °C | CeSb$_2$ |
| DPG013 | Ce:Pd:Sb | 1:1:20 | 1150 °C for 8 hrs<br>5 °C/hr to 670 °C | CeSb$_2$ |
| DPG019 | Ce:Pd:Sb | 1:1.5:20 | 1150 °C for 8 hrs<br>5 °C/hr to 670 °C | CeSb$_2$ |
| DPG020 | Ce:Pd:Sb | 1:1:20 | 1150 °C for 10 hrs<br>5 °C/hr to 670 °C | CeSb$_2$ |
| DPG021 | Ce:Pd:Sb | 1:1:10 | 1150 °C for 10 hrs<br>5 °C/hr to 670 °C | CePdSb$_3$ |

A1.2.2 Single crystal and Powder X-ray diffraction

The samples were identified by both powder and single crystal X-ray diffraction.  The powder pattern of the product revealed the presence of a small amount of CeSb$_2$.  This phase can be identified by visual inspection and removed manually from the *Ln*PdSb$_3$ crystals. Single

crystal X-ray diffraction data were collected by mounting a block-shaped, silver fragment of each of the La and Ce analogues onto a glass fiber of a goniometer. Data collection parameters and crystallographic data are located in Table A1.2. Atomic positions and displacement parameters are located in Table A1.3.

**Table A1.2**  Crystallographic Data for LaPdSb$_3$ and CePdSb$_3$

| Formula | LaPdSb$_3$ | CePdSb$_3$ |
|---|---|---|
| Space Group | *Pbcm* | *Pbcm* |
| $a$ (Å) | 12.9210(4) | 12.7850(3) |
| $b$ (Å) | 6.3450(9) | 6.3210(7) |
| $c$ (Å) | 12.5030(9) | 12.4500(6) |
| $V$ (Å$^3$) | 1025.04(17) | 1006.13(12) |
| Crystal dimensions (mm$^3$) | 0.080 x 0.100 x 0.100 | 0.030 x 0.080 x 0.080 |
| $Z$ | 8 | 8 |
| Temperature (K) | 298 | 298 |
| Crystal Density (g/cm$^3$) | 7.913 | 10.097 |
| $\theta$ range (°) | 3.15 – 30.0 | 3.19 – 30.03 |
| $\mu$ (mm$^{-1}$) | 27.091 | 35.105 |
| Collected reflections | 2790 | 2738 |
| Unique reflections | 1557 | 1523 |
| $R_{\text{int}}$ | 0.0625 | 0.0692 |
| $h$ | $-18 \leq h \leq 18$ | $-17 \leq h \leq 17$ |
| $k$ | $-8 \leq k \leq 8$ | $-8 \leq k \leq 8$ |
| $l$ | $-17 \leq l \leq 17$ | $-17 \leq l \leq 17$ |
| $\Delta\rho_{\text{max}}$ (e Å$^{-3}$) | 3.425 | 7.597 |
| $\Delta\rho_{\text{min}}$ (e Å$^{-3}$) | -3.279 | -4.626 |
| Extinction coefficient | 0.00011(4) | 0.00061(11) |
| [a] $R[F^2 > 2\sigma(F^2)]$ | 0.0443 | 0.0593 |
| [b] $wR_2(F^2)$ | 0.0885 | 0.1534 |

[a] $R_1 = \sum || F_o | - | F_c || / \sum | F_o |$

[b] $wR_2 = \left[ \sum [w(F_o^2 - F_c^2)] / \sum [w(F_o^2)^2] \right]^{1/2}$  where  $w = 1/[\sigma^2 F_0^2 + (0.0401P)^2 + 11.4063P]$  for LaPdSb$_3$ and $w = 1/[\sigma^2 F_0^2 + (0.0187P)^2]$  for CePdSb$_3$.

**Table A1.3**   Atomic Positions and Displacement Parameters for $Ln$PdSb$_3$ ($Ln$ = La or Ce)

| Atom | Wyckoff site | $x$ | $y$ | $z$ | $U_{eq}$ (Å$^2$)$^a$ |
|------|------|------|------|------|------|
| La1 | 4$c$ | 0.69911(8) | ¼ | 0 | 0.0135(2) |
| La2 | 4$d$ | 0.30822(8) | 0.27462(17) | ¾ | 0.0142(3) |
| Pd1 | 8$e$ | 0.10190(7) | 0.04697(17) | 0.86579(8) | 0.0180(3) |
| Sb1 | 4$c$ | 0.97482(9) | ¼ | 0 | 0.0168(3) |
| Sb2 | 4$d$ | 0.77702(9) | 0.2635(2) | ¾ | 0.0155(3) |
| Sb3 | 8$e$ | 0.50306(6) | 0.51263(14) | 0.87808(6) | 0.0156(2) |
| Sb4 | 4$c$ | 0.23291(9) | ¼ | 0 | 0.0150(3) |
| Sb5 | 4$d$ | 0.93812(9) | 0.9219(2) | ¾ | 0.0165(3) |
| | | | | | |
| Ce1 | 4$c$ | 0.69815(9) | ¼ | 0 | 0.0099(3) |
| Ce2 | 4$d$ | 0.30869(9) | 0.27673(19) | ¾ | 0.0099(3) |
| Pd1 | 8$e$ | 0.10344(8) | 0.0475(2) | 0.86583(9) | 0.0136(3) |
| Sb1 | 4$c$ | 0.97381(11) | ¼ | 0 | 0.0128(4) |
| Sb2 | 4$d$ | 0.77250(11) | 0.2645(2) | ¾ | 0.0119(4) |
| Sb3 | 8$e$ | 0.50336(7) | 0.51373(16) | 0.87743(7) | 0.0120(3) |
| Sb4 | 4$c$ | 0.23642(12) | ¼ | 0 | 0.0111(3) |
| Sb5 | 4$d$ | 0.93723(10) | 0.9225(2) | ¾ | 0.0125(4) |

$^a U_{eq}$ is defined as one-third of the trace of the orthogonalized $U_{ij}$ tensor.

## A1.3   Results and Discussion

A1.3.1 Structure

CePdSb$_3$ adopts two polymorphic forms, the tetragonal CaBe$_2$Ge$_2$-type[12] and the orthorhombic CePdSb$_3$-type.[1,13] The two polymorphs were synthesized by different methods: arc-melting[4] and flux growth.[1,13] The arc-melted CaBe$_2$Ge$_2$-type was only characterized by powder X-ray diffraction,[4] while the CePdSb$_3$ type was characterized by both powder and single crystal X-ray diffraction. From here on, CePdSb$_3$ will refer to the new orthorhombic compound synthesized in our lab unless otherwise noted. The structure of CePdSb$_3$ is shown in Figure A1.1. This compound consists of layers of nearly square nets of Sb atoms and layers of slightly distorted face- and edge-sharing PdSb$_6$ octahedra. Between the Sb nets and Pd octahedra are

crystallographically inequivalent Ce atoms which adopt a square anti-prismatic and a mono-capped square anti-prismatic geometry.
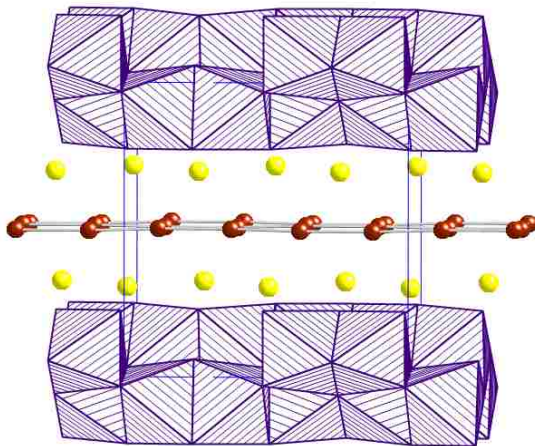


**Figure A1.1**   Crystal structure of *Ln*PdSb$_3$ where the yellow spheres refer to the La or Ce atoms, the maroon spheres refer to the Sb atoms and the purple polyhedral refer to the distorted Pd octahedra.

The *Ln* atoms occupy two inequivalent crystallographic sites and are located above and below the Sb square nets. *Ln*1 atoms adopt an 8-coordinate square anti-prismatic geometry comprised of 4 Sb3 atoms as the base, and 2 Sb2 and 2 Sb4 atoms from the PdSb$_6$ octahedra forming a second square as shown in Figure 3.2 for the La analogue. The *Ln*2 atoms in CePdSb$_3$ adopt a similar geometry as the *Ln*1 however there is an Sb5 capping the top of the square anti-prism. There is a capping atom present near the *Ln*1, however it is located at 3.5629(15) Å and 3.5244(17) Å away for the La and Ce analogues respectively. This is considered too far away for strong bonding/interactions to be considered between *Ln*1 and Sb1.

The nearly square Sb nets are along the *bc*-plane and are composed of Sb3 atoms. The Sb3—Sb3 distances for LaPdSb$_3$ range from 3.0539(16) Å and 3.2028(16) Å. For CePdSb$_3$, the Sb3—Sb3 distances range from 3.0582(18) Å and 3.1730(18) Å. There is a slight distortion to

72

the nets, but they are not as distorted as $CeNiSb_3$.[14] The distorted angles in the Sb nets are 86.96(3)° and 92.95(3)° for $LaPdSb_3$, and 86.71(4)° and 93.21(4)° for $CePdSb_3$. In the similar structure $CeCrSb_3$, the Sb net angles are perfect 90.00°.[15]

The Pd environment of $Ln$PdSb$_3$ is a distorted octahedral environment. The Pd—Sb distances range from 2.6781(13) – 2.8725(15) Å for $LaPdSb_3$ and 2.6786(14) – 2.8228(18) Å for $CePdSb_3$. They are comparable to those found in the binary compound PdSb (NiAs-type) of 2.737 Å, in which Pd adopts an octahedral coordination.[16] The Pd-centered octahedra in $LaPdSb_3$ and $CePdSb_3$ are highly distorted with Sb—Pd—Sb angles as acute as 73.87(3)° and 73.79(3)°. The PdSb$_6$ octahedra are edge sharing in the $b$-direction and are face-sharing in the $c$-direction. The Pd—Pd distances are 2.895(2) Å in $LaPdSb_3$ and 2.884(2) Å in $CePdSb_3$ which are comparable to the Pd-Pd distance of 2.751 Å in Pd metal.[17]

## A1.4   References

(1)    Thomas, E. L.; Gautreaux, D. P.; Chan, J. Y. *Acta Crystallogr. Sect. E: Struct. Rep. Online* **2006**, *E62*, i96-i98.

(2)    Marazza, R.; Rossi, D.; Ferro, R. *J. Less-Common Metals* **1980**, *75*, P25-P28.

(3)    Hofmann, W. K.; Jeitschko, W. *Monatsh. Chem.* **1985**, *116*, 569-580.

(4)    Cava, R. J.; Ramirez, A. P.; Takagi, H.; Krajewski, J. J.; Peck, W. F. *J. Magn. Magn. Mater.* **1993**, *128*, 124-128.

(5)    Sologub, O.; Hiebl, K.; Rogl, P.; Noël, H.; Bodak, O. *J. Alloys Compd.* **1994**, *210*, 153-157.

(6)    Gordon, R. A.; DiSalvo, F. J.; Poettgen, R. *J. Alloys Compd.* **1995**, *228*, 16-22.

(7)    Gordon, R. A.; DiSalvo, F. J. *Z. Naturforsch.* **1996**, *51*, 52-56.

(8)    Gordon, R. A.; DiSalvo, F. J.; Poettgen, R.; Brese, N. E. *J. Chem. Soc., Faraday Trans.* **1996**, *92*, 2167-2171.

(9)    Fisk, Z.; Hess, D. W.; Pethick, C. J.; Pines, D.; Smith, J. L.; Thompson, J. D.; Willis, J. O. *Science* **1988**, *239*, 33-42.

(10)    Cho, B. K.; Gordon, R. A.; Jones, C. D. W.; DiSalvo, F. J.; Kim, J. S.; Stewart, G. R. *Phys. Rev. B* **1998**, *57*, 15191-15196.

(11)    Muro, Y.; Takeda, N.; Ishikawa, M. *J. Alloys Compd.* **1997**, *257*, 23-29.

(12)    Eisenmann, B.; Schaefer, H.; May, N.; Müller, W. *Z. Naturforsch. B: Chem. Sci.* **1972**, *27*, 1155-1157.

(13)    Thamizhavel, A.; Nakashima, H.; Shiromoto, T.; Obiraki, Y.; Matsuda, T. D.; Haga, Y.; Ramakrishnan, S.; Takeuchi, T.; Settai, R.; Onuki, Y. *J. Phys. Soc. Jpn.* **2005**, *74*, 2617-2621.

(14)    Macaluso, R. T.; Wells, D. M.; Sykora, R. E.; Albrecht-Schmitt, T. E.; Mar, A.; Nakatsuji, S.; Lee, H.; Fisk, Z.; Chan, J. Y. *J. Solid State Chem.* **2004**, *177*, 293-298.

(15)    Brylak, M.; Jeitschko, W. *Z. Naturforsch. B: Chem. Sci.* **1995**, *50*, 899-904.

(16)    Pratt, J. N.; Myles, K. M.; Darby, J. B. J.; Mueller, M. H. *J. Less-Common Metals* **1968**, *14*, 427-433.

(17)    Donohue, P. C. *J. Solid State Chem.* **1975**, *12*, 80-3.

## APPENDIX 2 – EuCu$_9$Sn$_4$

### A2.1 Introduction

Many compounds of the NaZn$_{13}$ structure type have received attention because of the remarkable properties they exhibit. UBe$_{13}$, a heavy fermion superconductor, has an enormous specific heat coefficient of $\gamma$ = 1100 mJ mol$^{-1}$ K$^{-2}$.[1] LaCo$_{13}$ possesses the large ordering temperature $T_N$ = 1290 °C.[2] In 1994, a tetragonal derivative of the NaZn$_{13}$ structure was discovered in LaFe$_9$Si$_4$.[3] Many analogues adopting this tetragonal structure have been studied. Magnetic properties of $Ln$Cu$_9$Sn$_4$ compounds ($Ln$ = La – Nd) all order ferromagnetically from 5 – 15 while no magnetic ordering is observed down to 1.5 K in $Ln$Cu$_{9.4}$Sn$_{3.6}$, which adopts the cubic NaZn$_{13}$ structure type.[4] The atomic ordering of the tetragonal structure leads to magnetic ordering, while the disorder in the cubic $Ln$Cu$_{9.4}$Sn$_{3.6}$ hinders any magnetic order down to 2 K.[4] Recently, the structure and magnetic properties of EuCu$_9$Sn$_4$, EuCu$_4$Sn$_2$, and EuCuSn$_2$ were reported.[5] In our effort to continue the exploration of the $Ln$ – Cu – Sn phase space, high quality single crystals of EuCu$_9$Sn$_4$ were grown by Sn flux to study the transport properties of this structure type. The synthesis, crystal structure determination, and physical properties of high quality single crystals of EuCu$_9$Sn$_4$ are discussed herein.

### A2.2 Experimental

A2.2.1 Synthesis

Single crystals of EuCu$_9$Sn$_4$ were synthesized using a Sn flux growth method. Eu pieces (99.9%, Alfa Aesar), Cu powder (99.999%, Alfa Aesar), and Sn shot (99.99%, Alfa Aesar) were placed into an alumina crucible in a 1:1:20 stoichiometric ratio. After sealing the crucible into an evacuated fused-silica tube, the entire reaction vessel was placed into a furnace for heat treatment. The sample was heated at 1150 °C for 48 h followed by a slow-cooling at 5 °C/h down to 300 °C. After the sample temperature reached 300 °C, the excess flux was removed by

centrifugation.   The sample contained thin metallic plates, which were determined to be $EuCu_9Sn_4$.  There is no surface degradation to the crystal visible over a period of months.  Some of the crystals contained small amounts of Sn present on the surface which were removed mechanically.

A2.2.2 Single Crystal X-Ray Diffraction

Single crystal X-ray diffraction was performed on a crystal with dimensions of 0.025 x 0.1 x 0.125 $mm^3$.  The crystal was mounted onto the glass fiber of the goniometer with epoxy and data were collected on a Nonius Kappa CCD X-ray diffractometer ($MoK_\alpha$ = 0.71073 Å). The unit cell parameters were determined from images taken at a rotation of 15 °$\varphi$.  The structural model was solved by direct methods using SIR92 [6] and refined using SHELXL97.[7] The data were corrected for absorption and the displacement parameters were refined as anisotropic.  Crystallographic data and data collection parameters are listed in Table A2.1 and atomic positions and anisotropic displacement parameters are listed in Table A2.2.

**Table A2.1**    Crystallographic Data for $EuCu_9Sn_4$

| | |
|---|---|
| Formula | $EuCu_9Sn_4$ |
| Formula Units (amu) | 1198.58 |
| Space Group | $I4/mcm$ |
| $a$ (Å) | 8.641(2) |
| $c$ (Å) | 12.433(3) |
| $V$ (Å) | 928.3(4) |
| Crystal Size ($mm^3$) | 0.03/0.10/0.13 |
| Z | 4 |
| Temperature (°C) | 20(2) |
| Density (g $cm^{-1}$) | 8.576 |
| $\theta$ Range (°) | 3.28-30.03 |
| $\mu$ ($mm^{-1}$) | 37.254 |
| $R_{int}$ | 0.0455 |
| Collected Reflections | 1058 |
| Unique Reflections | 390 |
| $h$ | $-12 \leq h \leq 12$ |
| $k$ | $-8 \leq k \leq 8$ |
| $l$ | $-17 \leq l \leq 13$ |

| | |
|---|---|
| $\Delta\rho_{max}$ (e Å$^{-3}$) | 2.569 |
| $\Delta\rho_{min}$ (e Å$^{-3}$) | -2.425 |
| Extinction coefficient | 0.0038(5) |
| [a] $R[F^2 > 2\sigma(F^2)]$ | 0.0441 |
| [b] $wR_2(F^2)$ | 0.1282 |

[a] $R_1(F) = \sum \left\| F_0 \right| - \left| F_c \right\| / \sum \left| F_0 \right|$

[b] $R_w(F_0^2) = \sum [w(F_0^2 - F_c^2)] / \sum [w(F_0^2)^2]^{1/2}$ ; where $w = 1/[\sigma^2(F_0^2) + (0.0850P)^2 + 12.4528P]$

**Table A2.2**     Atomic Positions and Displacement Parameters for EuCu$_9$Sn$_4$

| Atom | Wyckoff Site | $x$ | $y$ | $z$ | $U_{eq}$ (Å$^2$)[a] |
|---|---|---|---|---|---|
| Eu1 | 4a | 0 | 0 | ¼ | 0.01318 |
| Cu1 | 16l | 0.108912 | 0.608912 | 0.174330 | 0.01376 |
| Cu2 | 16k | 0.798244 | 0.944009 | 0 | 0.01561 |
| Cu3 | 4d | 0 | ½ | 0 | 0.01186 |
| Sn1 | 16l | 0.315068 | 0.815065 | 0.125358 | 0.01106 |

[a] $U_{eq}$ is defined as one-third of the trace of the orthogonalized $U_{ij}$ tensor.

A2.2.3 Physical Property Measurements

Magnetic measurements on single crystals of EuCu$_9$Sn$_4$ were performed using a Quantum Desing MPMS Superconducting Quantum Interference Device (SQUID) magnetometer. Temperature-dependent susceptibility data were measured at an applied field of 0.1 T from 2 K – 300 K and the field-dependent magnetization data were measured at 2 K up to 7 T. Transport property measurements were conducted using a Quantum Design Physical Property Measurement System (PPMS) at ambient pressure. Resistivity data were measured at 0 T, 0.5 T and 9 T while magnetoresistance data up to 9 T were measured at 2 K.

## A2.3   Results and Discussion

A2.3.1 Structure

EuCu$_9$Sn$_4$ crystallizes in the tetragonal space group $I4/mcm$ (# 140) with lattice parameters of $a$ = 8.641(2) Å and $c$ = 12.433(3) Å. This is in agreement with the EuCu$_9$Sn$_4$

lattice parameters $a = 8.633(2)$ Å and $c = 12.425(2)$ Å reported by Mazzone *et al.*[5] The current work was all ready in progress before the Mazzone paper was published in early 2008. $EuCu_9Sn_4$ adopts the $LaFe_9Si_4$ structure type which is a distorted variation of the cubic $NaZn_{13}$ structure type.[3,8] There are five atomic positions in the $EuCu_9Sn_4$ structure: Eu1, Cu1, Cu2, Cu3, and Sn1 which are listed in Table A2.2 with the displacement parameters. The structure shown in Figure A2.1 consists of alternating layers of Cu3 icosahedra and slightly irregular Eu snub-cubes. Figure A2.1 (b) highlights the Cu3 and Eu environments. Table A2.3 displays selected interatomic distances within the Cu3 and Eu subunits. Though similar, the distances vary slightly confirming that both the Cu3 iscoahedra and Eu snub-cubes are somewhat distorted. The Eu analogue does not follow the lanthanide contraction seen in other $LnCu_9Sn_4$ compounds ($Ln = La - Nd$) suggesting that Eu may have an oxidation state of +2 in this compound.[4]
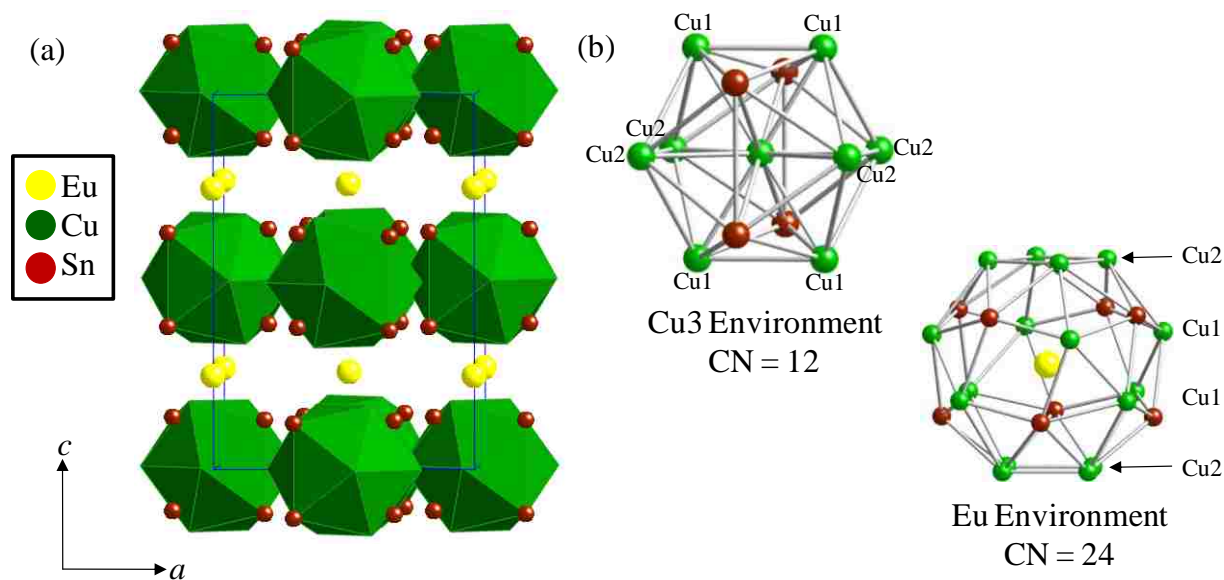


**Figure A2.1**  (a) Crystal structure of $EuCu_9Sn_4$ viewed down the *b* axis. (b) Images of environments of Cu3 icosahedra and Eu distorted snub-cubes.

78

**Table A2.3**    Selected Interatomic Distances (Å) of EuCu$_9$Sn$_4$ Subunits

| Eu Irregular Snub Cube | | Cu3-Icosahedra | |
|---|---|---|---|
| Eu1-Sn1(x8) | 3.5167(8) | Cu3-Sn1(x4) | 2.7453(9) |
| Eu1-Cu1(x8) | 3.6320(10) | Cu3-Cu1(x4) | 2.5434(15) |
| Eu1-Cu2(x8) | 3.5965(10) | Cu3-Cu2(x4) | 2.6222(15) |

A2.3.2 Physical Properties

The magnetic susceptibility of EuCu$_9$Sn$_4$ was measured from 2 – 300 K with an applied field of 0.1 T for several single crystals aligned side-by-side.    Figure A2.2 displays the
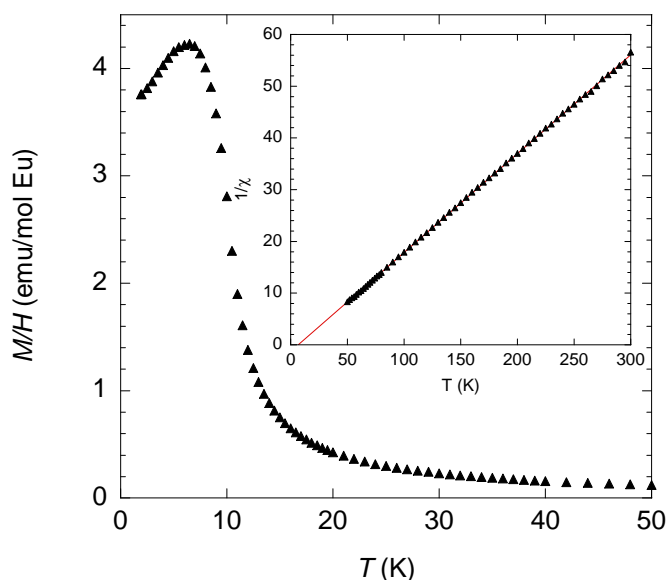


**Figure A2.2**   Magnetic Susceptibility of EuCu$_9$Sn$_4$ measured with an applied field of 0.1 T from 2 – 300 K.  Data from 2 – 50 K were shown to enhance the ordering seen below 20 K.  The inset displays the inverse susceptibity.

susceptibility data from 2 – 50 K and the inset shows the inverse susceptibility plot.  EuCu$_9$Sn$_4$

orders ferromagnetically at ~ 10 K.  This is in agreement with the published magnetic data where

this compound also shows ferromagnetic ordering at 10 K.[5]  The experimental effective magnetic

moment was determined from a Curie-Weiss fit of the inverse data from 50 – 300 K.  The

experimental moment of 6.48 $\mu_B$ is close to the calculated moment for Eu$^{2+}$ of 7.93.  This is

further evidence that this compound is divalent and is in agreement structure. The Weiss temperature ($\theta$) is 6.5 K is of ferromagnetic fluctuations. Mazzone *et al* reported a $\mu_{eff} = 7.96\ \mu_B$ and a Weiss temperature of $\theta = 7$ K which is consistent with this work.[5]

The magnetization as a function of field measured at 2 K for $EuCu_9Sn_4$ is shown in Figure A2.3. The magnetization increases sharply up to 1 T then begins to saturate. The experimental saturation moment is ~ 4.4 $\mu_B$ which is well below the calculated saturation moment for $Eu^{2+}$ is 7 $\mu_B$. This behavior is typical for rare earth compounds and can be explained by partial screening of the moments by the conduction electrons. The shape of the magnetization follows the behavior of a classical ferromagnet.
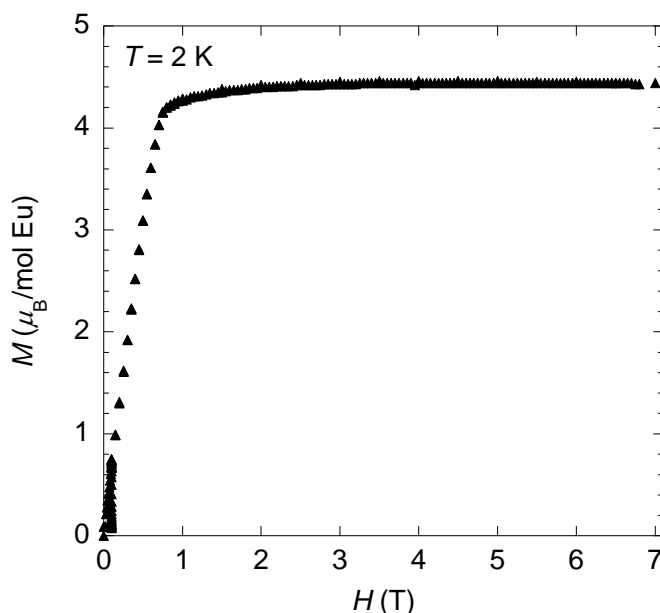


**Figure A2.3**  Magnetization of $EuCu_9Sn_4$ as a function of field measured at 2 K.

Resistivity measurements as a function of temperature were performed at 0 T, 0.05 T and 9 T and are shown in Figure A2.4. The resistivity at all fields shows simple metallic behavior. There is a slight downturn in the resistivity at 0 T at ~3.3 K which coincides with the superconducting transition of Sn. Data were collected in the presence of field to destroy the

80

critical field of Sn and at 0.05 T, the slight downturn is eliminated from the resistivity data

indicating the presence of a small amount of topical Sn.   The increase in resistivity seen at 9 T is

an indication of a change in resistance with the application of a magnetic field so
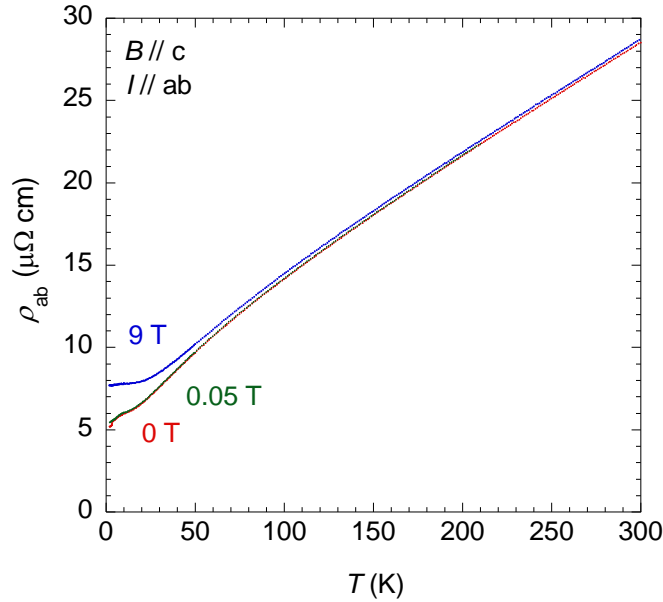


**Figure A2.4**   Resistivity measurements of $EuCu_9Sn_4$ as a function of temperature measured at 0 T, 0.05 T, and 9 T.
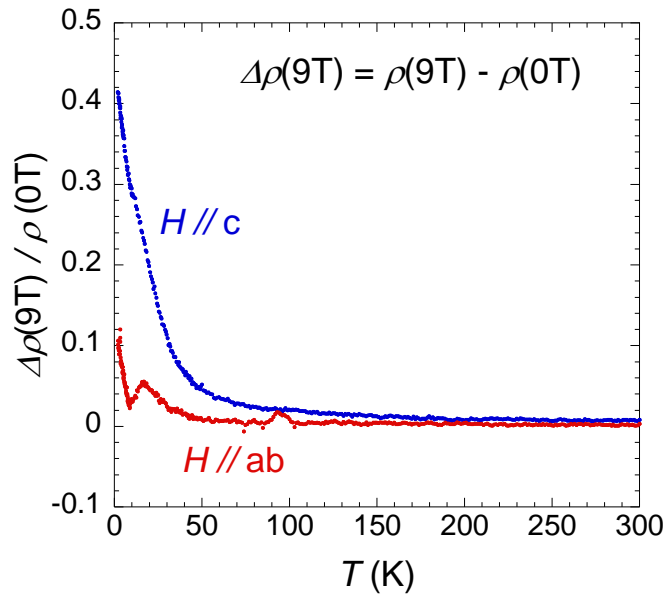


**Figure A2.5**   Change in resistivity of $EuCu_9Sn_4$ from 0 T to 9 T measured with field oriented in two directions: parallel to the *ab* plane and parallel to the *c* axis.

magnetoresistance was measured. Figure A2.5 shows the change in resistivity from 0 T to 9 T as a function of temperature. When the magnetic field is applied parallel to the *c* axis of the crystal, the magnetoresistance is ~ 40 % at 2 K. When the magnetic field is applied parallel to the *ab*-plane of the crystal, the change in resistivity is not as large. This is further evidence of the highly anisotropic nature of these crystals.

**A2.4 References**

(1)     Ott, H. R.; Rudigier, H.; Fisk, Z.; Smith, J. L. *Phys. Rev. Lett.* **1983**, *50*, 1595-1598.

(2)     Velge, W. A. J. J.; Buschow, K. H. J. *J. Appl. Phys.* **1968**, *39*, 1717-1720.

(3)     Tang, W.; Liang, J.; Chen, X.; Rao, G. *J. Appl. Phys.* **1994**, *76*, 4095-4098.

(4)     Singh, S.; Fornasini, M. L.; Manfrinetti, P.; Palenzona, A.; Dhar, S. K.; Paulose, P. L. *J. Alloys Compd.* **2001**, *317-318*, 560-566.

(5)     Mazzone, D.; Paulose, P. L.; Dhar, S. K.; Fornasini, M. L.; Manfrinetti, P. *J. Alloys Compd.* **2008**, *2008*.

(6)     Altomare, A.; Cascarno, G. L.; Giacovazzo, A.; Guagliardi, A. *J. Appl. Crystallogr.* **1993**, *26*, 343-350.

(7)     Sheldrick, G. M.; University of Gottingen: Germany, 1997.

(8)     Shoemaker, D. P.; Marsh, R. E.; Ewing, F. J.; Pauling, L. *Acta Cryst.* **1952**, *5*, 637-644.

**APPENDIX 3 –STRUCTURAL DETERMINATION OF VB$_2$**

**A3.2   Introduction**

Transition metal diborides have been extensively studied for many years.  However the recent discovery of superconducting behavior of MgB$_2$ at 39 K has refueled the interest in these simple diborides.[2]  Transition metal diborides exist for all first row transition metals between Sc – Fe.  The wide range of isostructural compounds make this structure type intriguing because of the chance to study the property changes throughout all the isostructural compounds.  Recently, our collaborators discovered that VB$_2$ has a very large magnetoresistance of ~ 1100 % at low temperatures.[1]  This extremely large magnetoresistive behavior is highly dependent on the quality of the single crystals measured.[1]  To gain better insight into the properties of this structure, very accurate lattice parameters were needed for energy band calculations and to determine the Fermi surface of VB$_2$.  Therefore the single crystal X-ray diffraction data of VB$_2$ were collected at 293 K and 90 K on high quality single crystals and the results are reported herein.

**A3.2   Experimental and Results**

High quality single crystals of VB$_2$ were synthesized by Al flux by collaborators in the Department of Physics and Astronomy at Louisiana State University.[1]  The crystals grew as both rods and plates and powder X-ray diffraction was used to confirm that the sample was single phase.  Powder X-ray diffraction data were collected on a Bruker D8 Advance Diffractometer with monochromatic Cu K$_\alpha$ radiation ($\lambda$ = 1.540562 Å) at room temperature and it was determined that both crystal morphologies are VB$_2$.  Accurate lattice parameters were needed for energy band calculations, therefore the single crystal X-ray diffraction data were collected at 293

---

[1] Portions of this chapter reprinted by permission of The Institute of Physics:  Karki, A.B.; Gautreaux, D.P.; Chan, J.Y.; Harrison, N.; Browne, D.A.; Goodrich, R.G.; Young, D.P.; "Magnetotransport Properties and the Fermi Surface of Single Crystal VB$_2$", *J.Phys: Condens. Matter.* **2008**, *20,* 035209.

K and 90 K. A 0.05 x 0.075 x 0.125 mm$^3$ crystal fragment was glued to a glass fiber with epoxy and mounted on the goniometer of a Nonius Kappa CCD diffractometer equipped with Mo K$\alpha$ radiation ($\lambda$ = 0.71073 Å). For low temperature data collections, the crystal was mounted onto the fiber using vacuum grease and no epoxy was used. The temperature was regulated with a cooled nitrogen gas stream produced by an Oxford Cryostream Cooler. Initial unit cell parameters were determined from images taken at a rotation of 15 °$\varphi$. The structural model was solved by direct methods using SIR97[3] and refined using SHELXL97.[4] The data were corrected for absorption and the displacement parameters were refined as anisotropic. Selected crystallographic data and data collection parameters are listed in Table A3.1. Atomic positions and anisotropic displacement parameters are listed in Table A3.2 for both data collections. VB$_2$ adopts the well known AlB$_2$ structure type and is displayed in Figure A3.1. The structure consists of alternating layers of vanadium atoms and graphite like sheets of boron. There are no structural discrepancies between our VB$_2$ structure and the known AlB$_2$ structure type. The structural information obtained from this study was used for energy band calculations and the results are reported in the *Journal of Physics: Condensed Matter*.

**Table A3.1**     Crystallographic Data for VB$_2$

| Sample | AK104 | AK104 |
|---|---|---|
| Space Group | *P6/mmm* | *P6/mmm* |
| Temperature (K) | 293 | 90 |
| $a$ (Å) | 3.0000(4) | 2.9980(10) |
| $b$ (Å) | 3.0000(4) | 2.9980(10) |
| $c$ (Å) | 3.0620(8) | 3.044(2) |
| $V$ (Å$^3$) | 23.866(8) | 23.69(2) |
| Z | 1 | 1 |
| Density (g cm$^{-1}$)5.049 | 5.085 | |
| $\theta$ Range (°) | 7.86-29.55 | 6.70-29.57 |
| $\mu$ (mm$^{-1}$) | 9.274 | 9.341 |
| $\Delta\rho_{max}$ (e Å$^{-3}$) | 0.697 | 0.690 |
| $\Delta\rho_{min}$ (e Å$^{-3}$) | -0.428 | -0.521 |

| | | | |
|---|---|---|---|
| [a] $R[F^2 > 2\sigma(F^2)]$ | 0.0188 | | 0.0252 |
| [b] $wR_2(F^2)$ | 0.0400 | | 0.0563 |

[a] $R_1(F) = \sum \left\| F_0 \right| - \left| F_c \right\| / \sum \left| F_0 \right|$

[b] $R_w(F_0^2) = \sum [w(F_0^2 - F_c^2)] / \sum [w(F_0^2)^2]^{1/2}$ ; where $w = 1/[\sigma^2(F_0^2) + (0.0167P)^2]$,

$w = 1/[\sigma^2(F_0^2) + (0.1000P)^2]$, for 293 K and 90 K respectively

**Table A3.2**    Atomic Positions and Displacement Parameters for $VB_2$

| | Atom | Wyckoff Site | $x$ | $y$ | $z$ | $U_{eq}$ (Å$^2$)[a] |
|---|---|---|---|---|---|---|
| 293 K | | | | | | |
| | V1 | 1$a$ | 0 | 0 | ¼ | 0.0033(16) |
| | B1 | 2$d$ | ⅓ | ⅔ | ½ | 0.000(2) |
| 90 K | | | | | | |
| | V1 | 1$a$ | 0 | 0 | ¼ | 0.0033(16) |
| | B1 | 2$d$ | ⅓ | ⅔ | ½ | 0.0036(19) |

[a] $U_{eq}$ is defined as one-third of the trace of the orthogonalized $U_{ij}$ tensor.
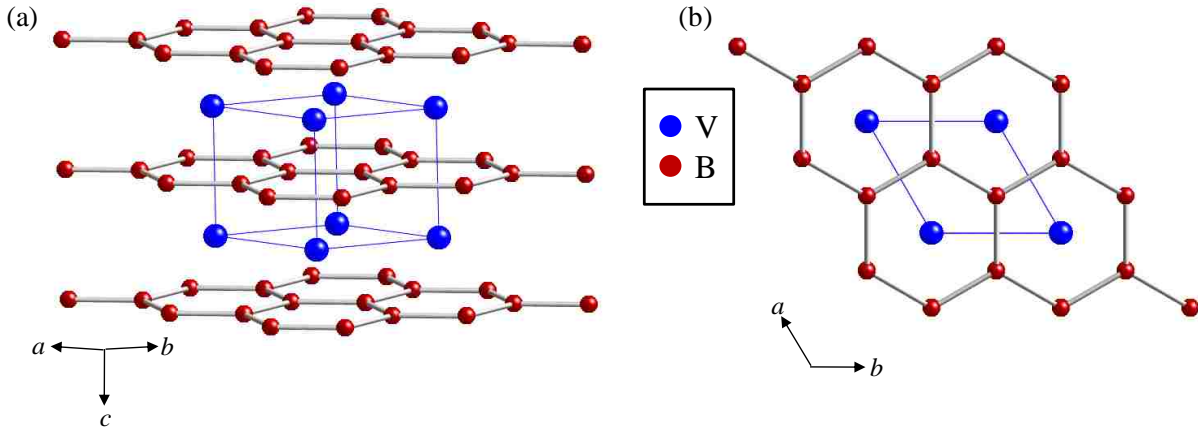


**Figure A3.1**    (a) Layered crystal structure of $VB_2$ viewed in the [110] direction.  (b) View down the $c$-axis of the crystal structure of $VB_2$.

## A3.2   References

(1)    Karki, A. B.; Gautreaux, D. P.; Chan, J. Y.; Harrison, N.; Browne, D.; Goodrich, R. G.; Young, D. P. *J. Phys.: Condens. Matter* **2008**, *20*, 035209.

(2)    Nagamatsu, J.; Nakagawa, N.; Muranaka, T.; Zenitani, Y.; Akimitsu, J. *Nature* **2001**, *410*, 63-64.

(3)     Altomare, A.; Burla, M. C.; Camalli, M.; Cascarno, G. L.; Giacovazzo, A.; Guagliardi, A.; Moliterni, A. G. G.; Polidori, G.; Spagna, R. J. *J. Appl. Crystallogr.* **1999**, *32*, 115-119.

(4)     Sheldrick, G. M.; University of Gottingen: Germany, 1997.

**APPENDIX 4 – $Y_{2-x}Ce_xTi_2O_7$**

**A4.1   Introduction**

Many research groups are focused on finding alternative fuel sources because of the uncertainty of the world's supply of fossil fuels.   An appealing alternative fuel source is hydrogen because it is abundantly found in $H_2O$.   Splitting of $H_2O$ by means such as photocatalysis or electrocatalysis would yield the desired $H_2$ product.   $CeO_2$ is used in automobile catalytic converters and has the ability to release $O_2$ ($2\ CeO_2 \leftrightarrow Ce_2O_3 + \frac{1}{2}\ O_2$).[1] This ability to release $O_2$ might suggest applications of $CeO_2$ as a water oxidation catalyst.  Solid oxides are ideal materials for water oxidation electrodes because they are likely to be inert under the high positive potentials required.

There are very few practical electrocatalytic materials for generating $H_2$ by the oxidation of $H_2O$ and catalysts of this reaction are of great interest.  The introduction of Ce into $Y_2Ti_2O_7$ may also introduce redox activity, therefore, samples of $Y_{2-x}Ce_xTi_2O_7$ were synthesized for the investigation of their electrocatalytic behavior.   A complete solid solution is not expected because the end members of the series, $Y_2Ti_2O_7$ and $Ce_2Ti_2O_7$, adopt cubic and monoclinic structure respectively.[2,3]  Powder neutron diffraction data and physical properties are reported herein for $Y_{2-x}Ce_xTi_2O_7$ (nominal $x = 0, 0.15, 0.35$).

**A4.2   Experimental and Results**

A4.2.1 Synthesis

$Y_{2-x}Ce_xTi_2O_7$ ($x = 0, 0.15, 0.35$) compounds have been synthesized using solid state ceramic synthesis.  Samples are prepared using a combination of grinding and mixing the constituent oxide powders, then pressing a pellet of the resulting mixture.   The amounts of reactant oxide powders needed to make ~7 g of product were obtained using the following reaction:  $2\ TiO_2 + x\ CeO_2 + (\frac{2-x}{2})\ Y_2O_3 \rightarrow Y_{2-x}Ce_xTi_2O_7$.  Each sample was mixed and pressed

into a pellet with a diameter of ~ 10 mm. The pellets were then dwelled at temperatures of 1000 °C, 1100 °C, 1300 °C, 1400 °C, and 1450 °C. The samples remained at each temperature for ~ 2 days with intermittent grinding and repressing of the pellet between each heat treatment. Powder X-ray diffraction patterns were measured between each heat treatment to determine if the phase assemblage has reached equilibrium.

A4.2.2 Neutron Powder Diffraction

Neutron powder diffraction (NPD) data were collected for all samples on BT-1 with a Cu(311) monochromator ($\lambda$ = 1.5403 Å). Experimental and statistical data are provided in Table A4.1. The NPD data were refined using Rietveld refinement. The observed NPD data are in very good agreement with the calculated NPD data and are shown in Figure A4.1. There are some small impurity peaks (< 4%), which can be attributed to a rutile $TiO_2$ impurity. The $Y_{2-x}Ce_xTi_2O_7$ ($x$ = 0, 0.34, and 0.62) compounds crystallize in the cubic space group $Fd\overline{3}m$ (No. 227, origin choice 2). The atomic positions and thermal parameters for all three compounds are shown in Table A4.2. There are no oxygen deficiencies in any of the pyrochlore compounds. The Ce atoms occupy the 16$c$ site which was expected based on the ionic radii of the atoms in the compound. Although $Ce_2Ti_2O_7$ adopts a monoclinic structure type, the introduction of Ce ions at $x$ < 0.63 into the cubic pyrochlore structure does not induce any structural phase changes.

**Table A4.1**  Experimental and Statistical Neutron Data for $Y_{2-x}Ce_xTi_2O_7$

| Nominal Composition | $Y_2Ti_2O_7$ | $Y_{1.85}Ce_{0.15}Ti_2O_7$ | $Y_{1.65}Ce_{0.35}Ti_2O_7$ |
|---|---|---|---|
| Observed Composition | $Y_2Ti_2O_7$ | $Y_{1.66}Ce_{0.34}Ti_2O_7$ | $Y_{1.37}Ce_{0.63}Ti_2O_7$ |
| Chi$^2$ | 1.849 | 2.223 | 2.285 |
| $R_p$ | 3.96 | 3.82 | 4.05 |
| $wR_p$ | 4.82 | 4.49 | 5.04 |
| $a$ (Å) | 10.09983(18) | 10.10634(17) | 10.11409(5) |
| $TiO_2$ (% wt) | 3.21 | 1.95 | 0.18221 |
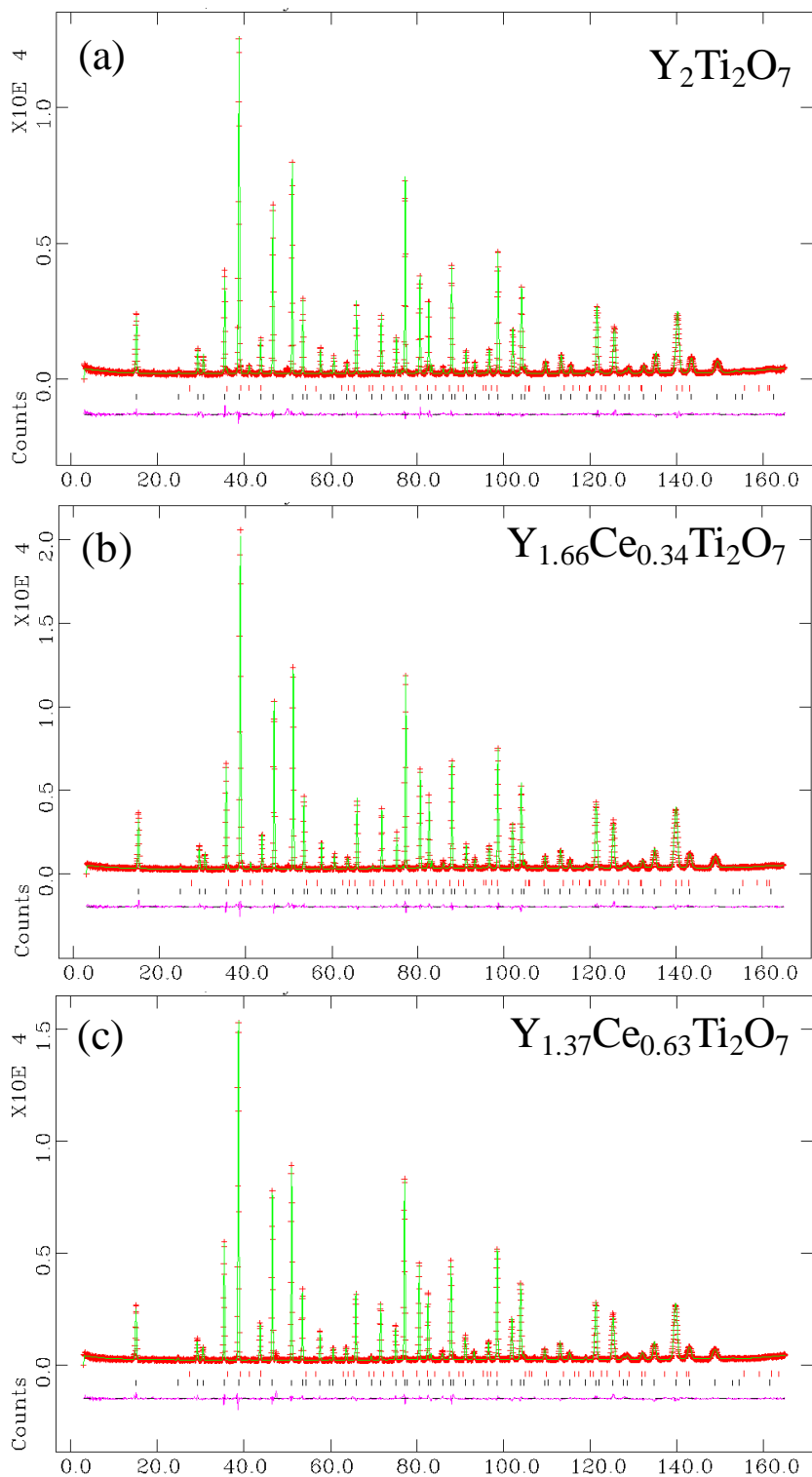
**Figure A4.1** Neutron powder diffraction patterns of (a) $Y_2Ti_2O_7$, (b) $Y_{1.66}Ce_{0.34}Ti_2O_7$, and (c) $Y_{1.37}Ce_{0.63}Ti_2O_7$ where the red crosses are the observed NPD pattern, solid black tick marks are the calculated NPD profiles of $Y_{2-x}Ce_xTi_2O_7$, solid red tick marks are the calculated NPD profiles of rutile $TiO_2$, and magenta patterns are the difference NPD profiles for $Y_{2-x}Ce_xTi_2O_7$.

**Table A4.2**    Atomic Positions and Thermal Parameters of $Y_{2-x}Ce_xTi_2O_7$

| Atom | Wyckoff Site | $x$ | $y$ | $z$ | Occupancy | $U_{iso}$ |
|---|---|---|---|---|---|---|
| $Y_2Ti_2O_7$ | | | | | | |
| Y | 16c | 0 | 0 | 0 | 1.0 | 0.00859(18) |
| Ti | 16d | ½ | ½ | ½ | 1.0 | 0.00506(30) |
| O1 | 48f | 0.420986(61) | ⅛ | ⅛ | 1.0 | 0.00811(13) |
| O2 | 8a | ⅛ | ⅛ | ⅛ | 1.0 | 0.00564(28) |
| $Y_{1.66}Ce_{0.34}Ti_2O_7$ | | | | | | |
| Y | 16c | 0 | 0 | 0 | 0.830(11) | 0.00779(22) |
| Ce | 16c | 0 | 0 | 0 | 0.170(11) | 0.00779(22) |
| Ti | 16d | ½ | ½ | ½ | 1.0 | 0.00593(27) |
| O1 | 48f | 0.421195(51) | ⅛ | ⅛ | 1.0 | 0.00884(13) |
| O2 | 8a | ⅛ | ⅛ | ⅛ | 1.0 | 0.00579(24) |
| $Y_{1.37}Ce_{0.63}Ti_2O_7$ | | | | | | |
| Y | 16c | 0 | 0 | 0 | 0.686(12) | 0.00921(28) |
| Ce | 16c | 0 | 0 | 0 | 0.314(12) | 0.00921(28) |
| Ti | 16d | ½ | ½ | ½ | 1.0 | 0.00762(33) |
| O1 | 48f | 0.420986(61) | ⅛ | ⅛ | 1.0 | 0.01082(15) |
| O2 | 8a | ⅛ | ⅛ | ⅛ | 1.0 | 0.00659(28) |

A4.2.3 Physical Properties

The magnetic susceptibility and electrical resistivity of $Y_{2-x}Ce_xTi_2O_7$ ($x$ = 0, 0.34, 0.63) were measured. $Y_{2-x}Ce_xTi_2O_7$ ($x$ = 0, 0.34, 0.63) were all insulators. The magnetic susceptibility data was measured at 0.1 T for $Y_{1.66}Ce_{0.34}Ti_2O_7$ and $Y_{1.37}Ce_{0.63}Ti_2O_7$ and are displayed in Figure A4.2. Both $Y_{1.66}Ce_{0.34}Ti_2O_7$ and $Y_{1.37}Ce_{0.63}Ti_2O_7$ are paramagnetic down to 2 K and $Y_2Ti_2O_7$ is not magnetic. Effective moments of 0.44 $\mu_B$ and 0.55 $\mu_B$ were obtained from a modified Curie-Weiss fit of the data from 2 – 275 K for $Y_{1.66}Ce_{0.34}Ti_2O_7$ and $Y_{1.37}Ce_{0.63}Ti_2O_7$ respectively. A modified Curie-Weiss fit was used because the inverse susceptibility plots were not linear. The calculated magnetic moment for a $Ce^{3+}$ ion is 2.54 $\mu_B$, while $Ce^{4+}$ is not magnetic. Weiss temperatures ($\theta$) of -0.81 K and -1.01 K were obtained for $Y_{1.66}Ce_{0.34}Ti_2O_7$ and $Y_{1.37}Ce_{0.63}Ti_2O_7$ respectively. The field-dependent magnetization data were measured for both compounds at 3 K and are shown in Figure A4.3. The magnetization of both compounds do not saturate in magnetic fields up to 9 T. The magnetization is well below the saturation moment for $Ce^{3+}$ of 2.14 $\mu_B$.
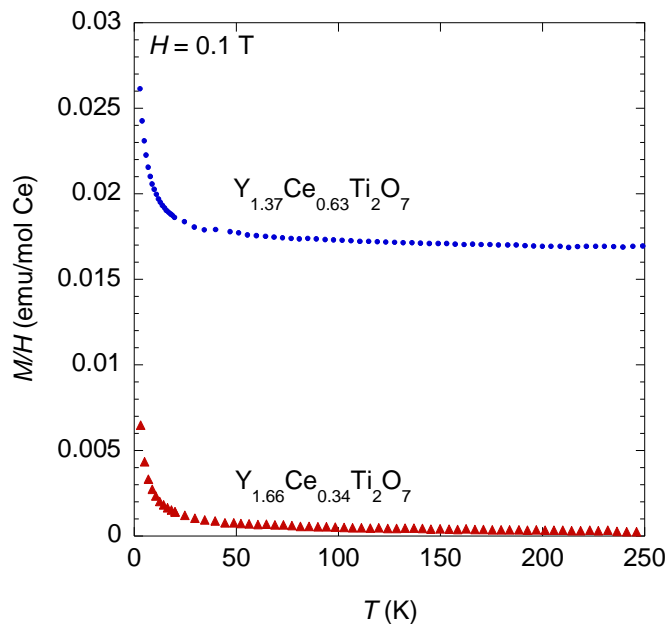
**Figure A4.2** Magnetic susceptibility of $Y_{1.66}Ce_{0.3394}Ti_2O_7$ and $Y_{1.37}Ce_{0.63}Ti_2O_7$ measured at 0.1 T where the red triangles and blue circles are $Y_{1.66}Ce_{0.34}Ti_2O_7$ and $Y_{1.37}Ce_{0.63}Ti_2O_7$ respectively.
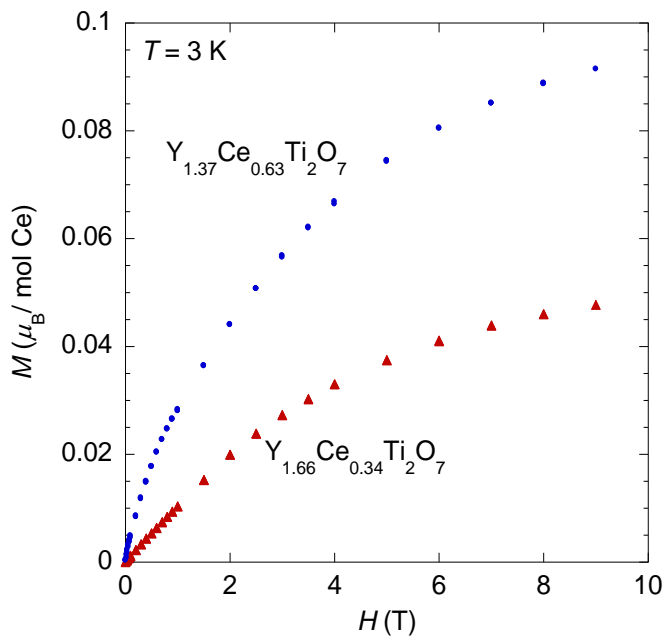


**Figure A4.3** Magnetization of $Y_{1.66}Ce_{0.3394}Ti_2O_7$ and $Y_{1.37}Ce_{0.63}Ti_2O_7$ measured at 3 K where the red triangles and blue circles are $Y_{1.66}Ce_{0.34}Ti_2O_7$ and $Y_{1.37}Ce_{0.63}Ti_2O_7$ respectively.

## A4.3 References

(1)     Dresselhaus, M. S.; Thomas, I. L. *Nature* **2001**, *414*, 332-337.

(2)     Brixner, L. H. *Inorg. Chem.* **1964**, *3*, 1065-1067.

(3)     Zakharov, N. A.; Stefanovich, S. Y.; Kustov, E. F.; Venevtsev, Y. N. *Kristall und Technik* **1980**, *15*, 29-33.

(4)     Milanova, M. M.; Kakihana, M.; Arima, M.; Yashima, M.; Yoshimura, M. *J. Alloys. Compds.* **1996**, *242*, 6-10.

## APPENDIX 5 – UNPUBLISHED CRYSTALLOGRAPHIC INFORMATION FILES

## A5.1   Rb$_4$Mn(MoO$_4$)$_3$

```
data_dixie67

_audit_creation_method             SHELXL-97
_chemical_name_systematic
;
 ?
;
_chemical_name_common              ?
_chemical_melting_point            ?
_chemical_formula_moiety           'Rb₄Mn(MoO₄)₃'
_chemical_formula_sum
 'Mn Mo3 O12 Rb4'
_chemical_formula_weight           876.64

loop_
 _atom_type_symbol
 _atom_type_description
 _atom_type_scat_dispersion_real
 _atom_type_scat_dispersion_imag
 _atom_type_scat_source
 'Mn'  'Mn'   0.3368   0.7283
 'International Tables Vol C Tables 4.2.6.8 and 6.1.1.4'
 'Mo'  'Mo'  -1.6832   0.6857
 'International Tables Vol C Tables 4.2.6.8 and 6.1.1.4'
 'O'   'O'    0.0106   0.0060
 'International Tables Vol C Tables 4.2.6.8 and 6.1.1.4'
 'Rb'  'Rb'  -0.9393   2.9676
 'International Tables Vol C Tables 4.2.6.8 and 6.1.1.4'

_symmetry_cell_setting             'hexagonal'
_symmetry_space_group_name_H-M     'P63/mmc'

loop_
 _symmetry_equiv_pos_as_xyz
 'x, y, z'
 '-x, -y, z+1/2'
 '-y, -x, -z+1/2'
 'y, x, -z'
 'x-y, -y, -z'
 '-x+y, y, -z+1/2'
 'x, x-y, -z+1/2'
 '-x, -x+y, -z'
 '-y, x-y, z'
 'y, -x+y, z+1/2'
 'x-y, x, z+1/2'
 '-x+y, -x, z'
 '-x, -y, -z'
 'x, y, -z-1/2'
 'y, x, z-1/2'
 '-y, -x, z'
 '-x+y, y, z'
 'x-y, -y, z-1/2'
 '-x, -x+y, z-1/2'
 'x, x-y, z'
 'y, -x+y, -z'
 '-y, x-y, -z-1/2'
 '-x+y, -x, -z-1/2'
 'x-y, x, -z'

_cell_length_a                     6.0990(10)
_cell_length_b                     6.0990(10)
_cell_length_c                     23.711(3)
_cell_angle_alpha                  90.00
_cell_angle_beta                   90.00
_cell_angle_gamma                  120.00
```

```
_cell_volume                        763.8(2)
_cell_formula_units_Z               2
_cell_measurement_temperature       293(2)
_cell_measurement_reflns_used       ?
_cell_measurement_theta_min         ?
_cell_measurement_theta_max         ?

_exptl_crystal_description          'plate shaped fragment'
_exptl_crystal_colour               'light brown'
_exptl_crystal_size_max             0.075
_exptl_crystal_size_mid             0.075
_exptl_crystal_size_min             0.025
_exptl_crystal_density_meas         ?
_exptl_crystal_density_diffrn       3.812
_exptl_crystal_density_method       'not measured'
_exptl_crystal_F_000                790
_exptl_absorpt_coefficient_mu       15.922
_exptl_absorpt_correction_type      'multi-scan'
_exptl_absorpt_correction_T_min     ?
_exptl_absorpt_correction_T_max     ?
_exptl_absorpt_process_details      'HKL Scalepack (Otwinowski & Minor 19'

_exptl_special_details
;
 ?
;

_diffrn_ambient_temperature         293(2)
_diffrn_radiation_wavelength        0.71073
_diffrn_radiation_type              MoK\a
_diffrn_radiation_source            'fine-focus sealed tube'
_diffrn_radiation_monochromator     graphite
_diffrn_measurement_device_type     'KappaCCD'
_diffrn_measurement_method          ' \w scans \k offsets'
_diffrn_detector_area_resol_mean    ?
_diffrn_standards_number            0
_diffrn_standards_interval_count    ?
_diffrn_standards_interval_time     ?
_diffrn_standards_decay_%           none
_diffrn_reflns_number               2762
_diffrn_reflns_av_R_equivalents     0.0531
_diffrn_reflns_av_sigmaI/netI       0.0379
_diffrn_reflns_limit_h_min          -8
_diffrn_reflns_limit_h_max          8
_diffrn_reflns_limit_k_min          -6
_diffrn_reflns_limit_k_max          6
_diffrn_reflns_limit_l_min          -32
_diffrn_reflns_limit_l_max          32
_diffrn_reflns_theta_min            3.44
_diffrn_reflns_theta_max            29.98
_reflns_number_total                489
_reflns_number_gt                   376
_reflns_threshold_expression        >2sigma(I)

_computing_data_collection          'COLLECT (Nonius, 2000)'
_computing_cell_refinement    'Denzo and Scalepack (Otwinowski & Minor, 1997)'
_computing_data_reduction     'Denzo and Scalepack (Otwinowski & Minor, 1997)'
_computing_structure_solution       'SHELXS-97 (Sheldrick, 1990)'
_computing_structure_refinement     'SHELXL-97 (Sheldrick, 1997)'
_computing_molecular_graphics       ?
_computing_publication_material     'SHELXL-97 (Sheldrick, 1997)'
_refine_special_details
;
 Refinement of F^2^ against ALL reflections.  The weighted R-factor wR and
 goodness of fit S are based on F^2^, conventional R-factors R are based
 on F, with F set to zero for negative F^2^. The threshold expression of
 F^2^ > 2sigma(F^2^) is used only for calculating R-factors(gt) etc. and is
 not relevant to the choice of reflections for refinement.  R-factors based
 on F^2^ are statistically about twice as large as those based on F, and R-
 factors based on ALL data will be even larger.
_refine_ls_structure_factor_coef  Fsqd
```

```
_refine_ls_matrix_type              full
_refine_ls_weighting_scheme         calc
_refine_ls_weighting_details
 'calc w=1/[\s^2^(Fo^2^)+(0.0421P)^2^+0.7989P] where P=(Fo^2^+2Fc^2^)/3'
_atom_sites_solution_primary        direct
_atom_sites_solution_secondary      difmap
_atom_sites_solution_hydrogens      geom
_refine_ls_hydrogen_treatment       none
_refine_ls_extinction_method        SHELXL
_refine_ls_extinction_coef          0.0049(8)
_refine_ls_extinction_expression
 'Fc^*^=kFc[1+0.001xFc^2^\l^3^/sin(2\q)]^-1/4^'
_refine_ls_number_reflns            489
_refine_ls_number_parameters        37
_refine_ls_number_restraints        0
_refine_ls_R_factor_all             0.0396
_refine_ls_R_factor_gt              0.0288
_refine_ls_wR_factor_ref            0.0810
_refine_ls_wR_factor_gt             0.0749
_refine_ls_goodness_of_fit_ref      1.061
_refine_ls_restrained_S_all         1.061
_refine_ls_shift/su_max             0.000
_refine_ls_shift/su_mean            0.000
loop_
 _atom_site_label
 _atom_site_type_symbol
 _atom_site_fract_x
 _atom_site_fract_y
 _atom_site_fract_z
 _atom_site_U_iso_or_equiv
 _atom_site_adp_type
 _atom_site_occupancy
 _atom_site_symmetry_multiplicity
 _atom_site_calc_flag
 _atom_site_refinement_flags
 _atom_site_disorder_assembly
 _atom_site_disorder_group
Rb1 Rb 0.3333 0.6667 0.15755(3) 0.0344(3) Uani 1 6 d S . .
Rb2 Rb 0.6667 0.3333 0.02849(3) 0.0283(3) Uani 1 6 d S . .
Mn1 Mn 0.0000 0.0000 0.2500 0.0281(4) Uani 1 12 d S . .
Mo1 Mo 1.0000 0.0000 0.09016(2) 0.0196(2) Uani 1 6 d S . .
Mo2 Mo 0.6667 0.3333 0.22782(6) 0.0255(5) Uani 0.481(3) 6 d SP . .
O1 O 0.0000 0.0000 0.1645(2) 0.056(2) Uani 1 6 d S . .
O2 O 0.1555(3) 0.3109(6) 0.06565(15) 0.0406(9) Uani 1 2 d S . .
O3 O 0.6667 0.3333 0.1557(4) 0.047(6) Uani 0.50(2) 6 d SP . .
O4 O 0.3859(12) 0.3283(13) 0.2500 0.041(2) Uani 0.506(9) 2 d SP . .


loop_
 _atom_site_aniso_label
 _atom_site_aniso_U_11
 _atom_site_aniso_U_22
 _atom_site_aniso_U_33
 _atom_site_aniso_U_23
 _atom_site_aniso_U_13
 _atom_site_aniso_U_12
Rb1 0.0391(4) 0.0391(4) 0.0250(5) 0.000 0.000 0.01957(18)
Rb2 0.0279(3) 0.0279(3) 0.0290(4) 0.000 0.000 0.01396(15)
Mn1 0.0360(6) 0.0360(6) 0.0123(8) 0.000 0.000 0.0180(3)
Mo1 0.0224(3) 0.0224(3) 0.0140(4) 0.000 0.000 0.01119(14)
Mo2 0.0281(6) 0.0281(6) 0.0203(6) 0.000 0.000 0.0140(3)
O1 0.076(4) 0.076(4) 0.015(3) 0.000 0.000 0.0380(18)
O2 0.0463(17) 0.0235(18) 0.0444(19) 0.0056(17) 0.0028(9) 0.0117(9)
O3 0.062(8) 0.062(8) 0.017(7) 0.000 0.000 0.031(4)
O4 0.034(4) 0.041(4) 0.045(4) 0.000 0.000 0.017(3)


_geom_special_details
;
 All esds (except the esd in the dihedral angle between two l.s. planes)
 are estimated using the full covariance matrix.  The cell esds are taken
 into account individually in the estimation of esds in distances, angles
 and torsion angles; correlations between esds in cell parameters are only
```

```
 used when they are defined by crystal symmetry.  An approximate (isotropic)
 treatment of cell esds is used for estimating esds involving l.s. planes.
;

loop_
 _geom_bond_atom_site_label_1
 _geom_bond_atom_site_label_2
 _geom_bond_distance
 _geom_bond_site_symmetry_2
 _geom_bond_publ_flag
Rb1 O2 2.877(3) . ?
Rb1 O2 2.877(3) 20_565 ?
Rb1 O2 2.877(3) 16_665 ?
Rb1 O4 3.135(5) 9_665 ?
Rb1 O4 3.135(5) 7_565 ?
Rb1 O4 3.135(5) 23_566 ?
Rb1 O4 3.135(5) 17 ?
Rb1 O4 3.135(5) 3_665 ?
Rb1 O4 3.135(5) . ?
Rb1 O3 3.5215(6) 1_455 ?
Rb1 O3 3.5215(6) 1_565 ?
Rb1 O3 3.5215(6) . ?
Rb2 O2 2.918(3) 8_655 ?
Rb2 O2 2.918(3) 4 ?
Rb2 O2 2.918(3) 13_665 ?
Rb2 O3 3.016(10) . ?
Rb2 O2 3.1765(11) 1_655 ?
Rb2 O2 3.1765(11) 16_655 ?
Rb2 O2 3.1765(11) 20_665 ?
Rb2 O2 3.1765(11) 20 ?
Rb2 O2 3.1765(11) 16_665 ?
Rb2 O2 3.1765(11) . ?
Rb2 Rb2 3.7715(8) 13_655 ?
Rb2 Rb2 3.7715(8) 13_765 ?
Mn1 O1 2.028(6) 14_556 ?
Mn1 O1 2.028(6) . ?
Mn1 O4 2.199(7) 3 ?
Mn1 O4 2.199(7) . ?
Mn1 O4 2.199(6) 23_556 ?
Mn1 O4 2.199(6) 7 ?
Mn1 O4 2.199(6) 9 ?
Mn1 O4 2.199(6) 17 ?
Mn1 Rb1 4.1478(6) 14_546 ?
Mn1 Rb1 4.1478(7) 14_556 ?
Mn1 Rb1 4.1478(6) 1_545 ?
Mn1 Rb1 4.1478(6) 1_445 ?
Mo1 O2 1.742(3) 16_655 ?
Mo1 O2 1.742(3) 20_655 ?
Mo1 O2 1.742(3) 1_655 ?
Mo1 O1 1.762(6) 1_655 ?
Mo1 Rb2 3.8128(6) 1_545 ?
Mo1 Rb2 3.8128(7) 1_655 ?
Mo1 Rb1 3.8669(6) 1_645 ?
Mo1 Rb1 3.8669(7) 1_655 ?
Mo1 Rb1 3.8669(7) 1_545 ?
Mo2 Mo2 1.052(3) 14_556 ?
Mo2 O3 1.710(10) . ?
Mo2 O4 1.777(6) 17_655 ?
Mo2 O4 1.777(6) 9_655 ?
Mo2 O4 1.777(7) 23_666 ?
Mo2 O4 1.777(7) 7 ?
Mo2 O4 1.777(6) 3_665 ?
Mo2 O4 1.777(6) . ?
Mo2 Rb1 3.8955(9) 1_545 ?
Mo2 Rb1 3.8955(9) 1_655 ?
O1 Mo1 1.762(6) 1_455 ?
O1 Rb1 3.5251(6) 1_545 ?
O1 Rb1 3.5251(6) 1_445 ?
```

O2 Mo1 1.742(3) 1_455 ?
O2 Rb2 2.918(3) 13_665 ?
O2 Rb2 3.1765(11) 1_455 ?
O3 Rb1 3.5215(6) 1_655 ?
O3 Rb1 3.5215(6) 1_545 ?
O4 O4 1.651(14) 7 ?
O4 O4 1.743(13) 3_665 ?
O4 Mo2 1.777(6) 14_556 ?
O4 Rb1 3.135(5) 14_556 ?

loop_
 _geom_angle_atom_site_label_1
 _geom_angle_atom_site_label_2
 _geom_angle_atom_site_label_3
 _geom_angle
 _geom_angle_site_symmetry_1
 _geom_angle_site_symmetry_3
 _geom_angle_publ_flag
O2 Rb1 O2 68.88(10) . 20_565 ?
O2 Rb1 O2 68.88(10) . 16_665 ?
O2 Rb1 O2 68.88(10) 20_565 16_665 ?
O2 Rb1 O4 163.67(11) . 9_665 ?
O2 Rb1 O4 118.15(11) 20_565 9_665 ?
O2 Rb1 O4 99.05(11) 16_665 9_665 ?
O2 Rb1 O4 163.67(11) . 7_565 ?
O2 Rb1 O4 99.05(11) 20_565 7_565 ?
O2 Rb1 O4 118.15(11) 16_665 7_565 ?
O4 Rb1 O4 32.3(2) 9_665 7_565 ?
O2 Rb1 O4 118.15(12) . 23_566 ?
O2 Rb1 O4 99.05(11) 20_565 23_566 ?
O2 Rb1 O4 163.67(11) 16_665 23_566 ?
O4 Rb1 O4 76.50(14) 9_665 23_566 ?
O4 Rb1 O4 51.1(2) 7_565 23_566 ?
O2 Rb1 O4 99.05(11) . 17 ?
O2 Rb1 O4 118.15(11) 20_565 17 ?
O2 Rb1 O4 163.67(11) 16_665 17 ?
O4 Rb1 O4 90.37(18) 9_665 17 ?
O4 Rb1 O4 76.50(14) 7_565 17 ?
O4 Rb1 O4 32.3(2) 23_566 17 ?
O2 Rb1 O4 118.15(11) . 3_665 ?
O2 Rb1 O4 163.67(12) 20_565 3_665 ?
O2 Rb1 O4 99.05(11) 16_665 3_665 ?
O4 Rb1 O4 51.1(2) 9_665 3_665 ?
O4 Rb1 O4 76.50(14) 7_565 3_665 ?
O4 Rb1 O4 90.37(18) 23_566 3_665 ?
O4 Rb1 O4 76.50(14) 17 3_665 ?
O2 Rb1 O4 99.05(11) . . ?
O2 Rb1 O4 163.67(12) 20_565 . ?
O2 Rb1 O4 118.15(11) 16_665 . ?
O4 Rb1 O4 76.50(14) 9_665 . ?
O4 Rb1 O4 90.37(18) 7_565 . ?
O4 Rb1 O4 76.50(14) 23_566 . ?
O4 Rb1 O4 51.1(2) 17 . ?
O4 Rb1 O4 32.3(2) 3_665 . ?
O2 Rb1 O3 70.37(13) . 1_455 ?
O2 Rb1 O3 70.37(13) 20_565 1_455 ?
O2 Rb1 O3 130.05(18) 16_665 1_455 ?
O4 Rb1 O3 125.37(17) 9_665 1_455 ?
O4 Rb1 O3 95.59(17) 7_565 1_455 ?
O4 Rb1 O3 49.48(18) 23_566 1_455 ?
O4 Rb1 O3 49.48(18) 17 1_455 ?
O4 Rb1 O3 125.37(18) 3_665 1_455 ?
O4 Rb1 O3 95.59(17) . 1_455 ?
O2 Rb1 O3 130.05(18) . 1_565 ?
O2 Rb1 O3 70.37(13) 20_565 1_565 ?
O2 Rb1 O3 70.37(13) 16_665 1_565 ?
O4 Rb1 O3 49.48(18) 9_665 1_565 ?
O4 Rb1 O3 49.48(18) 7_565 1_565 ?
O4 Rb1 O3 95.59(17) 23_566 1_565 ?
O4 Rb1 O3 125.37(17) 17 1_565 ?
O4 Rb1 O3 95.59(17) 3_665 1_565 ?
O4 Rb1 O3 125.37(18) . 1_565 ?
O3 Rb1 O3 119.984(7) 1_455 1_565 ?
O2 Rb1 O3 70.37(13) . . ?
O2 Rb1 O3 130.05(18) 20_565 . ?
O2 Rb1 O3 70.37(13) 16_665 . ?
O4 Rb1 O3 95.59(17) 9_665 . ?
O4 Rb1 O3 125.37(17) 7_565 . ?
O4 Rb1 O3 125.37(17) 23_566 . ?
O4 Rb1 O3 95.59(17) 17 . ?
O4 Rb1 O3 49.48(18) 3_665 . ?
O4 Rb1 O3 49.48(18) . . ?
O3 Rb1 O3 119.984(8) 1_455 . ?
O3 Rb1 O3 119.984(8) 1_565 . ?
O2 Rb2 O2 67.79(11) 8_655 4 ?
O2 Rb2 O2 67.79(11) 8_655 13_665 ?
O2 Rb2 O2 67.79(11) 4 13_665 ?
O2 Rb2 O3 139.91(7) 8_655 . ?
O2 Rb2 O3 139.91(7) 4 . ?
O2 Rb2 O3 139.91(7) 13_665 . ?
O2 Rb2 O2 70.42(11) 8_655 1_655 ?
O2 Rb2 O2 137.36(3) 4 1_655 ?
O2 Rb2 O2 103.66(6) 13_665 1_655 ?
O3 Rb2 O2 73.89(6) . 1_655 ?
O2 Rb2 O2 70.42(11) 8_655 16_655 ?
O2 Rb2 O2 103.66(6) 4 16_655 ?
O2 Rb2 O2 137.36(3) 13_665 16_655 ?
O3 Rb2 O2 73.89(6) . 16_655 ?
O2 Rb2 O2 53.20(11) 1_655 16_655 ?
O2 Rb2 O2 103.66(6) 8_655 20_665 ?
O2 Rb2 O2 137.36(3) 4 20_665 ?
O2 Rb2 O2 70.42(11) 13_665 20_665 ?
O3 Rb2 O2 73.89(6) . 20_665 ?
O2 Rb2 O2 61.63(11) 1_655 20_665 ?
O2 Rb2 O2 112.62(5) 16_655 20_665 ?
O2 Rb2 O2 103.66(6) 8_655 20 ?
O2 Rb2 O2 70.42(11) 4 20 ?
O2 Rb2 O2 137.36(3) 13_665 20 ?
O3 Rb2 O2 73.89(6) . 20 ?
O2 Rb2 O2 112.62(5) 1_655 20 ?
O2 Rb2 O2 61.63(11) 16_655 20 ?
O2 Rb2 O2 147.49(12) 20_665 20 ?
O2 Rb2 O2 137.36(3) 8_655 16_665 ?
O2 Rb2 O2 103.66(6) 4 16_665 ?
O2 Rb2 O2 70.42(11) 13_665 16_665 ?
O3 Rb2 O2 73.89(6) . 16_665 ?
O2 Rb2 O2 112.62(5) 1_655 16_665 ?
O2 Rb2 O2 147.49(12) 16_655 16_665 ?
O2 Rb2 O2 53.20(11) 20_665 16_665 ?
O2 Rb2 O2 112.62(5) 20 16_665 ?
O2 Rb2 O2 137.36(3) 8_655 . ?
O2 Rb2 O2 70.42(11) 4 . ?
O2 Rb2 O2 103.66(6) 13_665 . ?
O3 Rb2 O2 73.89(6) . . ?
O2 Rb2 O2 147.49(12) 1_655 . ?
O2 Rb2 O2 112.62(5) 16_655 . ?
O2 Rb2 O2 112.62(5) 20_665 . ?
O2 Rb2 O2 53.20(11) 20 . ?
O2 Rb2 O2 61.63(11) 16_665 . ?
O2 Rb2 Rb2 54.924(18) 8_655 13_655 ?
O2 Rb2 Rb2 54.924(18) 4 13_655 ?
O2 Rb2 Rb2 109.10(7) 13_665 13_655 ?
O3 Rb2 Rb2 110.99(2) . 13_655 ?
O2 Rb2 Rb2 93.70(6) 1_655 13_655 ?
O2 Rb2 Rb2 48.74(6) 16_655 13_655 ?
O2 Rb2 Rb2 153.25(6) 20_665 13_655 ?
O2 Rb2 Rb2 48.74(6) 20 13_655 ?
O2 Rb2 Rb2 153.25(6) 16_665 13_655 ?
O2 Rb2 Rb2 93.70(6) . 13_655 ?
O2 Rb2 Rb2 54.924(18) 8_655 13_765 ?
O2 Rb2 Rb2 109.10(7) 4 13_765 ?
O2 Rb2 Rb2 54.924(18) 13_665 13_765 ?

O3 Rb2 Rb2 110.99(2) . 13_765 ?
O2 Rb2 Rb2 48.74(6) 1_655 13_765 ?
O2 Rb2 Rb2 93.70(6) 16_655 13_765 ?
O2 Rb2 Rb2 48.74(6) 20_665 13_765 ?
O2 Rb2 Rb2 153.25(6) 20 13_765 ?
O2 Rb2 Rb2 93.70(6) 16_665 13_765 ?
O2 Rb2 Rb2 153.25(6) . 13_765 ?
Rb2 Rb2 Rb2 107.91(2) 13_655 13_765 ?
O1 Mn1 O1 180.0 14_556 . ?
O1 Mn1 O4 90.000(2) 14_556 3 ?
O1 Mn1 O4 90.000(2) . 3 ?
O1 Mn1 O4 90.000(2) 14_556 . ?
O1 Mn1 O4 90.000(2) . . ?
O4 Mn1 O4 164.1(4) 3 . ?
O1 Mn1 O4 90.000(2) 14_556 23_556 ?
O1 Mn1 O4 90.000(2) . 23_556 ?
O4 Mn1 O4 44.1(4) 3 23_556 ?
O4 Mn1 O4 120.000(1) . 23_556 ?
O1 Mn1 O4 90.000(2) 14_556 7 ?
O1 Mn1 O4 90.000(2) . 7 ?
O4 Mn1 O4 120.000(1) 3 7 ?
O4 Mn1 O4 44.1(4) . 7 ?
O4 Mn1 O4 75.9(4) 23_556 7 ?
O1 Mn1 O4 90.000(1) 14_556 9 ?
O1 Mn1 O4 90.000(1) . 9 ?
O4 Mn1 O4 75.9(4) 3 9 ?
O4 Mn1 O4 120.000(2) . 9 ?
O4 Mn1 O4 120.000(3) 23_556 9 ?
O4 Mn1 O4 164.1(4) 7 9 ?
O1 Mn1 O4 90.000(1) 14_556 17 ?
O1 Mn1 O4 90.000(1) . 17 ?
O4 Mn1 O4 120.000(3) 3 17 ?
O4 Mn1 O4 75.9(4) . 17 ?
O4 Mn1 O4 164.1(4) 23_556 17 ?
O4 Mn1 O4 120.000(4) 7 17 ?
O4 Mn1 O4 44.1(4) 9 17 ?
O1 Mn1 Rb1 58.097(10) 14_556 14_546 ?
O1 Mn1 Rb1 121.903(10) . 14_546 ?
O4 Mn1 Rb1 83.26(15) 3 14_546 ?
O4 Mn1 Rb1 83.26(15) . 14_546 ?
O4 Mn1 Rb1 47.97(13) 23_556 14_546 ?
O4 Mn1 Rb1 47.97(13) 7 14_546 ?
O4 Mn1 Rb1 141.89(10) 9 14_546 ?
O4 Mn1 Rb1 141.89(10) 17 14_546 ?
O1 Mn1 Rb1 58.097(10) 14_556 14_556 ?
O1 Mn1 Rb1 121.903(10) . 14_556 ?
O4 Mn1 Rb1 141.89(9) 3 14_556 ?
O4 Mn1 Rb1 47.97(13) . 14_556 ?
O4 Mn1 Rb1 141.89(9) 23_556 14_556 ?
O4 Mn1 Rb1 83.26(15) 7 14_556 ?
O4 Mn1 Rb1 83.26(16) 9 14_556 ?
O4 Mn1 Rb1 47.97(13) 17 14_556 ?
Rb1 Mn1 Rb1 94.650(14) 14_546 14_556 ?
O1 Mn1 Rb1 121.903(10) 14_556 1_545 ?
O1 Mn1 Rb1 58.097(10) . 1_545 ?
O4 Mn1 Rb1 83.26(15) 3 1_545 ?
O4 Mn1 Rb1 83.26(15) . 1_545 ?
O4 Mn1 Rb1 47.97(13) 23_556 1_545 ?
O4 Mn1 Rb1 47.97(13) 7 1_545 ?
O4 Mn1 Rb1 141.89(10) 9 1_545 ?
O4 Mn1 Rb1 141.89(10) 17 1_545 ?
Rb1 Mn1 Rb1 63.81(2) 14_546 1_545 ?
Rb1 Mn1 Rb1 129.765(6) 14_556 1_545 ?
O1 Mn1 Rb1 121.903(10) 14_556 1_445 ?
O1 Mn1 Rb1 58.097(10) . 1_445 ?
O4 Mn1 Rb1 47.97(13) 3 1_445 ?
O4 Mn1 Rb1 141.89(9) . 1_445 ?
O4 Mn1 Rb1 83.26(15) 23_556 1_445 ?
O4 Mn1 Rb1 141.89(9) 7 1_445 ?
O4 Mn1 Rb1 47.97(13) 9 1_445 ?
O4 Mn1 Rb1 83.26(16) 17 1_445 ?

Rb1 Mn1 Rb1 129.765(6) 14_546 1_445 ?
Rb1 Mn1 Rb1 129.765(6) 14_556 1_445 ?
Rb1 Mn1 Rb1 94.650(14) 1_545 1_445 ?
O2 Mo1 O2 109.46(12) 16_655 20_655 ?
O2 Mo1 O2 109.46(12) 16_655 1_655 ?
O2 Mo1 O2 109.46(12) 20_655 1_655 ?
O2 Mo1 O1 109.48(12) 16_655 1_655 ?
O2 Mo1 O1 109.48(12) 20_655 1_655 ?
O2 Mo1 O1 109.48(12) 1_655 1_655 ?
O2 Mo1 Rb2 55.72(3) 16_655 . ?
O2 Mo1 Rb2 137.96(12) 20_655 . ?
O2 Mo1 Rb2 55.72(3) 1_655 . ?
O1 Mo1 Rb2 112.551(14) 1_655 . ?
O2 Mo1 Rb2 55.72(3) 16_655 1_545 ?
O2 Mo1 Rb2 55.72(3) 20_655 1_545 ?
O2 Mo1 Rb2 137.96(12) 1_655 1_545 ?
O1 Mo1 Rb2 112.551(14) 1_655 1_545 ?
Rb2 Mo1 Rb2 106.223(15) . 1_545 ?
O2 Mo1 Rb2 137.96(12) 16_655 1_655 ?
O2 Mo1 Rb2 55.72(3) 20_655 1_655 ?
O2 Mo1 Rb2 55.72(3) 1_655 1_655 ?
O1 Mo1 Rb2 112.551(14) 1_655 1_655 ?
Rb2 Mo1 Rb2 106.223(15) . 1_655 ?
Rb2 Mo1 Rb2 106.223(15) 1_545 1_655 ?
O2 Mo1 Rb1 124.55(3) 16_655 1_645 ?
O2 Mo1 Rb1 43.89(11) 20_655 1_645 ?
O2 Mo1 Rb1 124.55(3) 1_655 1_645 ?
O1 Mo1 Rb1 65.591(13) 1_655 1_645 ?
Rb2 Mo1 Rb1 178.143(19) . 1_645 ?
Rb2 Mo1 Rb1 74.811(11) 1_545 1_645 ?
Rb2 Mo1 Rb1 74.811(11) 1_655 1_645 ?
O2 Mo1 Rb1 124.55(3) 16_655 1_655 ?
O2 Mo1 Rb1 124.55(3) 20_655 1_655 ?
O2 Mo1 Rb1 43.89(11) 1_655 1_655 ?
O1 Mo1 Rb1 65.591(13) 1_655 1_655 ?
Rb2 Mo1 Rb1 74.811(11) . 1_655 ?
Rb2 Mo1 Rb1 178.143(19) 1_545 1_655 ?
Rb2 Mo1 Rb1 74.811(11) 1_655 1_655 ?
Rb1 Mo1 Rb1 104.114(15) 1_645 1_655 ?
O2 Mo1 Rb1 43.89(11) 16_655 1_545 ?
O2 Mo1 Rb1 124.55(3) 20_655 1_545 ?
O2 Mo1 Rb1 124.55(3) 1_655 1_545 ?
O1 Mo1 Rb1 65.591(13) 1_655 1_545 ?
Rb2 Mo1 Rb1 74.811(11) . 1_545 ?
Rb2 Mo1 Rb1 74.811(11) 1_545 1_545 ?
Rb2 Mo1 Rb1 178.143(19) 1_655 1_545 ?
Rb1 Mo1 Rb1 104.114(15) 1_645 1_545 ?
Rb1 Mo1 Rb1 104.113(15) 1_655 1_545 ?
Mo2 Mo2 O3 180.000(2) 14_556 . ?
Mo2 Mo2 O4 72.79(8) 14_556 17_655 ?
O3 Mo2 O4 107.21(8) . 17_655 ?
Mo2 Mo2 O4 72.79(8) 14_556 9_655 ?
O3 Mo2 O4 107.21(8) . 9_655 ?
O4 Mo2 O4 55.4(4) 17_655 9_655 ?
Mo2 Mo2 O4 72.79(8) 14_556 23_666 ?
O3 Mo2 O4 107.21(8) . 23_666 ?
O4 Mo2 O4 58.7(4) 17_655 23_666 ?
O4 Mo2 O4 111.63(7) 9_655 23_666 ?
Mo2 Mo2 O4 72.79(8) 14_556 7 ?
O3 Mo2 O4 107.21(8) . 7 ?
O4 Mo2 O4 111.63(7) 17_655 7 ?
O4 Mo2 O4 58.7(4) 9_655 7 ?
O4 Mo2 O4 145.53(16) 23_666 7 ?
Mo2 Mo2 O4 72.79(8) 14_556 3_665 ?
O3 Mo2 O4 107.21(8) . 3_665 ?
O4 Mo2 O4 111.63(7) 17_655 3_665 ?
O4 Mo2 O4 145.53(16) 9_655 3_665 ?
O4 Mo2 O4 55.4(4) 23_666 3_665 ?
O4 Mo2 O4 111.63(7) 7 3_665 ?
Mo2 Mo2 O4 72.78(8) 14_556 . ?
O3 Mo2 O4 107.22(8) . . ?

98

```
O4 Mo2 O4 145.53(16) 17_655 . ?                        Mo2 O4 Mn1 126.8(3) . . ?
O4 Mo2 O4 111.63(7) 9_655 . ?                          O4 O4 Rb1 135.18(9) 7 14_556 ?
O4 Mo2 O4 111.63(7) 23_666 . ?                         O4 O4 Rb1 73.86(12) 3_665 14_556 ?
O4 Mo2 O4 55.4(4) 7 . ?                                Mo2 O4 Rb1 101.34(15) 14_556 14_556 ?
O4 Mo2 O4 58.7(4) 3_665 . ?                            Mo2 O4 Rb1 127.6(3) . 14_556 ?
Mo2 Mo2 Rb1 115.32(2) 14_556 1_545 ?                   Mn1 O4 Rb1 100.62(18) . 14_556 ?
O3 Mo2 Rb1 64.68(2) . 1_545 ?                          O4 O4 Rb1 135.18(9) 7 . ?
O4 Mo2 Rb1 96.5(2) 17_655 1_545 ?                      O4 O4 Rb1 73.86(11) 3_665 . ?
O4 Mo2 Rb1 52.09(14) 9_655 1_545 ?                     Mo2 O4 Rb1 127.6(3) 14_556 . ?
O4 Mo2 Rb1 151.8(2) 23_666 1_545 ?                     Mo2 O4 Rb1 101.34(15) . . ?
O4 Mo2 Rb1 52.09(14) 7 1_545 ?                         Mn1 O4 Rb1 100.62(18) . . ?
O4 Mo2 Rb1 151.8(2) 3_665 1_545 ?                      Rb1 O4 Rb1 88.73(18) 14_556 . ?
O4 Mo2 Rb1 96.5(2) . 1_545 ?
Mo2 Mo2 Rb1 115.32(2) 14_556 1_655 ?                   _diffrn_measured_fraction_theta_max    0.996
O3 Mo2 Rb1 64.68(2) . 1_655 ?                          _diffrn_reflns_theta_full              29.98
O4 Mo2 Rb1 52.09(14) 17_655 1_655 ?                    _diffrn_measured_fraction_theta_full   0.996
O4 Mo2 Rb1 96.5(2) 9_655 1_655 ?                       _refine_diff_density_max    0.892
O4 Mo2 Rb1 52.09(14) 23_666 1_655 ?                    _refine_diff_density_min   -1.134
O4 Mo2 Rb1 151.8(2) 7 1_655 ?                          _refine_diff_density_rms    0.150
O4 Mo2 Rb1 96.5(2) 3_665 1_655 ?
O4 Mo2 Rb1 151.8(2) . 1_655 ?
Rb1 Mo2 Rb1 103.04(3) 1_545 1_655 ?
Mo2 Mo2 Rb1 115.32(2) 14_556 . ?
O3 Mo2 Rb1 64.68(2) . . ?
O4 Mo2 Rb1 151.8(2) 17_655 . ?
O4 Mo2 Rb1 151.8(2) 9_655 . ?
O4 Mo2 Rb1 96.5(2) 23_666 . ?
O4 Mo2 Rb1 96.5(2) 7 . ?
O4 Mo2 Rb1 52.09(14) 3_665 . ?
O4 Mo2 Rb1 52.09(14) . . ?
Rb1 Mo2 Rb1 103.04(3) 1_545 . ?
Rb1 Mo2 Rb1 103.04(3) 1_655 . ?
Mo1 O1 Mn1 180.0 1_455 . ?
Mo1 O1 Rb1 87.34(10) 1_455 1_545 ?
Mn1 O1 Rb1 92.66(10) . 1_545 ?
Mo1 O1 Rb1 87.34(10) 1_455 1_445 ?
Mn1 O1 Rb1 92.66(10) . 1_445 ?
Rb1 O1 Rb1 119.786(16) 1_545 1_445 ?
Mo1 O1 Rb1 87.34(10) 1_455 . ?
Mn1 O1 Rb1 92.66(10) . . ?
Rb1 O1 Rb1 119.786(16) 1_545 . ?
Rb1 O1 Rb1 119.786(16) 1_445 . ?
Mo1 O2 Rb1 111.29(16) 1_455 . ?
Mo1 O2 Rb2 149.57(17) 1_455 13_665 ?
Rb1 O2 Rb2 99.14(9) . 13_665 ?
Mo1 O2 Rb2 97.33(6) 1_455 1_455 ?
Rb1 O2 Rb2 100.71(6) . 1_455 ?
Rb2 O2 Rb2 76.34(6) 13_665 1_455 ?
Mo1 O2 Rb2 97.33(6) 1_455 . ?
Rb1 O2 Rb2 100.71(6) . . ?
Rb2 O2 Rb2 76.34(6) 13_665 . ?
Rb2 O2 Rb2 147.49(12) 1_455 . ?
Mo2 O3 Rb2 180.0 . . ?
Mo2 O3 Rb1 89.28(16) . 1_655 ?
Rb2 O3 Rb1 90.72(16) . 1_655 ?
Mo2 O3 Rb1 89.28(16) . 1_545 ?
Rb2 O3 Rb1 90.72(16) . 1_545 ?
Rb1 O3 Rb1 119.984(8) 1_655 1_545 ?
Mo2 O3 Rb1 89.28(16) . . ?
Rb2 O3 Rb1 90.72(16) . . ?
Rb1 O3 Rb1 119.984(8) 1_655 . ?
Rb1 O3 Rb1 119.984(8) 1_545 . ?
O4 O4 O4 120.000(2) 7 3_665 ?
O4 O4 Mo2 62.3(2) 7 14_556 ?
O4 O4 Mo2 60.6(2) 3_665 14_556 ?
O4 O4 Mo2 62.3(2) 7 . ?
O4 O4 Mo2 60.6(2) 3_665 . ?
Mo2 O4 Mo2 34.43(15) 14_556 . ?
O4 O4 Mn1 67.95(18) 7 . ?
O4 O4 Mn1 172.05(18) 3_665 . ?
Mo2 O4 Mn1 126.8(3) 14_556 . ?
```

## A5.2   Rb$_4$Zn(MoO$_4$)$_3$

```
data_dixie76

_audit_creation_method              SHELXL-97
_chemical_name_systematic
;
 ?
;
_chemical_name_common               ?
_chemical_melting_point             ?
_chemical_formula_moiety            'Rb₄Zn(MoO₄)₃'
_chemical_formula_sum
 'Mo3 O12 Rb4 Zn'
_chemical_formula_weight            887.07

loop_
 _atom_type_symbol
 _atom_type_description
 _atom_type_scat_dispersion_real
 _atom_type_scat_dispersion_imag
 _atom_type_scat_source
 'O'  'O'   0.0106   0.0060
 'International Tables Vol C Tables 4.2.6.8 and 6.1.1.4'
 'Zn'  'Zn'   0.2839   1.4301
 'International Tables Vol C Tables 4.2.6.8 and 6.1.1.4'
 'Rb'  'Rb'  -0.9393   2.9676
 'International Tables Vol C Tables 4.2.6.8 and 6.1.1.4'
 'Mo'  'Mo'  -1.6832   0.6857
 'International Tables Vol C Tables 4.2.6.8 and 6.1.1.4'

_symmetry_cell_setting              'orthorhombic'
_symmetry_space_group_name_H-M      'Pbca'

loop_
 _symmetry_equiv_pos_as_xyz
 'x, y, z'
 '-x+1/2, -y, z+1/2'
 'x+1/2, -y+1/2, -z'
 '-x, y+1/2, -z+1/2'
 '-x, -y, -z'
 'x-1/2, y, -z-1/2'
 '-x-1/2, y-1/2, z'
 'x, -y-1/2, z-1/2'

_cell_length_a                      12.485(2)
_cell_length_b                      10.8750(10)
_cell_length_c                      22.2660(10)
_cell_angle_alpha                   90.00
_cell_angle_beta                    90.00
_cell_angle_gamma                   90.00
_cell_volume                        3023.2(6)
_cell_formula_units_Z               8
_cell_measurement_temperature       293(2)
_cell_measurement_reflns_used       ?
_cell_measurement_theta_min         ?
_cell_measurement_theta_max         ?

_exptl_crystal_description          'plate-shaped fragment'
_exptl_crystal_colour               'blue-green'
_exptl_crystal_size_max             0.13
_exptl_crystal_size_mid             0.10
_exptl_crystal_size_min             0.05
_exptl_crystal_density_meas         ?
_exptl_crystal_density_diffrn       3.898
_exptl_crystal_density_method       'not measured'
_exptl_crystal_F_000                3200
_exptl_absorpt_coefficient_mu       16.843
_exptl_absorpt_correction_type      ?
_exptl_absorpt_correction_T_min     0.2273
```

```
_exptl_absorpt_correction_T_max    0.4864
_exptl_absorpt_process_details     ?

_exptl_special_details
;
 ?
;

_diffrn_ambient_temperature        293(2)
_diffrn_radiation_wavelength       0.71073
_diffrn_radiation_type             MoK\a
_diffrn_radiation_source           'fine-focus sealed tube'
_diffrn_radiation_monochromator    graphite
_diffrn_measurement_device_type    'KappaCCD'
_diffrn_measurement_method         ' \w scans \k offsets'
_diffrn_detector_area_resol_mean   ?
_diffrn_standards_number           0
_diffrn_standards_interval_count   ?
_diffrn_standards_interval_time    ?
_diffrn_standards_decay_%          none
_diffrn_reflns_number              8235
_diffrn_reflns_av_R_equivalents    0.0535
_diffrn_reflns_av_sigmaI/netI      0.0624
_diffrn_reflns_limit_h_min         -17
_diffrn_reflns_limit_h_max         17
_diffrn_reflns_limit_k_min         -15
_diffrn_reflns_limit_k_max         15
_diffrn_reflns_limit_l_min         -31
_diffrn_reflns_limit_l_max         31
_diffrn_reflns_theta_min           2.45
_diffrn_reflns_theta_max           30.02
_reflns_number_total               4419
_reflns_number_gt                  2922
_reflns_threshold_expression       >2sigma(I)

_computing_data_collection         'COLLECT (Nonius, 2000)'
_computing_cell_refinement    'Denzo and Scalepack (Otwinowski & Minor, 1997)'
_computing_data_reduction     'Denzo and Scalepack (Otwinowski & Minor, 1997)'
_computing_structure_solution      'SHELXS-97 (Sheldrick, 1990)'
_computing_structure_refinement    'SHELXL-97 (Sheldrick, 1997)'
_computing_molecular_graphics      ?
_computing_publication_material    'SHELXL-97 (Sheldrick, 1997)'

_refine_special_details
;
 Refinement of F^2^ against ALL reflections.  The weighted R-factor wR and
 goodness of fit S are based on F^2^, conventional R-factors R are based
 on F, with F set to zero for negative F^2^. The threshold expression of
 F^2^ > 2sigma(F^2^) is used only for calculating R-factors(gt) etc. and is
 not relevant to the choice of reflections for refinement.  R-factors based
 on F^2^ are statistically about twice as large as those based on F, and R-
 factors based on ALL data will be even larger.
;

_refine_ls_structure_factor_coef  Fsqd
_refine_ls_matrix_type            full
_refine_ls_weighting_scheme       calc
_refine_ls_weighting_details
 'calc w=1/[\s^2^(Fo^2^)+(0.0394P)^2^+9.0735P] where P=(Fo^2^+2Fc^2^)/3'
_atom_sites_solution_primary      direct
_atom_sites_solution_secondary    difmap
_atom_sites_solution_hydrogens    geom
_refine_ls_hydrogen_treatment     none
_refine_ls_extinction_method      SHELXL
_refine_ls_extinction_coef        0.000134(18)
_refine_ls_extinction_expression
 'Fc^*^=kFc[1+0.001xFc^2^\l^3^/sin(2\q)]^-1/4^'
_refine_ls_number_reflns          4419
_refine_ls_number_parameters      182
_refine_ls_number_restraints      0
_refine_ls_R_factor_all           0.0873
```

```
_refine_ls_R_factor_gt            0.0456
_refine_ls_wR_factor_ref          0.1062
_refine_ls_wR_factor_gt           0.0919
_refine_ls_goodness_of_fit_ref    1.032
_refine_ls_restrained_S_all       1.032
_refine_ls_shift/su_max           0.002
_refine_ls_shift/su_mean          0.000

loop_
 _atom_site_label
 _atom_site_type_symbol
 _atom_site_fract_x
 _atom_site_fract_y
 _atom_site_fract_z
 _atom_site_U_iso_or_equiv
 _atom_site_adp_type
 _atom_site_occupancy
 _atom_site_symmetry_multiplicity
 _atom_site_calc_flag
 _atom_site_refinement_flags
 _atom_site_disorder_assembly
 _atom_site_disorder_group
Mo01 Mo 0.37662(4) 0.74717(5) 0.90582(2) 0.00993(13) Uani 1 1 d . . .
Mo02 Mo 0.87294(4) 0.75407(5) 0.90704(2) 0.01007(13) Uani 1 1 d . . .
Mo03 Mo 0.37491(5) 0.42223(5) 0.73384(3) 0.01156(14) Uani 1 1 d . . .
Rb01 Rb 0.62709(5) 0.91860(6) 0.97183(3) 0.01378(15) Uani 1 1 d . . .
Rb02 Rb 0.87567(5) 1.08440(6) 1.03151(3) 0.01385(15) Uani 1 1 d . . .
Rb03 Rb 0.10545(6) 0.57003(6) 0.83948(3) 0.01477(15) Uani 1 1 d . . .
Rb04 Rb 0.62453(5) 0.59903(6) 0.84265(3) 0.01486(16) Uani 1 1 d . . .
Zn01 Zn 0.32067(7) 0.71724(7) 0.75429(3) 0.01259(18) Uani 1 1 d . . .
O1 O 0.3690(4) 0.7428(4) 0.6740(2) 0.0205(11) Uani 1 1 d . . .
O2 O 0.4986(4) 0.4614(4) 0.7629(2) 0.0165(10) Uani 1 1 d . . .
O3 O 0.3980(4) 0.7525(4) 0.82513(19) 0.0167(11) Uani 1 1 d . . .
O4 O 0.5121(4) 0.1802(4) 0.9333(2) 0.0188(11) Uani 1 1 d . . .
O5 O 0.2808(4) 0.5400(4) 0.75474(19) 0.0168(10) Uani 1 1 d . . .
O6 O 0.1704(4) 0.7760(4) 0.7622(2) 0.0178(10) Uani 1 1 d . . .
O7 O 0.2594(4) 0.6681(5) 0.9229(2) 0.0224(12) Uani 1 1 d . . .
O8 O 0.3683(4) 0.8969(4) 0.9333(2) 0.0201(11) Uani 1 1 d . . .
O9 O 0.3833(4) 0.4173(4) 0.65647(19) 0.0195(11) Uani 1 1 d . . .
O10 O 0.4851(4) 0.6700(4) 0.9381(2) 0.0206(11) Uani 1 1 d . . .
O11 O 0.6227(4) 0.4084(4) 0.92981(19) 0.0167(11) Uani 1 1 d . . .
O12 O 0.7585(4) 0.6840(4) 0.93782(19) 0.0174(11) Uani 1 1 d . . .

loop_
 _atom_site_aniso_label
 _atom_site_aniso_U_11
 _atom_site_aniso_U_22
 _atom_site_aniso_U_33
 _atom_site_aniso_U_23
 _atom_site_aniso_U_13
 _atom_site_aniso_U_12
Mo01 0.0118(3) 0.0101(3) 0.0080(3) 0.00017(19) -0.0003(2) -0.0005(2)
Mo02 0.0117(3) 0.0103(3) 0.0082(3) 0.0001(2) -0.0008(2) 0.0000(2)
Mo03 0.0122(3) 0.0101(3) 0.0124(3) -0.0004(2) -0.0004(2) -0.0001(2)
Rb01 0.0155(4) 0.0144(3) 0.0114(3) -0.0003(2) 0.0004(2) 0.0001(3)
Rb02 0.0141(4) 0.0142(3) 0.0132(3) 0.0010(2) -0.0005(2) 0.0001(3)
Rb03 0.0160(3) 0.0175(3) 0.0108(3) 0.0005(2) 0.0007(2) -0.0008(3)
Rb04 0.0171(4) 0.0176(3) 0.0099(3) -0.0003(2) 0.0004(3) -0.0029(3)
Zn01 0.0147(4) 0.0126(4) 0.0105(3) -0.0007(3) -0.0008(3) 0.0005(3)
O1 0.028(3) 0.025(3) 0.009(2) 0.001(2) -0.002(2) -0.004(2)
O2 0.014(3) 0.016(2) 0.020(2) -0.003(2) -0.004(2) -0.0019(19)
O3 0.023(3) 0.021(2) 0.006(2) 0.0009(18) -0.001(2) -0.007(2)
O4 0.017(3) 0.024(3) 0.016(2) -0.003(2) -0.001(2) -0.007(2)
O5 0.016(3) 0.013(2) 0.020(2) 0.0008(19) 0.004(2) 0.000(2)
O6 0.022(3) 0.012(2) 0.019(2) 0.002(2) 0.005(2) 0.000(2)
O7 0.018(3) 0.030(3) 0.020(2) 0.003(2) 0.000(2) -0.015(2)
O8 0.030(3) 0.014(2) 0.016(2) 0.0005(19) 0.005(2) 0.003(2)
O9 0.023(3) 0.023(3) 0.013(2) 0.000(2) -0.002(2) -0.003(2)
O10 0.022(3) 0.025(3) 0.015(2) 0.002(2) 0.001(2) 0.010(2)
O11 0.027(3) 0.008(2) 0.015(2) -0.0008(18) 0.002(2) 0.001(2)
O12 0.019(3) 0.023(3) 0.010(2) 0.004(2) -0.001(2) -0.003(2)
```

_geom_special_details
;
 All esds (except the esd in the dihedral angle between two l.s. planes)
 are estimated using the full covariance matrix.  The cell esds are taken
 into account individually in the estimation of esds in distances, angles
 and torsion angles; correlations between esds in cell parameters are only
 used when they are defined by crystal symmetry.  An approximate (isotropic)
 treatment of cell esds is used for estimating esds involving l.s. planes.
;

loop_
 _geom_bond_atom_site_label_1
 _geom_bond_atom_site_label_2
 _geom_bond_distance
 _geom_bond_site_symmetry_2
 _geom_bond_publ_flag
Mo01 O7 1.740(5) . ?
Mo01 O8 1.742(5) . ?
Mo01 O10 1.748(5) . ?
Mo01 O3 1.817(4) . ?
Mo01 Rb04 3.7621(10) . ?
Mo01 Rb03 3.8157(9) 7_665 ?
Mo01 Rb02 3.8665(9) 3_467 ?
Mo01 Rb02 3.9018(9) 5_677 ?
Mo01 Rb01 3.9261(9) . ?
Mo01 Rb03 4.1660(10) . ?
Mo02 O4 1.746(5) 7_765 ?
Mo02 O11 1.754(4) 7_765 ?
Mo02 O12 1.758(5) . ?
Mo02 O1 1.808(5) 6_657 ?
Mo02 Rb04 3.8102(9) . ?
Mo02 Rb03 3.8334(9) 1_655 ?
Mo02 Rb01 3.8347(9) . ?
Mo02 Rb02 3.8482(9) 5_777 ?
Mo02 Rb01 3.9230(9) 7_755 ?
Mo02 Rb04 4.0163(9) 7_765 ?
Mo03 O9 1.727(4) . ?
Mo03 O2 1.727(5) . ?
Mo03 O5 1.800(5) . ?
Mo03 O6 1.802(5) 7_655 ?
Mo03 Rb03 3.6787(10) 6_657 ?
Mo03 Rb04 3.9055(9) 4_646 ?
Mo03 Rb04 4.0459(9) 6_557 ?
Rb01 O9 2.860(4) 4_656 ?
Rb01 O8 2.915(5) 5_677 ?
Rb01 O4 2.939(5) 5_667 ?
Rb01 O7 3.018(5) 3_567 ?
Rb01 O12 3.126(5) . ?
Rb01 O11 3.263(5) 7_765 ?
Rb01 O4 3.300(5) 1_565 ?
Rb01 O12 3.309(5) 7_765 ?
Rb01 O10 3.319(5) . ?
Rb01 O8 3.352(5) . ?
Rb01 Rb02 3.8274(10) . ?
Rb02 O10 2.866(5) 7_765 ?
Rb02 O12 2.886(5) 7_765 ?
Rb02 O11 2.965(4) 7_765 ?
Rb02 O8 3.152(5) 5_677 ?
Rb02 O10 3.159(5) 3_567 ?
Rb02 O4 3.173(5) 3_567 ?
Rb02 O11 3.203(5) 3_567 ?
Rb02 O7 3.268(5) 3_567 ?
Rb02 O7 3.334(5) 5_677 ?
Rb02 Mo02 3.8482(9) 5_777 ?
Rb02 Mo01 3.8665(9) 3_567 ?
Rb03 O4 2.820(5) 7_665 ?
Rb03 O8 2.830(5) 7_655 ?
Rb03 O7 2.878(5) . ?
Rb03 O2 2.893(5) 6_557 ?
Rb03 O5 2.908(5) . ?

Rb03 O6 2.939(4) . ?
Rb03 O9 3.234(5) 6_557 ?
Rb03 O3 3.468(5) 7_655 ?
Rb03 O1 3.512(5) 6_557 ?
Rb03 Zn01 3.6581(11) . ?
Rb03 Mo03 3.6787(10) 6_557 ?
Rb03 Mo01 3.8157(9) 7_655 ?
Rb04 O2 2.805(5) . ?
Rb04 O11 2.840(4) . ?
Rb04 O12 2.853(5) . ?
Rb04 O10 2.853(5) . ?
Rb04 O5 2.986(5) 6_657 ?
Rb04 O6 3.079(5) 6_657 ?
Rb04 O3 3.307(5) . ?
Rb04 O1 3.450(5) 6_657 ?
Rb04 O9 3.463(5) 4_656 ?
Rb04 Zn01 3.5083(11) 6_657 ?
Zn01 O3 1.889(5) . ?
Zn01 O1 1.908(5) . ?
Zn01 O6 1.990(5) . ?
Zn01 O5 1.991(5) . ?
Zn01 Rb04 3.5083(10) 6_557 ?
O1 Mo02 1.808(5) 6_557 ?
O1 Rb04 3.450(5) 6_557 ?
O1 Rb03 3.512(5) 6_657 ?
O2 Rb03 2.893(5) 6_657 ?
O3 Rb03 3.468(5) 7_665 ?
O4 Mo02 1.746(5) 7_755 ?
O4 Rb03 2.820(5) 7_655 ?
O4 Rb01 2.939(5) 5_667 ?
O4 Rb02 3.173(5) 3_467 ?
O4 Rb01 3.300(5) 1_545 ?
O5 Rb04 2.986(5) 6_557 ?
O6 Mo03 1.802(5) 7_665 ?
O6 Rb04 3.079(5) 6_557 ?
O7 Rb01 3.018(5) 3_467 ?
O7 Rb02 3.268(5) 3_467 ?
O7 Rb02 3.334(5) 5_677 ?
O8 Rb03 2.830(5) 7_665 ?
O8 Rb01 2.915(5) 5_677 ?
O8 Rb02 3.152(5) 5_677 ?
O9 Rb01 2.860(4) 4_646 ?
O9 Rb03 3.234(5) 6_657 ?
O9 Rb04 3.463(5) 4_646 ?
O10 Rb02 2.866(5) 7_755 ?
O10 Rb02 3.159(5) 3_467 ?
O11 Mo02 1.754(4) 7_755 ?
O11 Rb02 2.965(4) 7_755 ?
O11 Rb02 3.203(5) 3_467 ?
O11 Rb01 3.263(5) 7_755 ?
O12 Rb02 2.886(5) 7_755 ?
O12 Rb01 3.309(5) 7_755 ?

loop_
 _geom_angle_atom_site_label_1
 _geom_angle_atom_site_label_2
 _geom_angle_atom_site_label_3
 _geom_angle
 _geom_angle_site_symmetry_1
 _geom_angle_site_symmetry_3
 _geom_angle_publ_flag
O7 Mo01 O8 109.6(2) . . ?
O7 Mo01 O10 109.0(2) . . ?
O8 Mo01 O10 110.5(2) . . ?
O7 Mo01 O3 110.9(2) . . ?
O8 Mo01 O3 109.0(2) . . ?
O10 Mo01 O3 107.9(2) . . ?
O7 Mo01 Rb04 124.23(18) . . ?
O8 Mo01 Rb04 125.49(17) . . ?
O10 Mo01 Rb04 46.42(15) . . ?
O3 Mo01 Rb04 61.52(16) . . ?

O7 Mo01 Rb03 126.07(18) . 7_665 ?
O8 Mo01 Rb03 43.88(15) . 7_665 ?
O10 Mo01 Rb03 123.74(17) . 7_665 ?
O3 Mo01 Rb03 65.11(15) . 7_665 ?
Rb04 Mo01 Rb03 101.60(2) . 7_665 ?
O7 Mo01 Rb02 57.15(18) . 3_467 ?
O8 Mo01 Rb02 138.15(15) . 3_467 ?
O10 Mo01 Rb02 53.58(17) . 3_467 ?
O3 Mo01 Rb02 112.78(15) . 3_467 ?
Rb04 Mo01 Rb02 74.818(18) . 3_467 ?
Rb03 Mo01 Rb02 176.41(2) 7_665 3_467 ?
O7 Mo01 Rb02 58.29(18) . 5_677 ?
O8 Mo01 Rb02 52.23(17) . 5_677 ?
O10 Mo01 Rb02 134.74(15) . 5_677 ?
O3 Mo01 Rb02 117.21(16) . 5_677 ?
Rb04 Mo01 Rb02 177.31(2) . 5_677 ?
Rb03 Mo01 Rb02 75.751(18) 7_665 5_677 ?
Rb02 Mo01 Rb02 107.831(18) 3_467 5_677 ?
O7 Mo01 Rb01 145.37(15) . . ?
O8 Mo01 Rb01 58.17(17) . . ?
O10 Mo01 Rb01 57.10(17) . . ?
O3 Mo01 Rb01 103.76(15) . . ?
Rb04 Mo01 Rb01 71.823(19) . . ?
Rb03 Mo01 Rb01 70.199(17) 7_665 . ?
Rb02 Mo01 Rb01 108.069(19) 3_467 . ?
Rb02 Mo01 Rb01 106.63(2) 5_677 . ?
O7 Mo01 Rb03 33.42(15) . . ?
O8 Mo01 Rb03 120.52(17) . . ?
O10 Mo01 Rb03 123.61(17) . . ?
O3 Mo01 Rb03 77.51(15) . . ?
Rb04 Mo01 Rb03 109.76(2) . . ?
Rb03 Mo01 Rb03 109.629(18) 7_665 . ?
Rb02 Mo01 Rb03 72.196(17) 3_467 . ?
Rb02 Mo01 Rb03 71.809(18) 5_677 . ?
Rb01 Mo01 Rb03 178.37(2) . . ?
O4 Mo02 O11 108.5(2) 7_765 7_765 ?
O4 Mo02 O12 109.8(2) 7_765 . ?
O11 Mo02 O12 109.1(2) 7_765 . ?
O4 Mo02 O1 109.0(2) 7_765 6_657 ?
O11 Mo02 O1 110.7(2) 7_765 6_657 ?
O12 Mo02 O1 109.7(2) . 6_657 ?
O4 Mo02 Rb04 126.29(16) 7_765 . ?
O11 Mo02 Rb04 123.88(16) 7_765 . ?
O12 Mo02 Rb04 45.04(14) . . ?
O1 Mo02 Rb04 64.70(16) 6_657 . ?
O4 Mo02 Rb03 42.99(15) 7_765 1_655 ?
O11 Mo02 Rb03 126.12(16) 7_765 1_655 ?
O12 Mo02 Rb03 122.84(16) . 1_655 ?
O1 Mo02 Rb03 66.03(16) 6_657 1_655 ?
Rb04 Mo02 Rb03 103.75(2) . 1_655 ?
O4 Mo02 Rb01 138.32(15) 7_765 . ?
O11 Mo02 Rb01 57.97(16) 7_765 . ?
O12 Mo02 Rb01 53.48(16) . . ?
O1 Mo02 Rb01 112.65(16) 6_657 . ?
Rb04 Mo02 Rb01 72.329(19) . . ?
Rb03 Mo02 Rb01 175.86(2) 1_655 . ?
O4 Mo02 Rb02 54.56(16) 7_765 5_777 ?
O11 Mo02 Rb02 55.61(16) 7_765 5_777 ?
O12 Mo02 Rb02 136.22(14) . 5_777 ?
O1 Mo02 Rb02 114.06(16) 6_657 5_777 ?
Rb04 Mo02 Rb02 178.56(2) . 5_777 ?
Rb03 Mo02 Rb02 76.13(2) 1_655 5_777 ?
Rb01 Mo02 Rb02 107.82(2) . 5_777 ?
O4 Mo02 Rb01 56.58(16) 7_765 7_755 ?
O11 Mo02 Rb01 141.58(14) 7_765 7_755 ?
O12 Mo02 Rb01 56.90(16) . 7_755 ?
O1 Mo02 Rb01 107.68(16) 6_657 7_755 ?
Rb04 Mo02 Rb01 74.145(17) . 7_755 ?
Rb03 Mo02 Rb01 70.053(17) 1_655 7_755 ?
Rb01 Mo02 Rb01 107.189(18) . 7_755 ?
Rb02 Mo02 Rb01 107.088(19) 5_777 7_755 ?

```
O4 Mo02 Rb04 122.87(17) 7_765 7_765 ?
O11 Mo02 Rb04 37.74(14) 7_765 7_765 ?
O12 Mo02 Rb04 123.37(16) . 7_765 ?
O1 Mo02 Rb04 72.99(16) 6_657 7_765 ?
Rb04 Mo02 Rb04 106.581(18) . 7_765 ?
Rb03 Mo02 Rb04 109.976(19) 1_655 7_765 ?
Rb01 Mo02 Rb04 72.826(17) . 7_765 ?
Rb02 Mo02 Rb04 72.190(16) 5_777 7_765 ?
Rb01 Mo02 Rb04 179.21(2) 7_755 7_765 ?
O9 Mo03 O2 109.1(2) . . ?
O9 Mo03 O5 108.6(2) . . ?
O2 Mo03 O5 108.2(2) . . ?
O9 Mo03 O6 109.9(2) . 7_655 ?
O2 Mo03 O6 111.5(2) . 7_655 ?
O5 Mo03 O6 109.4(2) . 7_655 ?
O9 Mo03 Rb03 61.53(16) . 6_657 ?
O2 Mo03 Rb03 50.14(15) . 6_657 ?
O5 Mo03 Rb03 108.36(15) . 6_657 ?
O6 Mo03 Rb03 141.88(16) 7_655 6_657 ?
O9 Mo03 Rb04 62.43(16) . 4_646 ?
O2 Mo03 Rb04 112.54(16) . 4_646 ?
O5 Mo03 Rb04 138.97(15) . 4_646 ?
O6 Mo03 Rb04 50.14(15) 7_655 4_646 ?
Rb03 Mo03 Rb04 101.439(19) 6_657 4_646 ?
O9 Mo03 Rb04 68.99(16) . 6_557 ?
O2 Mo03 Rb04 136.99(16) . 6_557 ?
O5 Mo03 Rb04 42.77(14) . 6_557 ?
O6 Mo03 Rb04 108.91(16) 7_655 6_557 ?
Rb03 Mo03 Rb04 102.13(2) 6_657 6_557 ?
Rb04 Mo03 Rb04 104.214(18) 4_646 6_557 ?
O9 Rb01 O8 136.77(14) 4_656 5_677 ?
O9 Rb01 O4 133.59(14) 4_656 5_667 ?
O8 Rb01 O4 75.06(13) 5_677 5_667 ?
O9 Rb01 O7 143.03(13) 4_656 3_567 ?
O8 Rb01 O7 68.97(13) 5_677 3_567 ?
O4 Rb01 O7 69.58(14) 5_667 3_567 ?
O9 Rb01 O12 77.16(12) 4_656 . ?
O8 Rb01 O12 136.63(13) 5_677 . ?
O4 Rb01 O12 100.71(13) 5_667 . ?
O7 Rb01 O12 69.26(12) 3_567 . ?
O9 Rb01 O11 75.92(13) 4_656 7_765 ?
O8 Rb01 O11 102.26(13) 5_677 7_765 ?
O4 Rb01 O11 139.43(12) 5_667 7_765 ?
O7 Rb01 O11 71.82(12) 3_567 7_765 ?
O12 Rb01 O11 53.16(12) . 7_765 ?
O9 Rb01 O4 74.03(12) 4_656 1_565 ?
O8 Rb01 O4 66.66(12) 5_677 1_565 ?
O4 Rb01 O4 104.17(11) 5_667 1_565 ?
O7 Rb01 O4 135.18(13) 3_567 1_565 ?
O12 Rb01 O4 150.32(11) . 1_565 ?
O11 Rb01 O4 111.80(11) 7_765 1_565 ?
O9 Rb01 O12 78.18(12) 4_656 7_765 ?
O8 Rb01 O12 63.70(12) 5_677 7_765 ?
O4 Rb01 O12 137.64(12) 5_667 7_765 ?
O7 Rb01 O12 102.36(13) 3_567 7_765 ?
O12 Rb01 O12 115.46(6) . 7_765 ?
O11 Rb01 O12 63.30(11) 7_765 7_765 ?
O4 Rb01 O12 51.42(12) 1_565 7_765 ?
O9 Rb01 O10 75.27(13) 4_656 . ?
O8 Rb01 O10 137.34(13) 5_677 . ?
O4 Rb01 O10 63.19(12) 5_667 . ?
O7 Rb01 O10 102.32(13) 3_567 . ?
O12 Rb01 O10 63.94(12) . . ?
O11 Rb01 O10 114.75(11) 7_765 . ?
O4 Rb01 O10 114.27(12) 1_565 . ?
O12 Rb01 O10 152.81(11) 7_765 . ?
O9 Rb01 O8 72.54(12) 4_656 . ?
O8 Rb01 O8 104.68(11) 5_677 . ?
O4 Rb01 O8 65.70(12) 5_667 . ?
O7 Rb01 O8 134.79(13) 3_567 . ?
O12 Rb01 O8 112.73(12) . . ?

O11 Rb01 O8 147.90(12) 7_765 . ?
O4 Rb01 O8 64.82(11) 1_565 . ?
O12 Rb01 O8 114.78(12) 7_765 . ?
O10 Rb01 O8 50.94(11) . . ?
O9 Rb01 Rb02 112.70(10) 4_656 . ?
O8 Rb01 Rb02 53.69(10) 5_677 . ?
O4 Rb01 Rb02 113.71(9) 5_667 . ?
O7 Rb01 Rb02 55.52(11) 3_567 . ?
O12 Rb01 Rb02 92.47(9) . . ?
O11 Rb01 Rb02 48.64(8) 7_765 . ?
O4 Rb01 Rb02 92.12(8) 1_565 . ?
O12 Rb01 Rb02 47.02(8) 7_765 . ?
O10 Rb01 Rb02 153.56(8) . . ?
O8 Rb01 Rb02 154.67(8) . . ?
O9 Rb01 Mo02 70.01(10) 4_656 . ?
O8 Rb01 Mo02 125.31(10) 5_677 . ?
O4 Rb01 Mo02 124.96(10) 5_667 . ?
O7 Rb01 Mo02 73.04(9) 3_567 . ?
O12 Rb01 Mo02 26.88(9) . . ?
O11 Rb01 Mo02 27.11(7) 7_765 . ?
O4 Rb01 Mo02 130.75(8) 1_565 . ?
O12 Rb01 Mo02 88.59(8) 7_765 . ?
O10 Rb01 Mo02 87.84(8) . . ?
O8 Rb01 Mo02 129.97(8) . . ?
Rb02 Rb01 Mo02 72.623(19) . . ?
O10 Rb02 O12 72.87(14) 7_765 7_765 ?
O10 Rb02 O11 69.59(13) 7_765 7_765 ?
O12 Rb02 O11 72.21(13) 7_765 7_765 ?
O10 Rb02 O8 138.23(13) 7_765 5_677 ?
O12 Rb02 O8 66.11(13) 7_765 5_677 ?
O11 Rb02 O8 103.79(13) 7_765 5_677 ?
O10 Rb02 O10 100.23(12) 7_765 3_567 ?
O12 Rb02 O10 137.28(13) 7_765 3_567 ?
O11 Rb02 O10 66.13(12) 7_765 3_567 ?
O8 Rb02 O10 114.91(12) 5_677 3_567 ?
O10 Rb02 O4 65.90(13) 7_765 3_567 ?
O12 Rb02 O4 100.78(13) 7_765 3_567 ?
O11 Rb02 O4 134.89(13) 7_765 3_567 ?
O8 Rb02 O4 113.90(12) 5_677 3_567 ?
O10 Rb02 O4 114.93(12) 3_567 3_567 ?
O10 Rb02 O11 66.63(13) 7_765 3_567 ?
O12 Rb02 O11 138.06(13) 7_765 3_567 ?
O11 Rb02 O11 102.39(11) 7_765 3_567 ?
O8 Rb02 O11 149.54(12) 5_677 3_567 ?
O10 Rb02 O11 63.08(12) 3_567 3_567 ?
O4 Rb02 O11 52.92(11) 3_567 3_567 ?
O10 Rb02 O7 140.15(13) 7_765 3_567 ?
O12 Rb02 O7 106.39(13) 7_765 3_567 ?
O11 Rb02 O7 72.40(12) 7_765 3_567 ?
O8 Rb02 O7 63.10(12) 5_677 3_567 ?
O10 Rb02 O7 52.39(13) 3_567 3_567 ?
O4 Rb02 O7 147.11(12) 3_567 3_567 ?
O11 Rb02 O7 111.40(12) 3_567 3_567 ?
O10 Rb02 O7 105.39(13) 7_765 5_677 ?
O12 Rb02 O7 67.88(12) 7_765 5_677 ?
O11 Rb02 O7 139.20(12) 7_765 5_677 ?
O8 Rb02 O7 51.93(12) 5_677 5_677 ?
O10 Rb02 O7 149.37(12) 3_567 5_677 ?
O4 Rb02 O7 62.94(12) 3_567 5_677 ?
O11 Rb02 O7 112.67(12) 3_567 5_677 ?
O7 Rb02 O7 111.05(7) 3_567 5_677 ?
O10 Rb02 Rb01 113.13(10) 7_765 . ?
O12 Rb02 Rb01 57.00(10) 7_765 . ?
O11 Rb02 Rb01 55.69(10) 7_765 . ?
O8 Rb02 Rb01 48.18(9) 5_677 . ?
O10 Rb02 Rb01 90.72(9) 3_567 . ?
O4 Rb02 Rb01 154.30(9) 3_567 . ?
O11 Rb02 Rb01 152.33(8) 3_567 . ?
O7 Rb02 Rb01 49.59(8) 3_567 . ?
O7 Rb02 Rb01 94.35(9) 5_677 . ?
O10 Rb02 Mo02 67.37(10) 7_765 5_777 ?
```

105

```
O12 Rb02 Mo02 123.98(10) 7_765 5_777 ?
O11 Rb02 Mo02 124.10(10) 7_765 5_777 ?
O8 Rb02 Mo02 132.08(9) 5_677 5_777 ?
O10 Rb02 Mo02 88.33(9) 3_567 5_777 ?
O4 Rb02 Mo02 26.64(9) 3_567 5_777 ?
O11 Rb02 Mo02 26.86(8) 3̄_567 5_777 ?
O7 Rb02 Mo02 129.46(9) 3_567 5_777 ?
O7 Rb02 Mo02 86.32(9) 5_677 5_777 ?
Rb01 Rb02 Mo02 179.00(2) . 5_777 ?
O10 Rb02 Mo01 124.27(10) 7_765 3_567 ?
O12 Rb02 Mo01 127.79(10) 7_765 3_567 ?
O11 Rb02 Mo01 70.95(8) 7_765 3_567 ?
O8 Rb02 Mo01 88.47(9) 5_677 3_567 ?
O10 Rb02 Mo01 26.44(9) 3̄_567 3_567 ?
O4 Rb02 Mo01 131.42(9) 3_567 3_567 ?
O11 Rb02 Mo01 85.57(8) 3_567 3_567 ?
O7 Rb02 Mo01 26.56(9) 3_567 3_567 ?
O7 Rb02 Mo01 130.13(8) 5̄_677 3_567 ?
Rb01 Rb02 Mo01 71.848(17) . 3_567 ?
Mo02 Rb02 Mo01 107.150(19) 5_777 3_567 ?
O4 Rb03 O8 78.26(14) 7_665 7_655 ?
O4 Rb03 O7 73.24(15) 7_665 . ?
O8 Rb03 O7 72.12(13) 7_655 . ?
O4 Rb03 O2 121.14(14) 7_665 6_557 ?
O8 Rb03 O2 111.27(13) 7_655 6_557 ?
O7 Rb03 O2 165.43(14) . 6_557 ?
O4 Rb03 O5 156.91(14) 7_665 . ?
O8 Rb03 O5 108.46(14) 7_655 . ?
O7 Rb03 O5 87.59(14) . . ?
O2 Rb03 O5 77.88(13) 6_557 . ?
O4 Rb03 O6 104.69(13) 7_665 . ?
O8 Rb03 O6 155.09(15) 7_655 . ?
O7 Rb03 O6 84.91(14) . . ?
O2 Rb03 O6 88.70(13) 6_557 . ?
O5 Rb03 O6 59.86(13) . . ?
O4 Rb03 O9 75.60(13) 7_665 6_557 ?
O8 Rb03 O9 74.77(13) 7_655 6_557 ?
O7 Rb03 O9 138.17(12) . 6_557 ?
O2 Rb03 O9 54.32(12) 6_557 6_557 ?
O5 Rb03 O9 127.29(12) . 6_557 ?
O6 Rb03 O9 130.12(13) . 6_557 ?
O4 Rb03 O3 119.00(13) 7_665 7_655 ?
O8 Rb03 O3 53.64(12) 7_655 7_655 ?
O7 Rb03 O3 115.90(13) . 7_655 ?
O2 Rb03 O3 60.99(12) 6_557 7_655 ?
O5 Rb03 O3 80.66(12) . 7_655 ?
O6 Rb03 O3 135.10(12) . 7_655 ?
O9 Rb03 O3 58.71(12) 6_557 7_655 ?
O4 Rb03 O1 53.02(12) 7_665 6_557 ?
O8 Rb03 O1 121.07(13) 7_655 6_557 ?
O7 Rb03 O1 114.70(14) . 6_557 ?
O2 Rb03 O1 76.34(12) 6_557 6_557 ?
O5 Rb03 O1 129.60(12) . 6_557 ?
O6 Rb03 O1 76.96(13) . 6_557 ?
O9 Rb03 O1 63.66(12) 6_557 6_557 ?
O3 Rb03 O1 120.96(12) 7_655 6_557 ?
O4 Rb03 Zn01 125.47(10) 7_665 . ?
O8 Rb03 Zn01 126.05(11) 7_655 . ?
O7 Rb03 Zn01 71.46(9) . . ?
O2 Rb03 Zn01 96.26(9) 6_557 . ?
O5 Rb03 Zn01 32.85(9) . . ?
O6 Rb03 Zn01 32.87(10) . . ?
O9 Rb03 Zn01 150.36(8) 6_557 . ?
O3 Rb03 Zn01 113.40(8) 7_655 . ?
O1 Rb03 Zn01 109.82(8) 6_557 . ?
O4 Rb03 Mo03 96.16(10) 7_665 6_557 ?
O8 Rb03 Mo03 97.32(10) 7_655 6_557 ?
O7 Rb03 Mo03 166.14(9) . 6_557 ?
O2 Rb03 Mo03 27.27(9) 6_557 6_557 ?
O5 Rb03 Mo03 104.59(9) . 6_557 ?
O6 Rb03 Mo03 106.80(10) . 6_557 ?

O9 Rb03 Mo03 27.99(8) 6_557 6_557 ?
O3 Rb03 Mo03 60.94(8) 7_655 6_557 ?
O1 Rb03 Mo03 62.51(8) 6_557 6_557 ?
Zn01 Rb03 Mo03 122.40(2) . 6_557 ?
O4 Rb03 Mo01 97.75(10) 7_665 7_655 ?
O8 Rb03 Mo01 25.26(9) 7_655 7_655 ?
O7 Rb03 Mo01 92.98(10) . 7_655 ?
O2 Rb03 Mo01 87.49(9) 6_557 7_655 ?
O5 Rb03 Mo01 95.95(9) . 7_655 ?
O6 Rb03 Mo01 155.76(10) . 7_655 ?
O9 Rb03 Mo01 64.34(9) 6_557 7_655 ?
O3 Rb03 Mo01 28.38(7) 7_655 7_655 ?
O1 Rb03 Mo01 125.07(8) 6̄_557 7_655 ?
Zn01 Rb03 Mo01 124.08(2) . 7_655 ?
Mo03 Rb03 Mo01 79.375(18) 6_557 7_655 ?
O2 Rb04 O11 92.21(13) . . ?
O2 Rb04 O12 166.33(13) . . ?
O11 Rb04 O12 74.55(13) . . ?
O2 Rb04 O10 105.90(14) . . ?
O11 Rb04 O10 71.55(13) . . ?
O12 Rb04 O10 73.54(14) . . ?
O2 Rb04 O5 77.97(13) . 6_657 ?
O11 Rb04 O5 110.15(13) . 6_657 ?
O12 Rb04 O5 103.07(13) . 6_657 ?
O10 Rb04 O5 175.83(14) . 6_657 ?
O2 Rb04 O6 87.60(12) . 6_657 ?
O11 Rb04 O6 167.39(13) . 6_657 ?
O12 Rb04 O6 104.56(13) . 6_657 ?
O10 Rb04 O6 120.60(13) . 6_657 ?
O5 Rb04 O6 57.49(13) 6_657 6_657 ?
O2 Rb04 O3 73.47(13) . . ?
O11 Rb04 O3 116.24(13) . . ?
O12 Rb04 O3 115.16(13) . . ?
O10 Rb04 O3 55.23(12) . . ?
O5 Rb04 O3 125.55(12) 6_657 . ?
O6 Rb04 O3 75.77(12) 6_657 . ?
O2 Rb04 O1 132.08(13) . 6_657 ?
O11 Rb04 O1 114.28(13) . 6_657 ?
O12 Rb04 O1 54.13(12) . 6_657 ?
O10 Rb04 O1 119.80(13) . 6_657 ?
O5 Rb04 O1 56.06(12) 6_657 6_657 ?
O6 Rb04 O1 58.05(12) 6_657 6_657 ?
O3 Rb04 O1 121.02(12) . 6_657 ?
O2 Rb04 O9 121.42(12) . 4_656 ?
O11 Rb04 O9 136.52(11) . 4_656 ?
O12 Rb04 O9 71.85(12) . 4_656 ?
O10 Rb04 O9 73.04(12) . 4_656 ?
O5 Rb04 O9 103.74(12) 6_657 4_656 ?
O6 Rb04 O9 52.02(11) 6_657 4_656 ?
O3 Rb04 O9 58.13(11) . 4_656 ?
O1 Rb04 O9 64.69(12) 6_657 4_656 ?
O2 Rb04 Zn01 101.38(10) . 6_657 ?
O11 Rb04 Zn01 133.91(10) . 6_657 ?
O12 Rb04 Zn01 85.93(10) . 6_657 ?
O10 Rb04 Zn01 141.71(10) . 6_657 ?
O5 Rb04 Zn01 34.53(9) 6_657 6_657 ?
O6 Rb04 Zn01 34.38(9) 6_657 6_657 ?
O3 Rb04 Zn01 109.84(8) . 6_657 ?
O1 Rb04 Zn01 31.82(8) 6_657 6_657 ?
O9 Rb04 Zn01 69.93(8) 4_656 6_657 ?
O2 Rb04 Mo01 90.23(10) . . ?
O11 Rb04 Mo01 92.89(9) . . ?
O12 Rb04 Mo01 93.77(10) . . ?
O10 Rb04 Mo01 26.35(9) . . ?
O5 Rb04 Mo01 154.27(9) 6_657 . ?
O6 Rb04 Mo01 99.72(9) 6_657 . ?
O3 Rb04 Mo01 28.88(8) . . ?
O1 Rb04 Mo01 125.03(9) 6_657 . ?
O9 Rb04 Mo01 63.04(8) 4_656 . ?
Zn01 Rb04 Mo01 130.34(3) 6_657 . ?
O2 Rb04 Mo02 158.55(10) . . ?
```

```
O11 Rb04 Mo02 94.15(10) . . ?
O12 Rb04 Mo02 25.86(9) . . ?
O10 Rb04 Mo02 95.54(10) . . ?
O5 Rb04 Mo02 80.60(9) 6_657 . ?
O6 Rb04 Mo02 81.79(9) 6_657 . ?
O3 Rb04 Mo02 121.14(8) . . ?
O1 Rb04 Mo02 28.29(8) 6_657 . ?
O9 Rb04 Mo02 65.07(8) 4_656 . ?
Zn01 Rb04 Mo02 60.078(19) 6_657 . ?
Mo01 Rb04 Mo02 109.85(2) . . ?
O3 Zn01 O1 126.3(2) . . ?
O3 Zn01 O6 110.1(2) . . ?
O1 Zn01 O6 109.5(2) . . ?
O3 Zn01 O5 108.69(19) . . ?
O1 Zn01 O5 103.00(19) . . ?
O6 Zn01 O5 94.28(19) . . ?
O3 Zn01 Rb04 160.92(15) . 6_557 ?
O1 Zn01 Rb04 72.39(15) . 6_557 ?
O6 Zn01 Rb04 60.91(14) . 6_557 ?
O5 Zn01 Rb04 58.24(13) . 6_557 ?
O3 Zn01 Rb03 91.80(14) . . ?
O1 Zn01 Rb03 141.46(15) . . ?
O6 Zn01 Rb03 53.29(13) . . ?
O5 Zn01 Rb03 52.40(13) . . ?
Rb04 Zn01 Rb03 69.26(2) 6_557 . ?
Mo02 O1 Zn01 162.4(3) 6_557 . ?
Mo02 O1 Rb04 87.01(17) 6_557 6_557 ?
Zn01 O1 Rb04 75.78(15) . 6_557 ?
Mo02 O1 Rb03 85.90(17) 6_557 6_657 ?
Zn01 O1 Rb03 105.53(19) . 6_657 ?
Rb04 O1 Rb03 119.48(14) 6_557 6_657 ?
Mo03 O2 Rb04 150.4(2) . . ?
Mo03 O2 Rb03 102.59(19) . 6_657 ?
Rb04 O2 Rb03 91.27(13) . 6_657 ?
Mo01 O3 Zn01 138.1(3) . . ?
Mo01 O3 Rb04 89.60(17) . . ?
Zn01 O3 Rb04 115.7(2) . . ?
Mo01 O3 Rb03 86.51(16) . 7_665 ?
Zn01 O3 Rb03 105.83(18) . 7_665 ?
Rb04 O3 Rb03 120.16(14) . 7_665 ?
Mo02 O4 Rb03 112.0(2) 7_755 7_655 ?
Mo02 O4 Rb01 153.5(2) 7_755 5_667 ?
Rb03 O4 Rb01 93.99(14) 7_655 5_667 ?
Mo02 O4 Rb02 98.80(19) 7_755 3_467 ?
Rb03 O4 Rb02 104.28(15) 7_655 3_467 ?
Rb01 O4 Rb02 78.48(12) 5_667 3_467 ?
Mo02 O4 Rb01 97.2(2) 7_755 1_545 ?
Rb03 O4 Rb01 93.01(13) 7_655 1_545 ?
Rb01 O4 Rb01 75.83(11) 5_667 1_545 ?
Rb02 O4 Rb01 149.86(16) 3_467 1_545 ?
Mo03 O5 Zn01 121.6(3) . . ?
Mo03 O5 Rb03 137.7(2) . . ?
Zn01 O5 Rb03 94.75(17) . . ?
Mo03 O5 Rb04 113.07(19) . 6_557 ?
Zn01 O5 Rb04 87.23(16) . 6_557 ?
Rb03 O5 Rb04 87.44(13) . 6_557 ?
Mo03 O6 Zn01 123.3(2) 7_665 . ?
Mo03 O6 Rb03 142.3(2) 7_665 . ?
Zn01 O6 Rb03 93.84(16) . . ?
Mo03 O6 Rb04 103.17(19) 7_665 6_557 ?
Zn01 O6 Rb04 84.71(15) . 6_557 ?
Rb03 O6 Rb04 85.19(12) . 6_557 ?
Mo01 O7 Rb03 127.1(2) . . ?
Mo01 O7 Rb01 141.7(2) . 3_467 ?
Rb03 O7 Rb01 91.14(13) . 3_467 ?
Mo01 O7 Rb02 96.3(2) . 3_467 ?
Rb03 O7 Rb02 100.70(14) . 3_467 ?
Rb01 O7 Rb02 74.89(11) 3_467 3_467 ?
Mo01 O7 Rb02 95.4(2) . 5_677 ?
Rb03 O7 Rb02 99.09(15) . 5_677 ?
Rb01 O7 Rb02 74.88(11) 3_467 5_677 ?
```

```
Rb02 O7 Rb02 143.95(15) 3_467 5_677 ?
Mo01 O8 Rb03 110.9(2) . 7_665 ?
Mo01 O8 Rb01 153.7(2) . 5_677 ?
Rb03 O8 Rb01 94.29(14) 7_665 5_677 ?
Mo01 O8 Rb02 101.9(2) . 5_677 ?
Rb03 O8 Rb02 104.64(15) 7_665 5_677 ?
Rb01 O8 Rb02 78.13(11) 5_677 5_677 ?
Mo01 O8 Rb01 95.62(19) . . ?
Rb03 O8 Rb01 91.75(13) 7_665 . ?
Rb01 O8 Rb01 75.32(11) 5_677 . ?
Rb02 O8 Rb01 149.69(15) 5_677 . ?
Mo03 O9 Rb01 173.6(3) . 4_646 ?
Mo03 O9 Rb03 90.48(18) . 6_657 ?
Rb01 O9 Rb03 93.68(13) 4_646 6_657 ?
Mo03 O9 Rb04 91.35(18) . 4_646 ?
Rb01 O9 Rb04 90.53(12) 4_646 4_646 ?
Rb03 O9 Rb04 122.50(15) 6_657 4_646 ?
Mo01 O10 Rb04 107.2(2) . . ?
Mo01 O10 Rb02 157.6(2) . 7_755 ?
Rb04 O10 Rb02 94.75(14) . 7_755 ?
Mo01 O10 Rb02 100.0(2) . 3_467 ?
Rb04 O10 Rb02 100.75(14) . 3_467 ?
Rb02 O10 Rb02 79.77(12) 7_755 3_467 ?
Mo01 O10 Rb01 96.65(19) . . ?
Rb04 O10 Rb01 93.62(14) . . ?
Rb02 O10 Rb01 77.09(12) 7_755 . ?
Rb02 O10 Rb01 153.63(16) 3_467 . ?
Mo02 O11 Rb04 120.0(2) 7_755 . ?
Mo02 O11 Rb02 147.0(2) 7_755 7_755 ?
Rb04 O11 Rb02 92.90(12) . 7_755 ?
Mo02 O11 Rb02 97.53(18) 7_755 3_467 ?
Rb04 O11 Rb02 100.00(14) . 3_467 ?
Rb02 O11 Rb02 77.61(11) 7_755 3_467 ?
Mo02 O11 Rb01 94.92(18) 7_755 7_755 ?
Rb04 O11 Rb01 99.40(13) . 7_755 ?
Rb02 O11 Rb01 75.67(10) 7_755 7_755 ?
Rb02 O11 Rb01 147.56(15) 3_467 7_755 ?
Mo02 O12 Rb04 109.10(19) . . ?
Mo02 O12 Rb02 156.3(2) . 7_755 ?
Rb04 O12 Rb02 94.30(14) . 7_755 ?
Mo02 O12 Rb01 99.64(19) . . ?
Rb04 O12 Rb01 97.86(14) . . ?
Rb02 O12 Rb01 80.02(12) 7_755 . ?
Mo02 O12 Rb01 96.66(19) . 7_755 ?
Rb04 O12 Rb01 98.07(13) . 7_755 ?
Rb02 O12 Rb01 75.97(10) 7_755 7_755 ?
Rb01 O12 Rb01 152.02(15) . 7_755 ?

_diffrn_measured_fraction_theta_max    1.000
_diffrn_reflns_theta_full              30.02
_diffrn_measured_fraction_theta_full   1.000
_refine_diff_density_max     2.495
_refine_diff_density_min    -1.940
_refine_diff_density_rms     0.317
```

## A5.3 Orthorhombic Rb₄Cu(MoO₄)₃

```
data_dixie78

_audit_creation_method          SHELXL-97
_chemical_name_systematic
;
 ?
;
_chemical_name_common           ?
_chemical_melting_point         ?
_chemical_formula_moiety        'Rb4Cu(MoO4)3'
_chemical_formula_sum
 'Cu Mo3 O12 Rb4'
_chemical_formula_weight        885.24

loop_
 _atom_type_symbol
 _atom_type_description
 _atom_type_scat_dispersion_real
 _atom_type_scat_dispersion_imag
 _atom_type_scat_source
 'O'  'O'   0.0106   0.0060
 'International Tables Vol C Tables 4.2.6.8 and 6.1.1.4'
 'Cu'  'Cu'   0.3201   1.2651
 'International Tables Vol C Tables 4.2.6.8 and 6.1.1.4'
 'Rb'  'Rb'  -0.9393   2.9676
 'International Tables Vol C Tables 4.2.6.8 and 6.1.1.4'
 'Mo'  'Mo'  -1.6832   0.6857
 'International Tables Vol C Tables 4.2.6.8 and 6.1.1.4'

_symmetry_cell_setting          'orthorhombic'
_symmetry_space_group_name_H-M   'Pnma'

loop_
 _symmetry_equiv_pos_as_xyz
 'x, y, z'
 '-x+1/2, -y, z+1/2'
 'x+1/2, -y+1/2, -z+1/2'
 '-x, y+1/2, -z'
 '-x, -y, -z'
 'x-1/2, y, -z-1/2'
 '-x-1/2, y-1/2, z-1/2'
 'x, -y-1/2, z'

_cell_length_a                  10.581(2)
_cell_length_b                  23.213(4)
_cell_length_c                  6.0780(10)
_cell_angle_alpha               90.00
_cell_angle_beta                90.00
_cell_angle_gamma               90.00
_cell_volume                    1492.9(5)
_cell_formula_units_Z           4
_cell_measurement_temperature   298(2)
_cell_measurement_reflns_used   ?
_cell_measurement_theta_min     ?
_cell_measurement_theta_max     ?

_exptl_crystal_description      'plate-shaped fragment'
_exptl_crystal_colour           'blue green'
_exptl_crystal_size_max         0.17
_exptl_crystal_size_mid         0.15
_exptl_crystal_size_min         0.08
_exptl_crystal_density_meas     ?
_exptl_crystal_density_diffrn   3.939
_exptl_crystal_density_method   'not measured'
_exptl_crystal_F_000            1596
_exptl_absorpt_coefficient_mu   16.872
_exptl_absorpt_correction_type  ?
```

```
_exptl_absorpt_correction_T_min    0.1562
_exptl_absorpt_correction_T_max    0.3643
_exptl_absorpt_process_details     ?

_exptl_special_details
;
 ?
;

_diffrn_ambient_temperature        298(2)
_diffrn_radiation_wavelength       0.71073
_diffrn_radiation_type             MoK\a
_diffrn_radiation_source           'fine-focus sealed tube'
_diffrn_radiation_monochromator    graphite
_diffrn_measurement_device_type    'KappaCCD'
_diffrn_measurement_method         ' \w scans \k offsets'
_diffrn_detector_area_resol_mean   ?
_diffrn_standards_number           0
_diffrn_standards_interval_count   ?
_diffrn_standards_interval_time    ?
_diffrn_standards_decay_%          none
_diffrn_reflns_number              3948
_diffrn_reflns_av_R_equivalents    0.0295
_diffrn_reflns_av_sigmaI/netI      0.0401
_diffrn_reflns_limit_h_min         -14
_diffrn_reflns_limit_h_max         14
_diffrn_reflns_limit_k_min         -32
_diffrn_reflns_limit_k_max         32
_diffrn_reflns_limit_l_min         -8
_diffrn_reflns_limit_l_max         8
_diffrn_reflns_theta_min           3.46
_diffrn_reflns_theta_max           30.02
_reflns_number_total               2222
_reflns_number_gt                  1582
_reflns_threshold_expression       >2sigma(I)

_computing_data_collection         'COLLECT (Nonius, 2000)'
_computing_cell_refinement    'Denzo and Scalepack (Otwinowski & Minor, 1997)'
_computing_data_reduction     'Denzo and Scalepack (Otwinowski & Minor, 1997)'
_computing_structure_solution      'SHELXS-97 (Sheldrick, 1990)'
_computing_structure_refinement    'SHELXL-97 (Sheldrick, 1997)'
_computing_molecular_graphics      ?
_computing_publication_material    'SHELXL-97 (Sheldrick, 1997)'
_refine_special_details
;
 Refinement of F^2^ against ALL reflections.  The weighted R-factor wR and
 goodness of fit S are based on F^2^, conventional R-factors R are based
 on F, with F set to zero for negative F^2^. The threshold expression of
 F^2^ > 2sigma(F^2^) is used only for calculating R-factors(gt) etc. and is
 not relevant to the choice of reflections for refinement.  R-factors based
 on F^2^ are statistically about twice as large as those based on F, and R-
 factors based on ALL data will be even larger.
;

_refine_ls_structure_factor_coef Fsqd
_refine_ls_matrix_type             full
_refine_ls_weighting_scheme        calc
_refine_ls_weighting_details
 'calc w=1/[\s^2^(Fo^2^)+(0.0207P)^2^+31.5979P] where P=(Fo^2^+2Fc^2^)/3'
_atom_sites_solution_primary       direct
_atom_sites_solution_secondary     difmap
_atom_sites_solution_hydrogens     geom
_refine_ls_hydrogen_treatment      none
_refine_ls_extinction_method       SHELXL
_refine_ls_extinction_coef         0.00084(11)
_refine_ls_extinction_expression
 'Fc^*^=kFc[1+0.001xFc^2^\l^3^/sin(2\q)]^-1/4^'
_refine_ls_number_reflns           2222
_refine_ls_number_parameters       107
_refine_ls_number_restraints       0
_refine_ls_R_factor_all            0.0729
```

```
_refine_ls_R_factor_gt            0.0508
_refine_ls_wR_factor_ref          0.1188
_refine_ls_wR_factor_gt           0.1103
_refine_ls_goodness_of_fit_ref    1.052
_refine_ls_restrained_S_all       1.052
_refine_ls_shift/su_max           0.001
_refine_ls_shift/su_mean          0.000


loop_
 _atom_site_label
 _atom_site_type_symbol
 _atom_site_fract_x
 _atom_site_fract_y
 _atom_site_fract_z
 _atom_site_U_iso_or_equiv
 _atom_site_adp_type
 _atom_site_occupancy
 _atom_site_symmetry_multiplicity
 _atom_site_calc_flag
 _atom_site_refinement_flags
 _atom_site_disorder_assembly
 _atom_site_disorder_group
Mo1 Mo 0.00050(6) 0.59262(2) 0.50809(10) 0.01809(17) Uani 1 1 d . . .
Mo2 Mo 0.16952(16) 0.73000(6) 0.9616(3) 0.0285(3) Uani 0.48 1 d P . .
Rb1 Rb 0.33338(8) 0.47125(3) 0.50086(12) 0.0258(2) Uani 1 1 d . . .
Rb2 Rb 0.33349(10) 0.66056(3) 0.47298(16) 0.0378(2) Uani 1 1 d . . .
Cu1 Cu 0.00041(14) 0.2500 0.5088(2) 0.0223(3) Uani 1 2 d S . .
O1 O 0.4181(6) 0.5647(3) 0.2159(10) 0.0361(15) Uani 1 1 d . . .
O2 O 0.4590(12) 0.2500 0.603(3) 0.075(4) Uani 1 2 d S . .
O3 O 0.4280(7) 0.5690(3) 0.7497(11) 0.0410(16) Uani 1 1 d . . .
O4 O -0.0003(8) 0.6692(3) 0.4940(14) 0.054(2) Uani 1 1 d . . .
O5 O 0.1542(6) 0.5672(3) 0.5002(11) 0.0388(15) Uani 1 1 d . . .
O6 O 0.8410(11) 0.2500 0.325(2) 0.057(3) Uani 1 2 d S . .
O7 O 0.6865(11) 0.2500 0.927(2) 0.070(4) Uani 1 2 d S . .
O8 O 0.1736(13) 0.6559(5) 0.983(2) 0.044(4) Uani 0.51 1 d P . .


loop_
 _atom_site_aniso_label
 _atom_site_aniso_U_11
 _atom_site_aniso_U_22
 _atom_site_aniso_U_33
 _atom_site_aniso_U_23
 _atom_site_aniso_U_13
 _atom_site_aniso_U_12
Mo1 0.0208(3) 0.0120(3) 0.0215(3) 0.0003(2) -0.0009(3) -0.0003(2)
Mo2 0.0306(7) 0.0183(5) 0.0367(9) -0.0010(5) -0.0027(7) 0.0000(5)
Rb1 0.0263(4) 0.0255(4) 0.0255(3) 0.0008(3) 0.0022(3) -0.0005(3)
Rb2 0.0461(5) 0.0228(4) 0.0445(5) -0.0002(3) 0.0065(5) -0.0011(4)
Cu1 0.0269(6) 0.0118(5) 0.0281(6) 0.000 -0.0024(6) 0.000
O1 0.040(3) 0.030(3) 0.038(3) 0.003(3) 0.017(3) -0.005(3)
O2 0.053(7) 0.084(10) 0.089(10) 0.000 -0.007(7) 0.000
O3 0.044(4) 0.041(4) 0.038(3) -0.007(3) -0.015(3) 0.000(3)
O4 0.065(5) 0.010(2) 0.087(6) 0.000 -0.022(5) -0.012(3)
O5 0.024(3) 0.037(3) 0.056(4) 0.004(3) 0.002(3) 0.006(3)
O6 0.046(6) 0.061(7) 0.063(7) 0.000 -0.013(6) 0.000
O7 0.034(6) 0.091(10) 0.083(9) 0.000 -0.017(6) 0.000
O8 0.038(7) 0.020(6) 0.073(10) 0.011(6) -0.002(8) -0.009(5)


_geom_special_details
;
 All esds (except the esd in the dihedral angle between two l.s. planes)
 are estimated using the full covariance matrix.  The cell esds are taken
 into account individually in the estimation of esds in distances, angles
 and torsion angles; correlations between esds in cell parameters are only
 used when they are defined by crystal symmetry.  An approximate (isotropic)
 treatment of cell esds is used for estimating esds involving l.s. planes.
;
loop_
 _geom_bond_atom_site_label_1
 _geom_bond_atom_site_label_2
 _geom_bond_distance
```

```
 _geom_bond_site_symmetry_2
 _geom_bond_publ_flag
Mo1 O5 1.731(6) . ?
Mo1 O1 1.741(6) 6_556 ?
Mo1 O3 1.748(6) 6_557 ?
Mo1 O4 1.780(6) . ?
Mo1 Rb2 3.7629(12) 6_556 ?
Mo1 Rb1 3.7759(11) 2_565 ?
Mo1 Rb1 3.8316(12) 5_566 ?
Mo1 Rb1 3.8460(11) 2_564 ?
Mo1 Rb2 3.8661(14) . ?
Mo1 Rb2 3.9443(13) 6_557 ?
Mo2 Mo2 0.929(3) 8_575 ?
Mo2 O2 1.674(13) 2_565 ?
Mo2 O8 1.726(11) . ?
Mo2 O7 1.730(11) 5_667 ?
Mo2 O6 1.805(12) 5_666 ?
Mo2 Rb2 3.798(2) . ?
Mo2 Rb2 3.908(2) 1_556 ?
Mo2 Rb2 3.924(2) 6_557 ?
Mo2 Rb2 4.2761(19) 8_575 ?
Rb1 O3 2.905(6) . ?
Rb1 O1 2.918(6) . ?
Rb1 O5 2.926(6) . ?
Rb1 O8 2.954(11) 2_564 ?
Rb1 O1 3.080(7) 2_565 ?
Rb1 O3 3.093(7) 5_666 ?
Rb1 O5 3.166(7) 2_565 ?
Rb1 O5 3.174(7) 2_564 ?
Rb1 O1 3.252(7) 5_666 ?
Rb1 O3 3.294(7) 2_564 ?
Rb1 Rb1 3.7591(10) 2_565 ?
Rb1 Rb1 3.7591(10) 2_564 ?
Rb2 O1 2.862(6) . ?
Rb2 O5 2.884(7) . ?
Rb2 O3 2.889(7) . ?
Rb2 O6 3.038(9) 5_666 ?
Rb2 O2 3.057(10) 5_666 ?
Rb2 O7 3.205(11) 5_666 ?
Rb2 O4 3.345(8) 6_656 ?
Rb2 O8 3.425(15) 1_554 ?
Rb2 O8 3.535(15) . ?
Rb2 O4 3.540(9) . ?
Rb2 O8 3.610(14) 6_657 ?
Rb2 Mo1 3.7629(12) 6_656 ?
Cu1 O4 1.876(6) 4_546 ?
Cu1 O4 1.876(6) 5_566 ?
Cu1 O7 2.007(12) 6_557 ?
Cu1 O6 2.023(11) 1_455 ?
Cu1 O2 2.400(15) 6_557 ?
Cu1 Rb2 3.9191(15) 2_565 ?
Cu1 Rb2 3.9191(15) 7_656 ?
Cu1 Rb2 4.0994(17) 4_546 ?
Cu1 Rb2 4.0994(17) 5_566 ?
Cu1 Rb2 4.2433(16) 7_655 ?
Cu1 Rb2 4.2433(16) 2_564 ?
O1 Mo1 1.741(6) 6_656 ?
O1 Rb1 3.080(7) 2_564 ?
O1 Rb1 3.252(7) 5_666 ?
O2 Mo2 1.674(13) 7_655 ?
O2 Mo2 1.674(13) 2_564 ?
O2 Cu1 2.400(15) 6_657 ?
O2 Rb2 3.057(10) 5_666 ?
O2 Rb2 3.057(10) 4_646 ?
O3 Mo1 1.748(6) 6_657 ?
O3 Rb1 3.093(7) 5_666 ?
O3 Rb1 3.294(7) 2_565 ?
O4 Cu1 1.876(6) 5_566 ?
O4 Rb2 3.345(8) 6_556 ?
O5 Rb1 3.166(7) 2_564 ?
O5 Rb1 3.174(7) 2_565 ?
```

```
O6 Mo2 1.805(12) 4_646 ?
O6 Mo2 1.805(12) 5_666 ?
O6 Cu1 2.023(11) 1_655 ?
O6 Rb2 3.038(9) 4_646 ?
O6 Rb2 3.038(9) 5_666 ?
O7 Mo2 1.730(11) 5_667 ?
O7 Mo2 1.730(11) 4_647 ?
O7 Cu1 2.007(12) 6_657 ?
O7 Rb2 3.205(11) 4_646 ?
O7 Rb2 3.205(11) 5_666 ?
O8 Rb1 2.954(11) 2_565 ?
O8 Rb2 3.425(15) 1_556 ?
O8 Rb2 3.610(14) 6_557 ?

loop_
 _geom_angle_atom_site_label_1
 _geom_angle_atom_site_label_2
 _geom_angle_atom_site_label_3
 _geom_angle
 _geom_angle_site_symmetry_1
 _geom_angle_site_symmetry_3
 _geom_angle_publ_flag
O5 Mo1 O1 108.8(3) . 6_556 ?
O5 Mo1 O3 109.2(3) . 6_557 ?
O1 Mo1 O3 108.8(3) 6_556 6_557 ?
O5 Mo1 O4 110.1(4) . . ?
O1 Mo1 O4 109.3(3) 6_556 . ?
O3 Mo1 O4 110.6(4) 6_557 . ?
O5 Mo1 Rb2 124.2(2) . 6_556 ?
O1 Mo1 Rb2 46.6(2) 6_556 6_556 ?
O3 Mo1 Rb2 125.4(2) 6_557 6_556 ?
O4 Mo1 Rb2 62.7(3) . 6_556 ?
O5 Mo1 Rb1 56.7(2) . 2_565 ?
O1 Mo1 Rb1 135.0(2) 6_556 2_565 ?
O3 Mo1 Rb1 54.1(2) 6_557 2_565 ?
O4 Mo1 Rb1 115.6(3) . 2_565 ?
Rb2 Mo1 Rb1 178.21(2) 6_556 2_565 ?
O5 Mo1 Rb1 137.3(2) . 5_566 ?
O1 Mo1 Rb1 51.9(2) 6_556 5_566 ?
O3 Mo1 Rb1 59.1(2) 6_557 5_566 ?
O4 Mo1 Rb1 112.4(3) . 5_566 ?
Rb2 Mo1 Rb1 73.63(2) 6_556 5_566 ?
Rb1 Mo1 Rb1 106.77(2) 2_565 5_566 ?
O5 Mo1 Rb1 54.3(2) . 2_564 ?
O1 Mo1 Rb1 57.2(2) 6_556 2_564 ?
O3 Mo1 Rb1 139.0(2) 6_557 2_564 ?
O4 Mo1 Rb1 110.4(3) . 2_564 ?
Rb2 Mo1 Rb1 75.72(3) 6_556 2_564 ?
Rb1 Mo1 Rb1 105.77(3) 2_565 2_564 ?
Rb1 Mo1 Rb1 105.12(2) 5_566 2_564 ?
O5 Mo1 Rb2 44.0(2) . . ?
O1 Mo1 Rb2 124.4(2) 6_556 . ?
O3 Mo1 Rb2 125.0(2) 6_557 . ?
O4 Mo1 Rb2 66.1(3) . . ?
Rb2 Mo1 Rb2 102.36(2) 6_556 . ?
Rb1 Mo1 Rb2 77.27(2) 2_565 . ?
Rb1 Mo1 Rb2 175.80(3) 5_566 . ?
Rb1 Mo1 Rb2 72.33(2) 2_564 . ?
O5 Mo1 Rb2 125.4(2) . 6_557 ?
O1 Mo1 Rb2 123.3(2) 6_556 6_557 ?
O3 Mo1 Rb2 41.9(2) 6_557 6_557 ?
O4 Mo1 Rb2 68.7(3) . 6_557 ?
Rb2 Mo1 Rb2 104.09(3) 6_556 6_557 ?
Rb1 Mo1 Rb2 74.41(2) 2_565 6_557 ?
Rb1 Mo1 Rb2 75.70(2) 5_566 6_557 ?
Rb1 Mo1 Rb2 179.02(2) 2_564 6_557 ?
Rb2 Mo1 Rb2 106.82(2) . 6_557 ?
Mo2 Mo2 O2 73.89(14) 8_575 2_565 ?
Mo2 Mo2 O8 175.4(5) 8_575 . ?
O2 Mo2 O8 104.9(5) 2_565 . ?
Mo2 Mo2 O7 74.43(12) 8_575 5_667 ?
```

```
O2 Mo2 O7 116.1(6) 2_565 5_667 ?          O8 Rb1 O3 71.3(3) 2_564 2_564 ?
O8 Mo2 O7 102.5(5) . 5_667 ?              O1 Rb1 O3 52.73(16) 2_565 2_564 ?
Mo2 Mo2 O6 75.10(11) 8_575 5_666 ?        O3 Rb1 O3 111.80(10) 5_666 2_564 ?
O2 Mo2 O6 111.9(6) 2_565 5_666 ?          O5 Rb1 O3 113.51(16) 2_565 2_564 ?
O8 Mo2 O6 109.4(5) . 5_666 ?              O5 Rb1 O3 60.70(16) 2_564 2_564 ?
O7 Mo2 O6 111.2(6) 5_667 5_666 ?          O1 Rb1 O3 148.35(15) 5_666 2_564 ?
Mo2 Mo2 Rb2 115.11(3) 8_575 . ?           O3 Rb1 Rb1 57.56(15) . 2_565 ?
O2 Mo2 Rb2 152.9(5) 2_565 . ?             O1 Rb1 Rb1 111.10(13) . 2_565 ?
O8 Mo2 Rb2 68.0(5) . . ?                  O5 Rb1 Rb1 55.01(14) . 2_565 ?
O7 Mo2 Rb2 91.0(4) 5_667 . ?              O8 Rb1 Rb1 111.9(3) 2_564 2_565 ?
O6 Mo2 Rb2 51.9(3) 5_666 . ?              O1 Rb1 Rb1 49.29(11) 2_565 2_565 ?
Mo2 Mo2 Rb2 114.36(3) 8_575 1_556 ?       O3 Rb1 Rb1 152.68(12) 5_666 2_565 ?
O2 Mo2 Rb2 93.8(5) 2_565 1_556 ?          O5 Rb1 Rb1 49.06(11) 2_565 2_565 ?
O8 Mo2 Rb2 61.1(5) . 1_556 ?              O5 Rb1 Rb1 153.43(11) 2_564 2_565 ?
O7 Mo2 Rb2 53.8(3) 5_667 1_556 ?          O1 Rb1 Rb1 92.45(11) 5_666 2_565 ?
O6 Mo2 Rb2 154.2(4) 5_664 1_556 ?         O3 Rb1 Rb1 94.67(12) 2_564 2_565 ?
Rb2 Mo2 Rb2 104.13(4) . 1_556 ?           O3 Rb1 Rb1 107.77(13) . 2_564 ?
Mo2 Mo2 Rb2 114.25(3) 8_575 6_557 ?       O1 Rb1 Rb1 53.15(14) . 2_564 ?
O2 Mo2 Rb2 47.6(3) 2_565 6_557 ?          O5 Rb1 Rb1 54.85(14) . 2_564 ?
O8 Mo2 Rb2 66.8(5) . 6_557 ?              O8 Rb1 Rb1 108.3(3) 2_564 2_564 ?
O7 Mo2 Rb2 150.3(5) 5_667 6_557 ?         O1 Rb1 Rb1 91.94(12) 2_565 2_564 ?
O6 Mo2 Rb2 98.5(3) 5_666 6_557 ?          O3 Rb1 Rb1 95.30(12) 5_666 2_564 ?
Rb2 Mo2 Rb2 108.59(4) . 6_557 ?           O5 Rb1 Rb1 153.45(11) 2_565 2_564 ?
Rb2 Mo2 Rb2 98.76(4) 1_556 6_557 ?        O5 Rb1 Rb1 49.03(11) 2_564 2_564 ?
Mo2 Mo2 Rb2 53.55(3) 8_575 8_575 ?        O1 Rb1 Rb1 153.99(11) 5_666 2_564 ?
O2 Mo2 Rb2 121.4(3) 2_565 8_575 ?         O3 Rb1 Rb1 48.09(11) 2_564 2_564 ?
O8 Mo2 Rb2 129.4(5) . 8_575 ?             Rb1 Rb1 Rb1 107.89(4) 2_565 2_564 ?
O7 Mo2 Rb2 75.8(4) 5_667 8_575 ?          O1 Rb2 O5 69.72(18) . . ?
O6 Mo2 Rb2 37.1(3) 5_666 8_575 ?          O1 Rb2 O3 68.77(19) . . ?
Rb2 Mo2 Rb2 61.56(4) . 8_575 ?            O5 Rb2 O3 69.01(18) . . ?
Rb2 Mo2 Rb2 128.12(5) 1_556 8_575 ?       O1 Rb2 O6 160.4(2) . 5_666 ?
Rb2 Mo2 Rb2 133.01(4) 6_557 8_575 ?       O5 Rb2 O6 95.2(2) . 5_666 ?
O3 Rb1 O1 67.79(19) . . ?                 O3 Rb2 O6 118.5(2) . 5_666 ?
O3 Rb1 O5 68.22(19) . . ?                 O1 Rb2 O2 102.7(2) . 5_666 ?
O1 Rb1 O5 68.39(18) . . ?                 O5 Rb2 O2 172.4(3) . 5_666 ?
O3 Rb1 O8 143.9(3) . 2_564 ?              O3 Rb2 O2 109.8(3) . 5_666 ?
O1 Rb1 O8 136.8(3) . 2_564 ?              O6 Rb2 O2 91.9(2) 5_666 5_666 ?
O5 Rb1 O8 138.1(3) . 2_564 ?              O1 Rb2 O7 96.3(2) . 5_666 ?
O3 Rb1 O1 106.79(19) . 2_565 ?            O5 Rb2 O7 119.1(2) . 5_666 ?
O1 Rb1 O1 135.98(10) . 2_565 ?            O3 Rb2 O7 160.3(3) . 5_666 ?
O5 Rb1 O1 69.35(17) . 2_565 ?             O6 Rb2 O7 79.9(3) 5_666 5_666 ?
O8 Rb1 O1 73.9(3) 2_564 2_565 ?           O2 Rb2 O7 59.5(3) 5_666 5_666 ?
O3 Rb1 O3 102.18(16) . 5_666 ?            O1 Rb2 O4 54.46(16) . 6_656 ?
O1 Rb1 O3 71.44(18) . 5_666 ?             O5 Rb2 O4 116.07(18) . 6_656 ?
O5 Rb1 O3 139.32(18) . 5_666 ?            O3 Rb2 O4 110.9(2) . 6_656 ?
O8 Rb1 O3 72.6(3) 2_564 5_666 ?           O6 Rb2 O4 128.4(2) 5_666 6_656 ?
O1 Rb1 O3 146.32(17) 2_565 5_666 ?        O2 Rb2 O4 56.9(3) 5_666 6_656 ?
O3 Rb1 O5 72.98(18) . 2_565 ?             O7 Rb2 O4 49.6(2) 5_666 6_656 ?
O1 Rb1 O5 140.00(18) . 2_565 ?            O1 Rb2 O8 69.8(3) . 1_554 ?
O5 Rb1 O5 104.1(2) . 2_565 ?              O5 Rb2 O8 72.6(2) . 1_554 ?
O8 Rb1 O5 75.7(3) 2_564 2_565 ?           O3 Rb2 O8 130.8(2) . 1_554 ?
O1 Rb1 O5 63.42(15) 2_565 2_565 ?         O6 Rb2 O8 94.2(3) 5_666 1_554 ?
O3 Rb1 O5 110.66(17) 5_666 2_565 ?        O2 Rb2 O8 104.2(3) 5_666 1_554 ?
O3 Rb1 O5 134.80(19) . 2_564 ?            O7 Rb2 O8 47.8(2) 5_666 1_554 ?
O1 Rb1 O5 68.14(18) . 2_564 ?             O4 Rb2 O8 61.6(3) 6_656 1_554 ?
O5 Rb1 O5 103.9(2) . 2_564 ?              O1 Rb2 O8 127.2(2) . . ?
O8 Rb1 O5 71.6(3) 2_564 2_564 ?           O5 Rb2 O8 67.2(2) . . ?
O1 Rb1 O5 111.48(16) 2_565 2_564 ?        O3 Rb2 O8 68.4(3) . . ?
O3 Rb1 O5 53.79(16) 5_666 2_564 ?         O6 Rb2 O8 51.3(3) 5_666 . ?
O5 Rb1 O5 146.9(2) 2_565 2_564 ?          O2 Rb2 O8 119.8(3) 5_666 . ?
O3 Rb1 O1 69.29(17) . 5_666 ?             O7 Rb2 O8 130.9(3) 5_666 . ?
O1 Rb1 O1 104.88(15) . 5_666 ?            O4 Rb2 O8 176.4(3) 6_656 . ?
O5 Rb1 O1 136.08(17) . 5_666 ?            O8 Rb2 O8 121.7(4) 1_554 . ?
O8 Rb1 O1 77.5(3) 2_564 5_666 ?           O1 Rb2 O4 112.08(18) . . ?
O1 Rb1 O1 113.84(9) 2_565 5_666 ?         O5 Rb2 O4 51.99(15) . . ?
O3 Rb1 O1 61.51(16) 5_666 5_666 ?         O3 Rb2 O4 111.48(19) . . ?
O5 Rb1 O1 52.16(15) 2_565 5_666 ?         O6 Rb2 O4 48.7(2) 5_666 . ?
O5 Rb1 O1 113.69(16) 2_564 5_666 ?        O2 Rb2 O4 133.1(2) 5_666 . ?
O3 Rb1 O3 138.78(9) . 2_564 ?             O7 Rb2 O4 85.7(2) 5_666 . ?
O1 Rb1 O3 101.18(18) . 2_564 ?            O4 Rb2 O4 123.49(15) 6_656 . ?
O5 Rb1 O3 70.82(17) . 2_564 ?             O8 Rb2 O4 62.6(3) 1_554 . ?
```

O8 Rb2 O4 59.5(3) . . ?
O1 Rb2 O8 72.8(2) . 6_657 ?
O5 Rb2 O8 129.0(2) . 6_657 ?
O3 Rb2 O8 65.8(3) . 6_657 ?
O6 Rb2 O8 126.6(3) 5_666 6_657 ?
O2 Rb2 O8 46.8(3) 5_666 6_657 ?
O7 Rb2 O8 98.1(3) 5_666 6_657 ?
O4 Rb2 O8 62.6(3) 6_656 6_657 ?
O8 Rb2 O8 123.7(2) 1_554 6_657 ?
O8 Rb2 O8 114.3(2) . 6_657 ?
O4 Rb2 O8 173.5(3) . 6_657 ?
O1 Rb2 Mo1 26.24(12) . 6_656 ?
O5 Rb2 Mo1 92.22(13) . 6_656 ?
O3 Rb2 Mo1 88.94(14) . 6_656 ?
O6 Rb2 Mo1 152.4(2) 5_666 6_656 ?
O2 Rb2 Mo1 80.2(2) 5_666 6_656 ?
O7 Rb2 Mo1 73.30(19) 5_666 6_656 ?
O4 Rb2 Mo1 28.22(11) 6_656 6_656 ?
O8 Rb2 Mo1 62.8(2) 1_554 6_656 ?
O8 Rb2 Mo1 153.35(19) . 6_656 ?
O4 Rb2 Mo1 121.35(14) . 6_656 ?
O8 Rb2 Mo1 64.9(2) 6_657 6_656 ?
O4 Cu1 O4 179.0(5) 4_546 5_566 ?
O4 Cu1 O7 90.1(3) 4_546 6_557 ?
O4 Cu1 O7 90.1(3) 5_566 6_557 ?
O4 Cu1 O6 89.7(3) 4_546 1_455 ?
O4 Cu1 O6 89.7(3) 5_566 1_455 ?
O7 Cu1 O6 157.6(5) 6_557 1_455 ?
O4 Cu1 O2 90.5(3) 4_546 6_557 ?
O4 Cu1 O2 90.5(3) 5_566 6_557 ?
O7 Cu1 O2 89.4(5) 6_557 6_557 ?
O6 Cu1 O2 113.0(5) 1_455 6_557 ?
O4 Cu1 Rb2 122.5(3) 4_546 2_565 ?
O4 Cu1 Rb2 58.5(2) 5_566 2_565 ?
O7 Cu1 Rb2 54.6(3) 6_557 2_565 ?
O6 Cu1 Rb2 140.5(2) 1_455 2_565 ?
O2 Cu1 Rb2 51.3(2) 6_557 2_565 ?
O4 Cu1 Rb2 58.5(2) 4_546 7_656 ?
O4 Cu1 Rb2 122.5(3) 5_566 7_656 ?
O7 Cu1 Rb2 54.6(3) 6_557 7_656 ?
O6 Cu1 Rb2 140.5(2) 1_455 7_656 ?
O2 Cu1 Rb2 51.3(2) 6_557 7_656 ?
Rb2 Cu1 Rb2 63.98(3) 2_565 7_656 ?
O4 Cu1 Rb2 59.5(3) 4_546 4_546 ?
O4 Cu1 Rb2 120.4(3) 5_566 4_546 ?
O7 Cu1 Rb2 147.17(14) 6_557 4_546 ?
O6 Cu1 Rb2 45.3(2) 1_455 4_546 ?
O2 Cu1 Rb2 79.4(3) 6_557 4_546 ?
Rb2 Cu1 Rb2 129.45(4) 2_565 4_546 ?
Rb2 Cu1 Rb2 95.67(3) 7_656 4_546 ?
O4 Cu1 Rb2 120.4(3) 4_546 5_566 ?
O4 Cu1 Rb2 59.5(3) 5_566 5_566 ?
O7 Cu1 Rb2 147.17(14) 6_557 5_566 ?
O6 Cu1 Rb2 45.3(2) 1_455 5_566 ?
O2 Cu1 Rb2 79.4(3) 6_557 5_566 ?
Rb2 Cu1 Rb2 95.67(3) 2_565 5_566 ?
Rb2 Cu1 Rb2 129.45(4) 7_656 5_566 ?
Rb2 Cu1 Rb2 60.86(3) 4_546 5_566 ?
O4 Cu1 Rb2 60.3(3) 4_546 7_655 ?
O4 Cu1 Rb2 118.9(3) 5_566 7_655 ?
O7 Cu1 Rb2 75.1(3) 6_557 7_655 ?
O6 Cu1 Rb2 85.5(3) 1_455 7_655 ?
O2 Cu1 Rb2 146.12(15) 6_557 7_655 ?
Rb2 Cu1 Rb2 128.76(5) 2_565 7_655 ?
Rb2 Cu1 Rb2 96.17(3) 7_656 7_655 ?
Rb2 Cu1 Rb2 97.46(3) 4_546 7_655 ?
Rb2 Cu1 Rb2 128.72(4) 5_566 7_655 ?
O4 Cu1 Rb2 118.9(3) 4_546 2_564 ?
O4 Cu1 Rb2 60.3(3) 5_566 2_564 ?
O7 Cu1 Rb2 75.1(3) 6_557 2_564 ?
O6 Cu1 Rb2 85.5(3) 1_455 2_564 ?

O2 Cu1 Rb2 146.12(15) 6_557 2_564 ?
Rb2 Cu1 Rb2 96.17(3) 2_565 2_564 ?
Rb2 Cu1 Rb2 128.76(5) 7_656 2_564 ?
Rb2 Cu1 Rb2 128.72(4) 4_546 2_564 ?
Rb2 Cu1 Rb2 97.46(3) 5_566 2_564 ?
Rb2 Cu1 Rb2 58.59(3) 7_655 2_564 ?
Mo1 O1 Rb2 107.1(3) 6_656 . ?
Mo1 O1 Rb1 153.4(3) 6_656 . ?
Rb2 O1 Rb1 99.07(18) . . ?
Mo1 O1 Rb1 101.6(3) 6_656 2_564 ?
Rb2 O1 Rb1 99.9(2) . 2_564 ?
Rb1 O1 Rb1 77.56(15) . 2_564 ?
Mo1 O1 Rb1 96.0(3) 6_656 5_666 ?
Rb2 O1 Rb1 99.4(2) . 5_666 ?
Rb1 O1 Rb1 75.12(15) . 5_666 ?
Rb1 O1 Rb1 148.6(2) 2_564 5_666 ?
Mo2 O2 Mo2 32.2(3) 7_655 2_564 ?
Mo2 O2 Cu1 130.8(7) 7_655 6_657 ?
Mo2 O2 Cu1 130.8(7) 2_564 6_657 ?
Mo2 O2 Rb2 134.0(6) 7_655 5_666 ?
Mo2 O2 Rb2 108.5(4) 2_564 5_666 ?
Cu1 O2 Rb2 91.0(3) 6_657 5_666 ?
Mo2 O2 Rb2 108.5(4) 7_655 4_646 ?
Mo2 O2 Rb2 134.0(6) 2_564 4_646 ?
Cu1 O2 Rb2 91.0(3) 6_657 4_646 ?
Rb2 O2 Rb2 85.6(3) 5_666 4_646 ?
Mo1 O3 Rb2 114.3(3) 6_657 . ?
Mo1 O3 Rb1 146.6(3) 6_657 . ?
Rb2 O3 Rb1 98.76(19) . . ?
Mo1 O3 Rb1 98.7(3) 6_657 5_666 ?
Rb2 O3 Rb1 102.6(2) . 5_666 ?
Rb1 O3 Rb1 77.82(16) . 5_666 ?
Mo1 O3 Rb1 93.8(3) 6_657 2_565 ?
Rb2 O3 Rb1 100.8(2) . 2_565 ?
Rb1 O3 Rb1 74.35(15) . 2_565 ?
Rb1 O3 Rb1 145.9(2) 5_666 2_565 ?
Mo1 O4 Cu1 177.7(5) . 5_566 ?
Mo1 O4 Rb2 89.1(3) . 6_556 ?
Cu1 O4 Rb2 93.0(3) 5_566 6_556 ?
Mo1 O4 Rb2 86.6(3) . . ?
Cu1 O4 Rb2 93.3(3) 5_566 . ?
Rb2 O4 Rb2 119.4(3) 6_556 . ?
Mo1 O5 Rb2 111.4(3) . . ?
Mo1 O5 Rb1 150.2(3) . . ?
Rb2 O5 Rb1 98.40(18) . . ?
Mo1 O5 Rb1 99.3(3) . 2_564 ?
Rb2 O5 Rb1 97.45(19) . 2_564 ?
Rb1 O5 Rb1 76.09(15) . 2_564 ?
Mo1 O5 Rb1 96.2(3) . 2_565 ?
Rb2 O5 Rb1 103.8(2) . 2_565 ?
Rb1 O5 Rb1 75.96(15) . 2_565 ?
Rb1 O5 Rb1 146.9(2) 2_564 2_565 ?
Mo2 O6 Mo2 29.8(2) 4_646 5_666 ?
Mo2 O6 Cu1 125.7(6) 4_646 1_655 ?
Mo2 O6 Cu1 125.7(6) 5_666 1_655 ?
Mo2 O6 Rb2 100.2(3) 4_646 4_646 ?
Mo2 O6 Rb2 121.9(4) 5_666 4_646 ?
Cu1 O6 Rb2 106.4(4) 1_655 4_646 ?
Mo2 O6 Rb2 121.9(4) 4_646 5_666 ?
Mo2 O6 Rb2 100.2(3) 5_666 5_666 ?
Cu1 O6 Rb2 106.4(4) 1_655 5_666 ?
Rb2 O6 Rb2 86.2(3) 4_646 5_666 ?
Mo2 O7 Mo2 31.1(2) 5_667 4_647 ?
Mo2 O7 Cu1 142.0(8) 5_667 6_657 ?
Mo2 O7 Cu1 142.0(8) 4_647 6_657 ?
Mo2 O7 Rb2 121.9(5) 5_667 4_646 ?
Mo2 O7 Rb2 100.4(4) 4_647 4_646 ?
Cu1 O7 Rb2 94.7(3) 6_657 4_646 ?
Mo2 O7 Rb2 100.4(4) 5_667 5_666 ?
Mo2 O7 Rb2 121.9(5) 4_647 5_666 ?
Cu1 O7 Rb2 94.7(3) 6_657 5_666 ?

```
Rb2 O7 Rb2 80.7(3) 4_646 5_666 ?
Mo2 O8 Rb1 176.3(8) . 2_565 ?
Mo2 O8 Rb2 92.7(5) . 1_556 ?
Rb1 O8 Rb2 90.7(3) 2_565 1_556 ?
Mo2 O8 Rb2 85.1(5) . . ?
Rb1 O8 Rb2 94.3(4) 2_565 . ?
Rb2 O8 Rb2 121.7(4) 1_556 . ?
Mo2 O8 Rb2 87.2(5) . 6_557 ?
Rb1 O8 Rb2 90.1(3) 2_565 6_557 ?
Rb2 O8 Rb2 115.3(4) 1_556 6_557 ?
Rb2 O8 Rb2 122.7(4) . 6_557 ?

_diffrn_measured_fraction_theta_max     0.996
_diffrn_reflns_theta_full               30.02
_diffrn_measured_fraction_theta_full    0.996
_refine_diff_density_max     2.333
_refine_diff_density_min    -1.226
_refine_diff_density_rms     0.228
```

# APPENDIX 6 – LETTERS OF PERMISSION

## American Chemical Society

Publications Division
Copyright Office

1155 Sixteenth Street. NW
Washington. DC 20036
Phone: (1) 202-872-4368 or -4367
Fax: (1) 202-776-8112 E-mail: copyright@acs.org

VIA FAX: 225-578-3458      DATE: April 24, 2008

TO:     Dixie Gautreaux, Department of Chemistry, Louisiana State University
232 Choppin Hall, Baton Rouge, LA 70803-1804

FROM: C. Arleen Courtney, Copyright Associate   *C. Arlee Courtney*

Thank you for your request for permission to include **your** paper(s) or portions of text from **your** paper(s) in your thesis. Permission is now automatically granted; please pay special attention to the implications paragraph below. The Copyright Subcommittee of the Joint Board/Council Committees on Publications approved the following:

Copyright permission for published and submitted material from theses and dissertations
ACS extends blanket permission to students to include in their theses and dissertations their own articles, or portions thereof, that have been published in ACS journals or submitted to ACS journals for publication, provided that the ACS copyright credit line is noted on the appropriate page(s).

Publishing implications of electronic publication of theses and dissertation material
Students and their mentors should be aware that posting of theses and dissertation material on the Web prior to submission of material from that thesis or dissertation to an ACS journal **may** affect publication in that journal. Whether Web posting is considered prior publication may be evaluated on a case-by-case basis by the journal's editor. If an ACS journal editor considers Web posting to be "prior publication", the paper will not be accepted for publication in that journal. If you intend to submit your unpublished paper to ACS for publication, check with the appropriate editor prior to posting your manuscript electronically.

If your paper has **not** yet been published by ACS, we have no objection to your including the text or portions of the text in your thesis/dissertation in **print and microfilm formats**; please note, however, that electronic distribution or Web posting of the unpublished paper as part of your thesis in electronic formats might jeopardize publication of your paper by ACS. Please print the following credit line on the first page of your article: "Reproduced (or 'Reproduced in part') with permission from [JOURNAL NAME], in press (or 'submitted for publication'). Unpublished work copyright [CURRENT YEAR] American Chemical Society." Include appropriate information.

If your paper has already been published by ACS and you want to include the text or portions of the text in your thesis/dissertation in **print or microfilm formats**, please print the ACS copyright credit line on the first page of your article: "Reproduced (or 'Reproduced in part') with permission from [FULL REFERENCE CITATION.] Copyright [YEAR] American Chemical Society." Include appropriate information.

**Submission to a Dissertation Distributor:** If you plan to submit your thesis to UMI or to another dissertation distributor, you should not include the unpublished ACS paper in your thesis if the thesis will be disseminated electronically, until ACS has published your paper. After publication of the paper by ACS, you may release the entire thesis (**not the individual ACS article by itself**) for electronic dissemination through the distributor; ACS's copyright credit line should be printed on the first page of the ACS paper.

**Use on an Intranet:** The inclusion of your ACS unpublished or published manuscript is permitted in your thesis in print and microfilm formats. If ACS has published your paper you may include the manuscript in your thesis on an intranet that is **not** publicly available. Your ACS article cannot be posted electronically on a publicly available medium (i.e. one that is not password protected), such as but not limited to, electronic archives, Internet, library server, etc. The only material from your paper that can be posted on a public electronic medium is the article abstract, figures, and tables, and you may link to the article's DOI or post the article's author-directed URL link provided by ACS. This paragraph does not pertain to the dissertation distributor paragraph above.     06/07/06

Dixie P. Gatreaux
PhD Candidate
Department of Chemistry
Louisiana State University
232 Choppin Hall
Baton Rouge
LA 70803-1804
USA

25 April 2008

## Copyright Permission

Dear Dixie

Permission is hereby granted, on behalf of the IUCr, for the reproduction of the material specified in your email subject to the following conditions.

1. Reproduction is intended in a primary journal, secondary journal, CD-ROM, book or thesis.

2. The original article in which the material appeared is cited.

3. IUCr's copyright permission is indicated in print. In electronic form, this acknowledgement must be hyperlinked to Crystallography Journals Online (http://journals.iucr.org/).

Material to be reproduced:

Title: The Layered Intermatallic Compound LaPdSb$_3$
Journal: Acta Crystallographica Section E Structural Reports Online
Year: 2006
Volume: E62
Pages: i96-i98

Yours sincerely

Peter Strickland
Managing Editor

To Whom It May Concern:

I am writing to request a signed letter granting permission to use material from a paper published in the Journal of Physics: Condensed Matter.  I am an author of this paper and the citation is as follows:

Karki, A.B., Gautreaux, D.P., Chan, J.Y., Harrison, N., Browne, D.A., Goodrich, R.G., Young, D.P. *J. Phys: Condens. Matter* **2008**, *20* , 035209 (5pp).

I am requesting the use of portions of the text refering to the single crystal structure determination.  This material will be placed in my dissertation.

Please fax or mail the letter to the address listed below.

Thank you very much.

--
Dixie P. Gautreaux
PhD Candidate
Department of Chemistry
Louisiana State University
232 Choppin Hall
Baton Rouge, LA 70803-1804
Fax: (225)578-3458

PERMISSION TO REPRODUCE AS REQUESTED
IS GIVEN PROVIDED THAT:

(a) the consent of the author(s) is obtained
(b) the source of the material including author/editor, title, date and publisher is acknowledged (✓)

IOP Publishing Ltd
Dirac House
Temple Back
BRISTOL          25/4/08   [signature]

(✓) *Please include mention of the Journal's homepage at: www.iop.org/journals/jpcm and provide a link back to the article's abstract on our website from the electronic version of your thesis (if appropriate).*

*Thank you!*

117

## ELSEVIER LIMITED LICENSE
## TERMS AND CONDITIONS

May 21, 2008

This is a License Agreement between Dixie P Gautreaux ("You") and Elsevier Limited ("Elsevier Limited"). The license consists of your order details, the terms and conditions provided by Elsevier Limited, and the payment terms and conditions.

| | |
|---|---|
| Supplier | Elsevier Limited<br>The Boulevard,Langford Lane<br>Kidlington,Oxford,OX5 1GB,UK |
| Registered Company Number | 1982084 |
| Customer name | Dixie P Gautreaux |
| Customer address | Louisiana State University<br>Baton Rouge, LA 70803 |
| License Number | 1916550968681 |
| License date | Mar 26, 2008 |
| Licensed content publisher | Elsevier Limited |
| Licensed content publication | Physica B: Condensed Matter |
| Licensed content title | Magnetization and transport properties of $\alpha$-CeNi$_{0.78}$Co$_{0.22}$Sb$_3$ |
| Licensed content author | Gautreaux Dixie P., Parent Michael, Moldovan Monica, Young David P. and Chan Julia Y. |
| Licensed content date | 1 April 2008 |
| Volume number | 403 |
| Issue number | 5-9 |
| Pages | 2 |
| Type of Use | Thesis / Dissertation |
| Portion | Full article |
| Format | Both print and electronic |
| You are an author of the Elsevier article | Yes |
| Are you translating? | No |
| Purchase order number | |
| Expected publication date | Aug 2008 |
| Elsevier VAT number | GB 494 6272 12 |
| Permissions price | 0.00 USD |
| Value added tax 0.0% | 0.0 USD |
| Total | 0.00 USD |
| Terms and Conditions | |

118

## INTRODUCTION

The publisher for this copyrighted material is Elsevier. By clicking "accept" in connection with completing this licensing transaction, you agree that the following terms and conditions apply to this transaction (along with the Billing and Payment terms and conditions established by Copyright Clearance Center, Inc. ("CCC"), at the time that you opened your Rightslink account and that are available at any time at http://myaccount.copyright.com).

## GENERAL TERMS

Elsevier hereby grants you permission to reproduce the aforementioned material subject to the terms and conditions indicated.

Acknowledgement: If any part of the material to be used (for example, figures) has appeared in our publication with credit or acknowledgement to another source, permission must also be sought from that source. If such permission is not obtained then that material may not be included in your publication/ copies. Suitable acknowledgement to the source must be made, either as a footnote or in a reference list at the end of your publication, as follows:

"Reprinted from Publication title, Vol number, Author(s), Title of article, Pages No., Copyright (Year), with permission from Elsevier [OR APPLICABLE SOCIETY COPYRIGHT OWNER]." Also Lancet special credit - "Reprinted from The Lancet, Vol. number, Author(s), Title of article, Pages No., Copyright (Year), with permission from Elsevier."

Reproduction of this material is confined to the purpose and/or media for which permission is hereby given.

**Thesis/Dissertation**: If your license is for use in a thesis/dissertation your thesis may be submitted to your institution in either print or electronic form. Should your thesis be published commercially, please reapply for permission. These requirements include permission for the Library and Archives of Canada to supply single copies, on demand, of the complete thesis and include permission for UMI to supply single copies, on demand, of the complete thesis. Should your thesis be published commercially, please reapply for permission.

119

**VITA**

Dixie Plaisance Gautreaux was born in April 1982, in Lockport, Louisiana, to her parents Joey and Kate Plaisance. She is the wife of Jarred Gautreaux of Lockport, Louisiana, and mother of Elise Reneé. She has one younger sister, Josie Plaisance Eschete. In May 2000, Dixie graduated sixth in her class from Central Lafourche High School in Mathews, Louisiana. Dixie received numerous academic and music scholarships to universities throughout the state. She attended Tulane University in New Orleans, Louisiana on a full Legislative scholarship from August 2000-May 2001, where she majored in chemistry and was a member of the Tulane Symphonic Winds and Green Wave Basketball Band. In August, 2001, she transferred to Nicholls State University in Thibodaux, Louisiana, where she majored in chemistry and was the president of the Nicholls Chemical Sciences Society. She was also a member of the NSU Concert Band, Symphonic Winds, and the Pride of NSU Marching Band. She received a Bachelor of Science in chemistry (*cum laude*) from Nicholls State University in December 2003.

Dixie began her graduate career at Louisiana State University in August, 2004, and received a Louisiana Board of Regents Fellowship. She joined the Chan group in January 2005, and began her doctoral research on ternary rare earth antimonides. She attended and presented posters at national scientific meetings: the 24th Rare Earth Research Conference in Keystone, Colorado, the 232nd ACS National Meeting & Exposition in San Francisco, California, and the International Conference on Strongly Correlated Electron Systems in Houston, Texas. In 2006, she was chosen to be a member of the US delegation at the 56th Meeting of the Nobel Laureates and Students in Lindau, Germany. In 2007, she was awarded a Strongly Correlated Electron Systems Conference Young Investigator Award and a Proctor and Gamble Research Award. She was awarded another Proctor and Gamble Research award in 2008. She was an officer on the

2005-2006 Chemistry Graduate Student Council. She was also very active in the department's service learning program where she visited nearby schools and performed chemistry demonstrations for the students.

Dixie will graduate from Louisiana State University on August 8, 2008, with a Doctor of Philosophy degree in chemistry. She has chosen a career in academics where she can teach and inspire young minds for years to come.